USGS
science for a changing world

Mineral Resources Program

Roles of Regional Structures and Country-Rock Facies in Defining Mineral Belts in Central Idaho Mineral Province with Detail for Yellow Pine and Thunder Mountain Mining Districts

Professional Paper 1884
Version 1.1, September 2023

U.S. Department of the Interior
U.S. Geological Survey

Cover. Photographs of historic mine sites from the central Idaho mineral province. Clockwise from upper left: gold placer piles, Leesburg mining district; Jumbo Mine mill building, Buffalo Hump mining district; Lucky Lad Mine mill building, Buffalo Hump mining district; Warren Creek floating gold dredge, Warren mining district; Bayhorse mine mill buildings, Bayhorse mining district; arrastra mill, Thunder Mountain mining district; Atlas Mine ball mill, Buffalo Hump mining district. Photographs by Karen Lund, U.S. Geological Survey.

Roles of Regional Structures and Country-Rock Facies in Defining Mineral Belts in Central Idaho Mineral Province with Detail for Yellow Pine and Thunder Mountain Mining Districts

Karen Lund, John N. Aleinikoff, and Christopher Holm-Denoma

Mineral Resources Program

Professional Paper 1884
Version 1.1, September 2023

U.S. Department of the Interior
U.S. Geological Survey

U.S. Geological Survey, Reston, Virginia: 2023
First release: 2023
Revised: September 2023 (ver 1.1)

Suggested citation:
Lund, K., Aleinikoff, J.N., and Holm-Denoma, C., 2023, Roles of regional structures and country-rock facies in defining mineral belts in central Idaho mineral province with detail for Yellow Pine and Thunder Mountain mining districts (ver. 1.1, September 2023): U.S. Geological Survey Professional Paper 1884, 53 p., https://doi.org/10.3133/pp1884.

Associated data for this publication:
Aleinikoff, J.N., Holm-Denoma, C.S., and Lund, K., 2023, SHRIMP U-Pb and LA-ICPMS U-Pb geochronologic data for igneous and metasedimentary rocks in central Idaho mineral province, U.S.A., 2023: U.S. Geological Survey data release, https://doi.org/10.5066/P931I3A3.

ISSN 2330-7102 (online)

Acknowledgments

A first draft of this manuscript was reviewed by K.V. Evans who helped clarify and organize ideas. His continued interest in this region is gratefully acknowledged. A second draft was reviewed by R.S. Lewis. Comments by both reviewers improved the final manuscript. Interactions with and assistance from many personnel of the U.S. Department of Agriculture Forest Service in the Red River and Grangeville Ranger Districts of the Nez Perce National Forest and in the Krassel District of the Payette National Forest made it possible to complete the field aspects of this research through the many years represented by this study.

Contents

Figures

Tables

Conversion Factors

International System of Units to U.S. customary units

Multiply	By	To obtain
Length		
meter (m)	3.281	foot (ft)
kilometer (km)	0.6214	mile (mi)

Temperature in degrees Fahrenheit (°F) may be converted to degrees Celsius (°C) as follows:

$$°C = (°F - 32) / 1.8.$$

Datum

Vertical coordinate information is referenced to the World Geodetic System 1984 Datum (WGS 84).

Horizontal coordinate information is referenced to the World Geodetic System 1984 Datum (WGS 84).

Altitude, as used in this report, refers to distance above the vertical datum.

Abbreviations

Ag	gold
Au	silver
CL	cathodoluminescence
Ga	billion years
Ma	million years
Mo	molybdenum
Pb	lead
SHRIMP	sensitive high-resolution ion microprobe
Th	thorium
TIMS	thermal ionization mass spectrometry
U	uranium
USGS	U.S. Geological Survey
Zn	zinc

Roles of Regional Structures and Country-Rock Facies in Defining Mineral Belts in Central Idaho Mineral Province with Detail for Yellow Pine and Thunder Mountain Mining Districts

Karen Lund, John N. Aleinikoff, and Christopher Holm-Denoma

Abstract

The central Idaho metallogenic province hosts numerous mineral deposit types. These include Late Cretaceous precious-polymetallic vein deposits, amagmatic Paleocene–Eocene breccia-hosted gold-tungsten-antimony deposits, and Eocene mercury deposits in metasedimentary roof pendants and in Late Cretaceous granitoids. Hot-springs gold deposits in Eocene volcanic rocks are also included in the central Idaho province. New sensitive high mass-resolution ion microprobe (SHRIMP) uranium-lead (U-Pb) ages for igneous rocks and for detrital zircon analyses of metasedimentary rocks along with geologic mapping clarify the geologic framework of the mineral deposits. This framework includes (1) structural controls for regional distribution of mining districts, (2) progressive structural development of individual districts, (3) regional sedimentary facies and their control of metals associations resulting in regional belts, and (4) influences of the several regional magmatic events.

In central Idaho, 15 mining districts form two clusters that are grouped about a 200-kilometer (km) long system of normal faults. The northwestern cluster is in the regional hanging wall west of large, west-side-down faults, and the mineral deposits are located along smaller faults and fractures that cut the regional hanging wall. The southeastern cluster is in the regional hanging wall east of a linked large east-side-down fault and along and controlled by related hanging wall faults. At the southern extent of the regional fault system, the Yellow Pine-Thunder Mountain districts span a nearly 24-km-wide, east-tilted crustal block of normal-fault dominoes, exposing original crustal depths from 5 to 10 km deep on the west in the Late Cretaceous to shallow-surface depths on the east in the Eocene.

Ore deposition in the northwestern district cluster was primarily Late Cretaceous and related to Idaho batholith plutons with only a single deposit related to a small Eocene intrusion; in the southeastern cluster, most deposits were initiated in the Late Cretaceous but with varying manifestations of overprinted Eocene mineralization activity. In the Yellow Pine-Thunder Mountain districts at the southern extent of the southern cluster, several mineralizing pulses occurred during hanging-wall collapse, such that (1) early deposits were multiply overprinted and (2) deposit depths, ages, and structural characteristics change progressively eastward. Originally deep-seated western Yellow Pine district deposits are Late Cretaceous viscoplastic mesothermal veins overprinted by Paleocene and Eocene breccia-hosted epithermal deposits. Central Yellow Pine district deposits contain early deeper vein systems but are primarily Paleocene and Eocene breccia-hosted epithermal deposits in Late Cretaceous plutonic rocks and Proterozoic–Paleozoic roof pendant rocks. Eastern district deposits are Eocene hot-springs-related deposits in the roof pendant. Thunder Mountain deposits farthest east are near-surface hot-springs deposits in Eocene volcanic and volcaniclastic rocks that overlie buried Cretaceous igneous and older roof pendant rocks.

The mining district clusters are sited across several northwest-striking paleostratigraphic belts that are exposed in roof pendants and are offset by the regional normal fault system. A northeastern belt is Mesoproterozoic strata associated with gold-silver-copper±cobalt deposits. A central belt of Neoproterozoic rocks is not associated with mineral deposits in the central Idaho mineral province. A southwestern belt composed of probable Paleozoic deep-water miogeoclinal slope rocks and late Paleozoic epicratonic basinal rocks is thin and narrowly exposed but associated with gold-silver-antimony-tungsten±mercury deposits. These metasedimentary rocks (and their metal associations) are parts of regional mineral belts in which metal endowments are related to particular sedimentary facies belts and their Cretaceous thrust-fault juxtaposition and where these features have proximity to Late Cretaceous or Eocene igneous rocks. Offset and preservation or erosional stripping of these facies belts, thrust plates, igneous settings, and the associated regional mineral belts were controlled by the sense and magnitude of displacements across the regional normal-fault system.

Introduction

The many mining districts of central Idaho compose a richly mineralized province with significant historic production and a broad variety of commodities (fig. 1, table 1). Diverse proposed mineralizing fluid sources include Cretaceous plutons, Eocene igneous rocks, Mesoproterozoic plutons, metamorphic events, or synsedimentary processes. Recent studies also suggest that cryptic basement character and an overprinted rift system may have influenced development of the metallogenic province. In this complicated geologic framework containing mineral deposits of such broad characteristics, widely accepted models for deposit genesis are generally lacking as is agreement about which geologic elements are critical to ultimately determining genesis.

The present study endeavors to clarify settings of the diverse mineral deposits of the central Idaho mineral province by presenting and evaluating details from the districts, including (1) igneous rock relations to mineralization; (2) compositions, ages, provenances, and facies-belt origins for metasedimentary roof pendants using geologic mapping and uranium-lead (U-Pb) geochronology; (3) structural and kinematic histories of mineral deposit host rocks, crustal depths at times of mineralization, and the temporal relations between deformation and mineralization; and (4) the role of structural history as a factor in deposit formation as well as in deposit preservation and exposure. Yellow Pine and Thunder Mountain districts at the southern extent of the mineral province are the most complex and recently explored parts of the province. New details from these southern districts employ sensitive high resolution ion microprobe (SHRIMP) U-Pb ages of and emplacement settings for Late Cretaceous Idaho batholith phases and new structural mapping to evaluate crustal evolution and mineral deposit formation.

The goals of the study are to investigate potential common genetic factors among districts, test the verity and origin of a proposed regional tungsten belt and the geographic distributions of other metal endowments in deposits regionally, and advance a geologic framework useful for resource assessment of this mineral-rich province.

Regional Geologic Setting

Much of central Idaho is underlain by cryptic basement domains and a rift belt that overprinted the Laurentian basement (fig. 1*A*, *B*). The Paleoproterozoic juvenile crust of the Wallace terrane and western extension of the Great Falls tectonic zone compose the older basement elements (Lund and others, 2015). This basement was first modified by Mesoproterozoic extension, which resulted in the formation of a northwest-striking Lemhi depositional basin (Lund and others, 2004; Lund and Tysdal, 2007). The overprinted Neoproterozoic through early Paleozoic rift belt, which formed the western margin of Laurentia, resulted in north-northwest-striking rift structures, modification of basement by rift-related magmatism, and a broad rift-drift miogeoclinal basin (Lund, 2008; Lund and others, 2010). In south-central Idaho, discrete deformation events in the middle and late Paleozoic, which disturbed miogeoclinal deposition, resulted in successor depositional troughs and overlap successions. Diverse mineral deposit types are associated with the Neoproterozoic–Paleozoic sedimentary depositional environments and facies belts (Link and others, 1995; Lund, 2008; Lund and others, 2016).

The western edge of Laurentia is at the Salmon River suture in west-central Idaho (fig. 1*B*), along which late Mesozoic oblique convergence between Laurentia and various Pacific terranes caused accretion of allochthonous terranes. This accretion resulted in Late Cretaceous east-northeast-directed compression across central Idaho that telescoped rocks of the several sedimentary basins in this hinterland of the Cordilleran fold and thrust belt (Lund and Snee, 1988; Lund, 2004). Limited early-stage, accretion-related slab-wedge melting resulted in tonalite-granodiorite sheets, whereas associated crustal thickening and melting resulted in younger voluminous S-type granites; together, these formed the Late Cretaceous Atlanta lobe of the Idaho batholith (Lund and Snee, 1988; Lund, 2004; Gaschnig and others, 2010). Changes in plate motion in the Paleocene–Eocene (Lithgow-Bertelloni and Richards, 1998; Liu and others, 2008) resulted first in Paleocene amagmatic crustal relaxation in the Atlanta lobe area (and Idaho batholith magmatism switched to the north, forming the Bitteroot lobe) followed by extensional deformation that culminated in the Eocene Challis magmatism. The study area lies at the eastern edge of the Atlanta lobe and at the western extent of both the Challis volcanic field and Challis plutons.

Development of Central Idaho Mineral-Deposit Models

Because diverse metasedimentary, plutonic, and volcanic rocks host epigenetic deposits in the central Idaho mining districts (figs. 2, 3), there is a broad range of proposed deposit origins and a common linkage to a variety of proposed mineral belts. These mineral belts have been characterized using geographic groupings or, commodities, but the belts, so defined, resulted in intersecting linear arrays of deposits (for example, Bookstrom and others, 1998). Although not ascribed to geologic causes, these include (1) northwest-striking Florence-Stibnite gold belt, (2) north-northeast-striking Dixie-Thunder Mountain gold belt, (3) northeast-striking Marshall Lake-Elk City polymetallic belt (Green, 1972), (4) northeast-striking Idaho-Montana porphyry belt (Green, 1972; Rostad and others, 1978; Armstrong and others, 1978), (5) north-northwest-striking tungsten belt (Cook, 1956), and (6) northwest-striking Idaho cobalt belt (Hughes, 1983; Hahn and Hughes, 1984). Most of these are substantially modified or abandoned by new studies and so are not shown on maps for the present study.

In interpretations of their genesis, polymetallic deposits in central Idaho were initially interpreted as related to the Late Cretaceous Idaho batholith (Lindgren, 1904; Thompson and Ballard, 1924; Beckwith, 1928; Ross, 1931; Shenon and Reed,

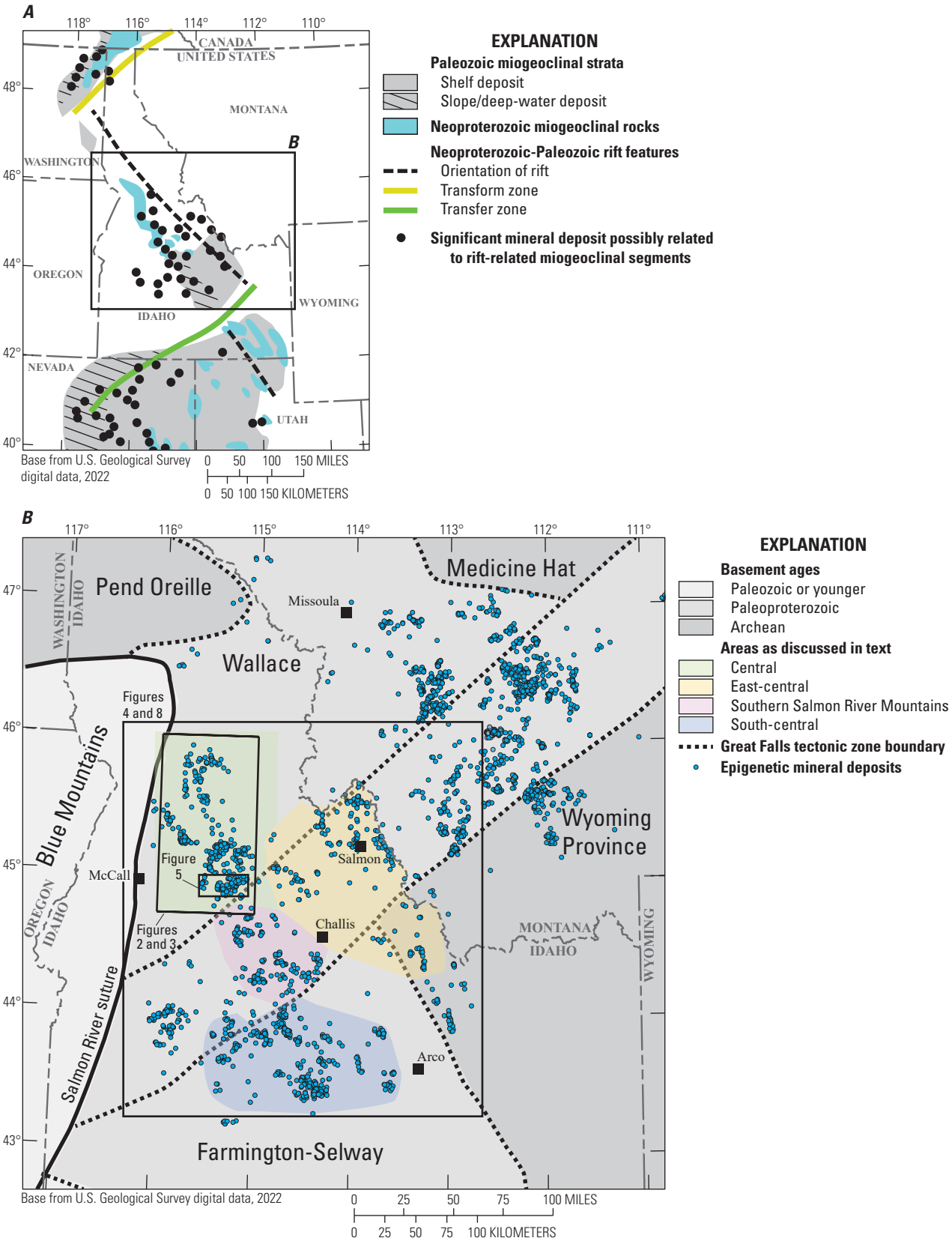

Figure 1. Index maps showing location of study area in northern Rocky Mountains. *A*, Map showing Neoproterozoic to early Paleozoic Laurentian rift features, location of miogeoclinal deposits, and related mineral deposits (Lund, 2008). *B*, Regional map showing cryptic basement domains from Lund and others (2015), distribution of epigenetic deposits from Klein and Sims (2007), and geographic areas discussed in text.

Table 1. Recorded metals production for lode and placer mining districts, central Idaho.

[--, not reported]

District name	Lode production							Placer production
	[a]Gold	[a]Silver	[b]Copper	[b]Lead	[b]Zinc	[b]Antimony	[b]Tungsten trioxide (WO_3)	[a]Gold
Northwestern districts								
Newsome[1]	1,236	298	--	--	--	--	--	97,000
Tenmile[1]	18,866	12,906	4,235	10,302	707	--	--	128,600
Orogrande[1]	20,827	11,698	2,871	20,941	--	--	present	32,000
Elk City[1]	27,646	11,315	750	847	400	--	--	--
Buffalo Hump[1]	33,534	33,579	11,118	49,253	--	--	--	--
Dixie[1]	2,408	1,534	927	2,483	--	--	--	40,000–75,000
Florence[1]	738	615	--	--	--	--	--	1,000,000
Marshall Lake and Resort[1]	21,102	13,204	13,204	10,302	707	present	present	225,600
Warren[1]	58,234	123,337	12,947	26,585	294	--	present	906,000
Southeastern districts								
Big Creek[2,4]	present	present	present	present	--	--	--	--
Ramey Ridge[2]	7,115	16,112	125,098	17,656	--	--	present	--
Edwardsburg[2,4]	1,568	351	present	--	--	--	present	3,500 estimated
Profile[2,4]	present	present	present	present	--	present	--	--
Yellow Pine[3]	549,778	1,687,914	--	--	--	75,618,556	17,306,110	--
Thunder Mountain[3]	117,993	153,681	--	--	--	--	--	--

[1]Lund and others, 1986; Lund and Esparza, 1990.

[2]Cater and others, 1973.

[3]Bookstrom and others, 1998.

[4]Big Creek had a total production of $265,379; Edwardsburg district had $97,485; Profile district had $7,993 (Cater and others, 1973).

[a]Troy ounces.

[b]Pounds.

1934). Later, Anderson (1951) argued the Cretaceous plutons of the Idaho batholith were barren intrusions that hosted mineral deposits only by means of magmatic recycling of metals from older sedimentary rocks or as host rocks through introduction of metals by Eocene magmatism. Thereafter, the interpretation of Eocene origins became most widely adopted (Bennett, 1980; Criss and Taylor, 1983; Fisher, 1985; Criss and others, 1991). Isotopic dating, undertaken to address the questions of origin, reveals that several central Idaho precious-polymetallic vein districts are temporally related to Late Cretaceous Idaho batholith two-mica granites (Lund and others, 1986; Gammons, 1988; Lund, 2004), whereas other Idaho vein districts are indeed related to Eocene magmatic and hydrothermal events (Leonard and Marvin, 1982; Fisher, 1985; Hardyman, 1985; Hardyman and Fisher, 1985; Kiilsgaard and Bennett, 1985). Dating of porphyry copper-molybdenum (Cu-Mo) deposits in the Idaho-Montana porphyry belt (Green, 1972; Rostad and others, 1978; Worthington, 2007) demonstrates that both Late Cretaceous and Eocene deposits are interspersed along the belt (Taylor and others, 2007). A corollary is that vast areas of central Idaho are underlain by Late Cretaceous plutons and Eocene igneous rocks that are texturally, compositionally, and temporally equivalent to those that host mineral deposits but that are barren. Thus, the distribution of mineral deposits bears little relation to the location of particular magmatic rocks, and there must be additional factors that were critical to mineral-deposit formation and the deposits' present location.

Several other geologic features are correlated with mineral deposit occurrences. Deposits of the Idaho-Montana porphyry belt overlie the cryptic Paleoproterozoic juvenile crust of the Great Falls tectonic zone (fig. 1*B*), and that basement character has been suggested as an influence on subsequent metallogeny (Sanford and Wooden, 1995; Klein and Sims, 2007; Lund and others, 2015). Additionally, several northwest-striking, linear arrays of diverse epigenetic deposits transect the underlying Great Falls tectonic zone and adjacent basement domains (Klein and Sims, 2007). These arrays parallel the zone where older basement was reworked during Neoproterozoic–Paleozoic rifting episodes, and the arrays also parallel the long axis of coeval miogeoclinal (rift-drift) sedimentary deposits, which are present along the length of this western Laurentian rift system (fig. 1*A*; Lund, 2008). Aspects of the prolonged rifting

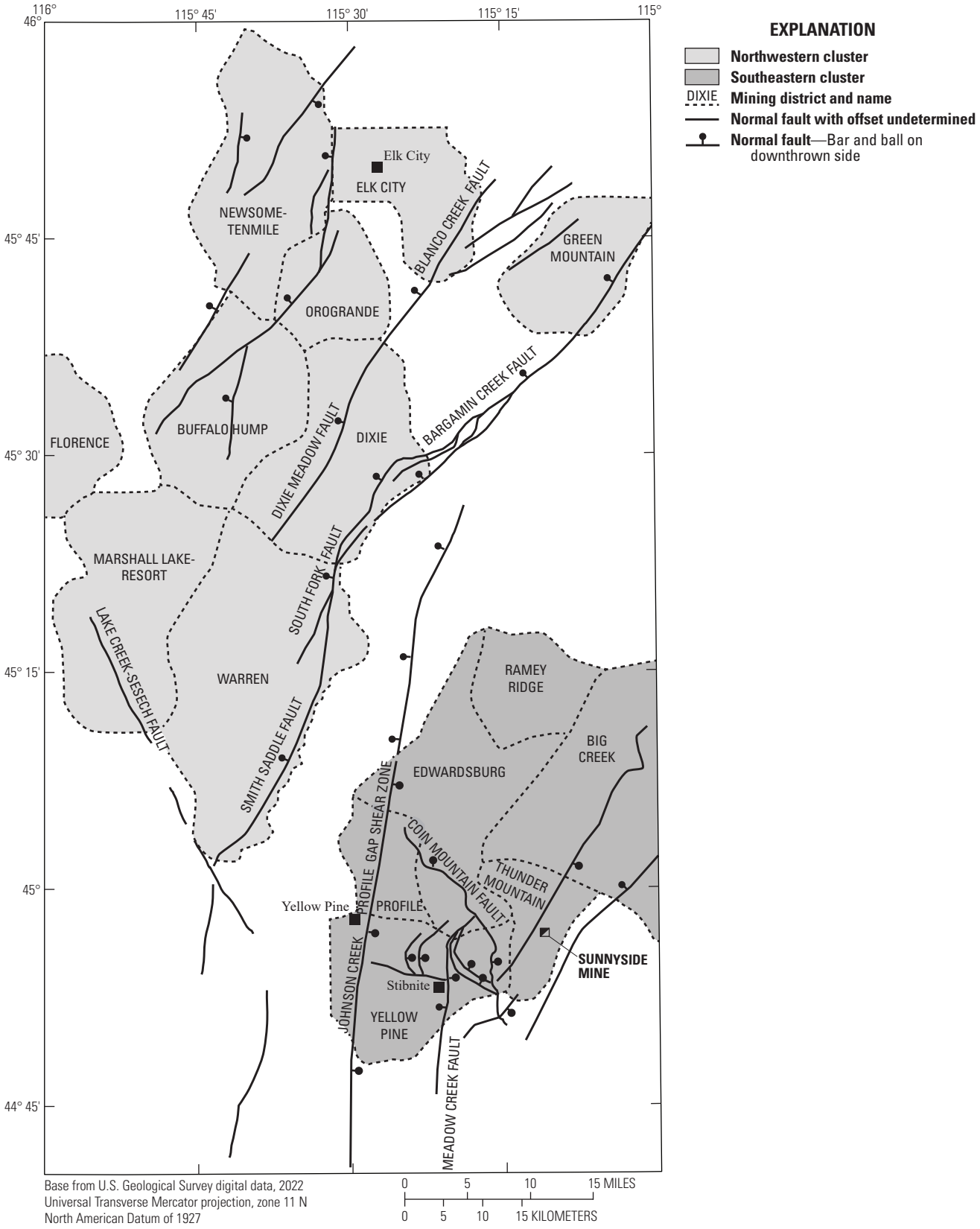

Figure 2. Mining districts (after Ross [1936] and Gustafson [1987]) and major faults of central Idaho. Light gray indicates those districts are referred to as northwestern cluster; dark gray indicates districts of southeastern cluster.

events, including sedimentary facies belts and synsedimentary down-to-the-basin extensional faults, are both linked with characteristic metal endowments (Turner and Otto, 1995; Lund, 2008; Lund and others, 2015).

Complex questions and conflicting ideas about ages, processes, and origins of central Idaho mineral deposits are illustrated by a modern descriptive mineral-resource assessment, encompassing many central Idaho mining districts, and illustrating the descriptive complexities. That study identifies 17 discrete epigenetic deposit types, many co-located as part of a single deposit and many described in context of the proposed mineral belts that crisscross the province (Bookstrom and others, 1998), as described above. A recent study centered on deposits at Stibnite provides significant details for those deposits and integrates those detail with previous district and regional information (Dail and Zinsser, 2020). Modern mapping and geochronology presented in the present study help clarify framework elements for the mineral deposits in this complex metallogenic province.

Characteristics of Central Idaho Mining Districts

Fifteen mining districts were organized historically across much of central Idaho as shown on figure 2. Most of the placer districts were discovered in the early 1860s (Idaho State Historical Society, 1985). Much-publicized gold rushes were initially associated with successive discoveries of gold placer deposits in the different districts. Discovery of lode deposits lagged in the various mining districts, but most activities related to lode mining commenced from the late 1890s to about 1915 (Idaho State Historical Society, 1985). Because lode mining and production was more difficult in this era, associated lode-gold rushes were smaller and generally occurred several decades after initial gold rushes. Production details for the districts are in table 1.

The mining districts group into northwestern and southeastern clusters which are distributed across a regional-scale zone of normal faults (fig. 2). The geologic setting of each district is complex, and the variety of metal commodities in different districts is extensive. To ascertain possible patterns among districts across the province, the geologic and mineral-deposit characteristics and settings for each district are tabulated in table 2 and described following.

Northwestern Mining Districts

Seven mining districts extend about 70 km northeast by 20 km east-west in a northwestern cluster of districts. They lie northwest of a series of normal faults (fig. 2). In the north, epigenetic deposits of the Elk City, Dixie, Buffalo Hump, and Orogrande districts are large quartz veins, wherein quartz has banded, massive, and open space textures. The veins are in persistent, north-northeast-striking fractures within the upper levels of Late Cretaceous (74 Ma, $^{40}Ar/^{39}Ar$ age determination from muscovite) muscovite-biotite granite and in overlying Mesoproterozoic roof pendants (figs. 2, 3; Lund and others, 1986). The precious-metal-rich, polymetallic-bearing assemblages for these districts (Thompson and Ballard, 1924; Beckwith, 1928; Shenon and Reed, 1934; Chauvot, 1986; Lund and others, 1986; Lund and Esparza, 1990) are relatively copper and base-metal rich for the province (tables 1, 2). Similarly, regional geochemical data exhibits anomalous cobalt-copper-gold associations for the area near these districts (Alminas, 1990). Veins of the Buffalo Hump district formed 72–71 Ma ($^{40}Ar/^{39}Ar$ age determinations from white mica, Chauvot, 1986; Lund and others, 1986), were genetically related to the muscovite-biotite granite host rock and were emplaced at about 4 km depth based on cooling data (Lund and others, 1986). A single Eocene stock along a several-kilometer long silicified fault zone in the Orogrande district (figs. 2, 3) hosts a relatively gold-rich deposit that notably contains tungsten (table 2; Thompson and Ballard, 1924; Shenon and Reed, 1934).

Quartz-vein deposits in the Marshall Lake-Resort and Warren districts are gold-silver-rich, polymetallic bearing, and some contain scheelite (Reed, 1937; Lorain, 1938; May, 1984; Bookstrom and others, 1998; Mitchell, 2000). Quartz in veins has banded, massive, and open space textures and veins are undeformed. Most veins in the Marshall Lake-Resort district are hosted by fractures in roof-pendant country rocks consisting of Mesoproterozoic, Neoproterozoic, and probably some undated Paleozoic units; other veins in this district are at the top of Late Cretaceous granodiorite and granite. Veins of the Warren district are in biotite granodiorite several hundred meters below the base level of nearby roof pendant exposures from the nearby Neoproterozoic or late Mesoproterozoic roof pendants. Granodiorite in the Warren and Marshall Lake-Resort districts is dated at 82.4 Ma (U-Pb age from zircon, this study), and quartz veins in the Marshall Lake-Resort district are dated at 74.5 Ma ($^{40}Ar/^{39}Ar$ age determinations from white mica, Lund, 2004). Regional geochemical data show a gold-antimony-tungsten association for these districts (Alminas, 1990; Watts and King, 1999).

Significant gold placers of several ages and settings also characterize northwestern districts (tables 1, 2). Most of the placer districts are in Eocene–Miocene, fault-bounded, extensional basins (Capps, 1939, 1940; Reid, 1960). Some gold placers are in tilted Miocene(?) sediments indicating post-Eocene faulting. Most of the gold placers are in Pleistocene glacial-related deposits and in younger, active stream deposits (Shenon and Reed, 1934; Reed, 1937, 1939; Lorain and Metzger, 1938; Capps, 1939, 1940). Placers in the Warren and Marshall Lake-Resort districts (Marshall Lakes and Resorts districts are combined in this report because the production records were combined in some published accounts) bear significant monazite-bearing black sand deposits as well (Reed, 1937; Savage, 1961).

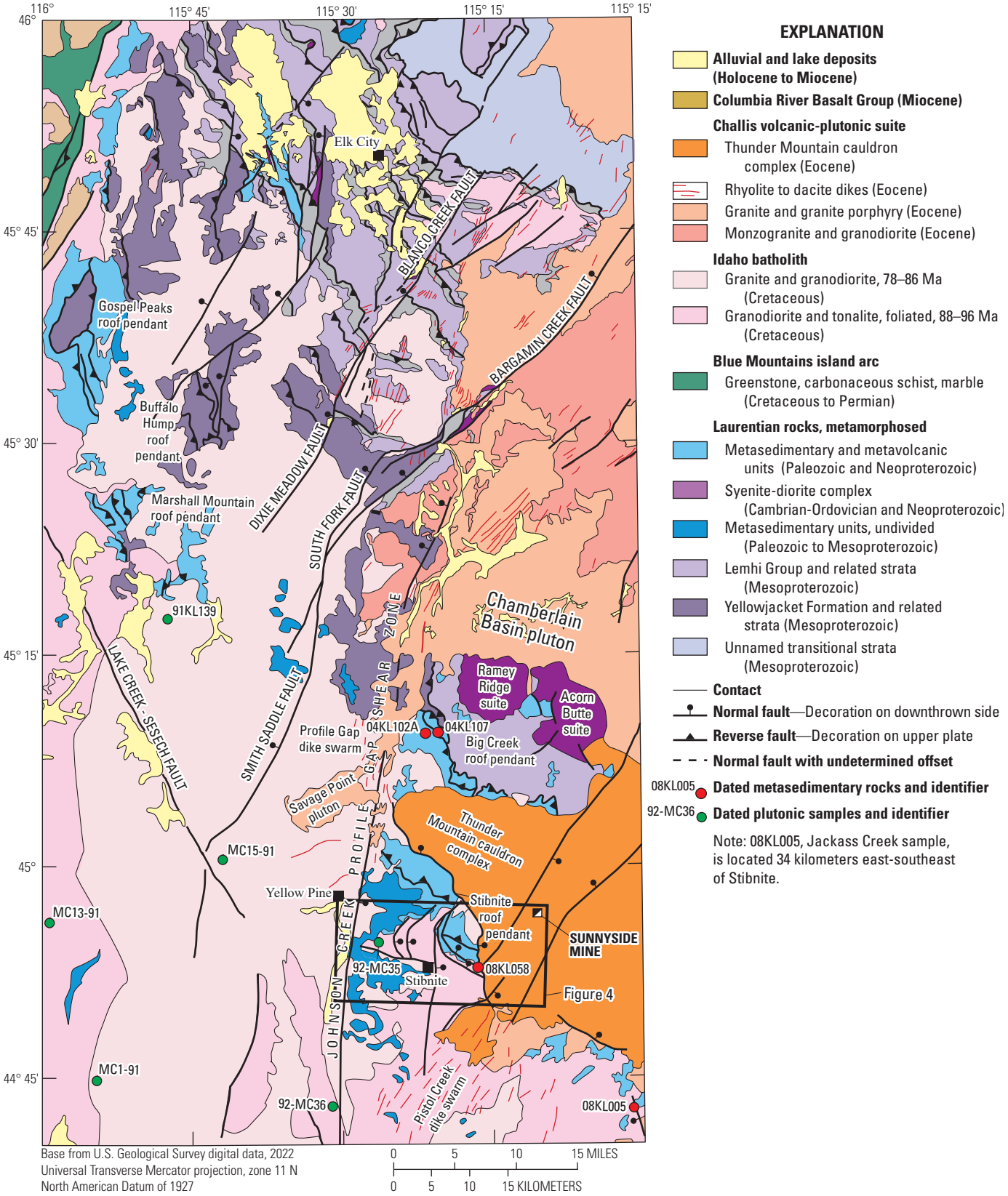

Figure 3. Generalized geologic map of central Idaho. Southern half modified from Lund (2004) and northern half compiled from new mapping, present study. Age data for metasedimentary rocks are in table 3 and plutonic samples are in table 4. (Ma, million years)

Table 2. Characteristics of mineral deposits for mining districts, central Idaho.

[m, meters; Ma, millions of years; Ar, argon; km, kilometers; U-Pb, uranium-lead; SHRIMP, sensitive high resolution ion microprobe; cm, centimeters; Re-Os, rhenium-osmium; --, not applicable]

District name	Metasedimentary host associations	Late Cretaceous plutonic host associations	Relation to Eocene igneous rocks	Deposit characteristics	Ore minerals (see table 1 for commodities and production)	Age(s) of mineralization	Sources of data
Northwestern mining districts							
Newsome and Tenmile	Mesoproterozoic, fine-grained, biotite-feldspar-quartz gneiss of Lemhi Group and local younger carbonate and quartzite gneiss	Minor Late Cretaceous granite and migmatite	--	Quartz veinlets and veins in silicified, faulted wall rock. Post-vein brecciation, gouge, and offsets of veins	Pyrite, chalcopyrite, arsenopyrite, galena, covellite, chalcocite, native gold, gold telluride	undetermined	Thompson and Ballard, 1924; Shenon and Reed, 1934; Reid, 1960
				Placers in Miocene–Holocene fault graben, as basin fill as much as 100 m above river level and active stream channels. As much as 25 m thick. Some eluvial placers	Gold	undetermined	Shenon and Reed, 1934; Capps, 1941
Orogrande	Mesoproterozoic, fine-grained, biotite-feldspar-quartz gneiss of Lemhi Group, Mesoproterozoic augen gneiss, and Mesoproterozoic feldspar-quartz metasandstone and sillimanite-biotite schist	Minor Late Cretaceous granite and granodiorite	Few post-ore andesite, porphyritic dacite dikes	Pinch and swell quartz veins (as much as 2 m wide) and disseminations in silicified country rock in shear zones. Some late-stage brecciation	Pyrite, chalcopyrite, galena, tetrahedrite, sphalerite, native gold, late-stage covellite	undetermined	Thompson and Ballard, 1924; Shenon and Reed, 1934; present study
			Eocene granite porphyry stock in north-striking Late Cretaceous shear zone	Ore minerals as disseminations and quartz stringers in Eocene granite porphyry	Pyrite, chalcopyrite, galena, molybdenite, tetradymite, free gold, gold telluride, wolframite, scheelite	Eocene	Thompson and Ballard, 1924; Shenon and Reed, 1934; Lund and Esparza, 1990; present study
			--	Placers in Miocene-Holocene fault graben occupied by active stream channel	Gold	Miocene to Holocene	Shenon and Reed, 1934; present study
Elk City	Mesoproterozoic, fine-grained, biotite-feldspar-quartz gneiss of Lemhi Group and Mesoproterozoic augen gneiss	Minor Late Cretaceous granite and migmatite	Small post-vein porphyritic andesite dikes noted along faults in several mines	Quartz veins and lenses in fracture zones. As much as 6 m wide and 100 m long. Subsequent fault offsets, parallel gouge, and brecciation	Pyrite, sphalerite, chalcopyrite, galena, native gold	undetermined	Shenon and Reed, 1934; present study
				Placers in Miocene–Holocene clay, sand, gravel, cobble deposits (as much as 35 m thick) located in fault graben and active stream channels	Gold	undetermined	Reed, 1934; Shenon and Reed, 1934; Capps, 1941; Reid, 1959, 1960; present study
Buffalo Hump	Mesoproterozoic calc-silicate gneiss of the Yellowjacket-Hoodoo package structurally over feldspar-quartz gneiss of Lemhi Group	Late Cretaceous 84 Ma tonalite (40Ar/39Ar on hornblende), granodiorite, and 74 Ma muscovite-biotite granite (40Ar/39Ar on muscovite)	--	North- to north-northeast-striking, comb and vuggy textured, multi-phase quartz veins, as much as 4 m wide, some for more than 0.5 km long, in fractures. Some shorter quartz offshoots	Pyrite, sphalerite, chalcopyrite, and tetrahedrite, galena, arsenopyrite, molybdenite, native gold, telluride, argentite, stibnite, covellite	71–72 Ma (40Ar/39Ar on white mica)	Thompson and Ballard, 1924; Beckwith, 1928; Shenon and Reed, 1934; Chauvot, 1986; Lund and others, 1986; Lund and Esparza, 1990; present study
Dixie	Mesoproterozoic, fine-grained, biotite-feldspar-quartz gneiss of Lemhi Group and Mesoproterozoic augen gneiss	Late Cretaceous muscovite-biotite granodiorite and granite	Few porphyritic rhyodacite dikes in district	Quartz veinlets localized, few large veins. Placer deposits in glacial outwash and modern stream channels. Central to a Miocene(?) graben structure	Pyrite, galena, sphalerite, chalcopyrite, native gold	undetermined	Capps, 1939, 1941; present study
Florence		Late Cretaceous tonalite and granodiorite	--	Quartz veinlets, short quartz veins, and silicified country rock	Native gold, telluride, cerargyrite, silver sulfides	undetermined	Reed, 1939; Capps, 1941
				Placers in older graben-fill lignite-peat, clay, sand, gravel, and cobble deposits, eluvial settings, modern stream channels	Gold, uranium	undetermined	

Table 2. Characteristics of mineral deposits for mining districts, central Idaho.—Continued

[m, meters; Ma, millions of years; Ar, argon; km, kilometers; U-Pb, uranium-lead; SHRIMP, sensitive high resolution ion microprobe; cm, centimeters; Re-Os, rhenium-osmium; --, not applicable]

District name	Metasedimentary host associations	Late Cretaceous plutonic host associations	Relation to Eocene igneous rocks	Deposit characteristics	Ore minerals (see table 1 for commodities and production)	Age(s) of mineralization	Sources of data
Northwestern mining districts—Continued							
Marshall Lake and Resort	Neoproterozoic metavolcanic rocks and probably younger quartzite, marble, andalusite-biotite schist. Mesoproterozoic biotite-feldspar quartz gneiss	Late Cretaceous muscovite-biotite granodiorite and granite	--	West-northwest striking, pinch and swell, quartz veins, as wide as 1.2 m	Gold, cerargyrite, galena, sphalerite, tetrahedrite, magnetite, scheelite	74.5 Ma (40Ar/39Ar on white mica)	Lorain, 1938; Capps, 1940, 1941; Savage, 1961; May, 1984; Lund and Esparza, 1990; Lund, 2004
				Pleistocene-Holocene glacial moraines and outwash reworked by modern streams. Deposits overlie tilted Miocene basin-fill in northwest-striking fault graben	Gold, corundum, monazite-bearing black sands, garnet, cinnabar, rutile, zircon, magnetite, illmenite	undetermined	
Warren	Neoproterozoic quartzite, feldspar-quartz metasandstone, sillimanite-biotite schist roof rocks above plutonic rocks at district margins; eroded over district	Late Cretaceous porphyritic muscovite-biotite granodiorite 82.4 Ma (U-Pb SHRIMP, this study)	--	East-striking, lenticular quartz veins, generally 30–60 cm wide, persisting for as much as 1 km in length. Located several hundred meters below projected base of Neoproterozoic roof rocks. In fractures that were reactivated after vein formation	Pyrite, sphalerite, tetrahedrite, arsenopyrite, stibnite, pyrargyrite, native gold, argentite, native silver, mottramite, scheelite, mimetite	undetermined	Reed, 1937; Lorain, 1938; Lorain and Metzger, 1938; Capps, 1941; Lund and Esparza, 1990; Lund, 2004; present study
				Placer deposits in successive Pleistocene-Holocene glacial moraines, interglacial outwash, modern stream channels. Overlying tilted Miocene basin fill	Gold, monazite-bearing black sands, zircon, garnet	undetermined	
Southeastern mining districts							
Big Creek and Ramey Ridge	Mesoproterozoic Lemhi Group locally overlain by Yellowjacket-Hoodoo package klippen Neoproterozoic syenite-diorite complex	--	Eocene volcanic rocks depositional on top; potentially underlain by Eocene granite. Eocene porphyritic dikes cut veins	East- or north-northeast-striking, lenticular quartz veins, as much a 1 m wide, in shear zones	Pyrite, chalcopyrite, chalcocite, galena, and magnetite; geochemical anomalies are gold, silver, copper, iron, and cobalt	undetermined	Shenon and Ross, 1936; Cater and others, 1973; Lund, 2004; Lund and others, 2010
				Northwest-striking, lenticular quartz veins in shear zone, persistent for more than 650 m	Pyrite, chalcopyrite, pyrrhotite, galena, local stibnite late in vein formation	79–65 Ma (40Ar/39Ar on white mica)	
Edwardsburg	Mesoproterozoic Lemhi Group structurally overlain by Yellowjacket-Hoodoo package Neoproterozoic and Paleozoic quartzite, marble, and sillimanite-biotite schist	Silicified, sericitized, sheared Late Cretaceous muscovite-biotite granodiorite and granite	Eocene granite porphyry intruded and underlies; Eocene porphyritic rhyolite and rhyodacite dikes parallel to and cutting veins	North-northeast-striking quartz veins in shear zones; at eastern margin of Johnson Creek-Profile Gap shear zone	Pyrite, chalcopyrite, sphalerite, galena, tetrahedrite, gold	undetermined	Shenon and Ross, 1936; Cater and others, 1973; Lund, 2004
				North-northeast-striking quartz veins and silicified disseminations in sheared and altered Late Cretaceous granitic rocks and metasedimentary screens. Early phases plastically deformed quartz, later phases associated with tensional openings and brecciation. Located along Johnson Creek-Profile Gap shear zone	Pyrite, arsenopyrite, stibnite, huebnerite, sphalerite, chalcopyrite, galena, tetrahedrite, pyrrhotite, telluride, scheelite, cinnabar, boulangerite, covellite	Early phases 79–73 Ma; younger phases 69–67 Ma; late phase and Ar loss 52–47 Ma (40Ar/39Ar)	Shenon and Ross, 1936; Gammons and others, 1985; Gammons, 1988; Lund, 2004
Profile	Neoproterozoic and Paleozoic quartzite, marble, and sillimanite-biotite schist; at south, Neoproterozoic–Mesoproterozoic feldspar-quartz metasandstone	Silicified, sericitized, sheared Late Cretaceous muscovite-biotite granodiorite and granite	Eocene porphyritic rhyolite and rhyodacite dikes parallel to and cutting veins in northern district; sparse andesite dikes in southern district	North-northeast-striking quartz veins and silicified stockwork, disseminations in sheared and altered granitic rocks and metasedimentary screens. Early tabular quartz veins, plastically deformed; later calcite filling in tensional openings and breccia. Located within Johnson Creek-Profile Gap shear zone	Pyrite, arsenopyrite, pyrrhotite, sphalerite, molybdenite, gold; late scheelite	undetermined	Shenon and Ross, 1936; Peterson, 1984; Gammons, 1988; Lund, 2004

Table 2. Characteristics of mineral deposits for mining districts, central Idaho.—Continued

[m, meters; Ma, millions of years; Ar, argon; km, kilometers; U-Pb, uranium-lead; SHRIMP, sensitive high resolution ion microprobe; cm, centimeters; Re-Os, rhenium-osmium; --, not applicable]

District name	Metasedimentary host associations	Late Cretaceous plutonic host associations	Relation to Eocene igneous rocks	Deposit characteristics	Ore minerals (see table 1 for commodities and production)	Age(s) of mineralization	Sources of data
Southeastern mining districts—Continued							
Yellow Pine	Neoproterozoic and Paleozoic quartzite, marble, and sillimanite-biotite schist in central and east Neoproterozoic–Mesoproterozic feldspar-quartz metasandstone and minor calc-silicate marble of unknown age in west	Silicified, sericitized, sheared Late Cretaceous tonalite and granodiorite	Few fine-grained andesite to rhyodacite dikes, some altered	West: early tabular quartz veins, plastically deformed; late quartz and calcite filling in tensional openings and breccia; within Johnson Creek-Profile Gap shear zone	West: early pyrite, arsenopyrite, pyrrhotite, molybdenite, sphalerite, gold; intermediate age scheelite	undetermined	Larsen and Livingston, 1921; Schrader and Ross, 1926; Shenon and Ross, 1936; White, 1940; Cooper, 1951; Lasmanis, 1981; Lewis, 1984; Peterson, 1984; Cookro, 1985; Cookro and others, 1988; Gammons, 1988; Bookstrom and others, 1998; Lund, 2004; table 4-3 of Gillerman and others, 2019
				Central (Stibnite area): quartz veins and silicified stockwork on north-striking fault segment in sheared and altered granitic rocks primarily precious-polymetallic deposits. Veins, disseminations, and replacements in sheared and altered granitic rocks and metasedimentary screens along fault conjugates and splays are gold rich. Intermediate age stockwork and disseminated antimony in hanging wall damage zone. Late-stage, breccia-related quartz-scheelite veins central to main structural pathways in hanging wall damage zone. Within damage zone of Meadow Creek fault and at junction of Meadow Creek and Sugar Creek faults, including along main fault, splay faults, and conjugate faults	Central (Stibnite area): early pyrite, arsenopyrite, pyrrhotite, molybdenite, sphalerite, gold; intermediate age stibnite, scheelite; late stibnite, scheelite, cinnabar, silver sulfosalts	Early phases at 86 Ma (Re-Os), main veins at 77.9 Ma, tungsten and antimony at about 57 and 51–47 Ma (40Ar/39Ar, U-Pb)	
				East: primarily stratabound parallel to strike of marble units near contacts with quartzite, few in north-northeast-striking gouge zones. In silicified zones, jasperoids, chalcedonic fumeroles; interpreted as shallow, epithermal systems. Within Stibnite roof pendant across 3 km in hanging wall of Meadow Creek fault, footwall of Thunder Mountain cauldron complex boundary fault	East: cinnabar with limited pyrite, realgar, orpiment, scheelite, stibnite	undetermined	
Thunder Mountain	Neoproterozoic and Paleozoic quartzite, marble, and sillimanite-biotite schist roof pendants underlie Thunder Mountain cauldron complex	Late Cretaceous granodiorite underlies Thunder Mountain cauldron complex	Eocene rhyolite welded and ash-flow tuffs 46.7 Ma and lacustrine beds with lignite and plant debris in north-northeast-striking caldera-collapse graben	Hot-spring-related, disseminated; in shallow, porosity- and composition-controlled layers and structures. Limited to units in young units within caldera-collapse graben. Graben-related, steeply dipping, silicified and argillized fault zones served as conduits for mineralizing fluid into permeable non-welded tuff layers and volcaniclastic debris-flow rocks	Native gold, electrum, pyrite	43 Ma (40Ar/39Ar)	Umpleby and Livingston, 1920; Ross, 1933; Cater and others, 1973; Shannon and Reynolds, 1975; Adams, 1985; Parsley, 1997; D. John, U.S. Geological Survey, oral commun.

Southeastern Mining Districts

Six mining districts extend about 40 km northeast by 35 km east-west in a southeastern cluster of mining districts. The districts lie along and southeast of a southern set of large normal faults (fig. 2). At the northern margins of this southeastern district cluster, epigenetic deposits of the Ramey Ridge and Big Creek districts (figs. 2, 3; table 2) are structurally controlled quartz veins (Cater and others, 1973) in metamorphosed Mesoproterozoic Lemhi Group (Lund, 2004) and Neoproterozoic syenite-diorite suites (Lund and others, 2010). Deposits hosted in these Mesoproterozoic metasedimentary rocks are the most copper-rich in the region. These deposits also bear gold and silver as well as local cobalt (table 1). Deposits hosted in the syenite-diorite complex rocks are precious-metal rich and include the single stibnite occurrence in the district (Cater and others, 1973). Ages for these deposits range from 79 to 65 Ma, but it is unclear if these are ages for mineralizing events or for regional cooling (Lund, 2004). A few generally fresh, unaltered Eocene dikes cut the vein deposits, indicating that mineralizing events occurred prior to the Eocene (Shenon and Ross, 1936; Cater and others, 1973).

The Edwardsburg and Profile districts extend north-south for about 30 km along the Johnson Creek-Profile Gap shear zone and are bounded on the east by the Coin Mountain fault (figs. 2, 3; tables 1, 2). Deposits in these districts are hosted by Late Cretaceous granite-granodiorite as well as by Neoproterozoic and Paleozoic metasedimentary rocks. In the Edwardsburg and Profile districts, the metasedimentary rocks are present as screens and elongated blocks along the fault zones and, at the southeastern corner of the Edwardsburg district, they form the northern Stibnite roof pendant (fig. 3; Lund, 2004). The deposits are gold-rich and silver-polymetallic bearing quartz vein, skarn, stockwork, and disseminations within sheared, silicified, and altered host rocks (Shenon and Ross, 1936; Peterson, 1984; Gammons, 1988; Lund, 2004). Quartz in the veins and in silicified wall rock commonly exhibits plastic deformation characteristics (Peterson, 1984; Gammons, 1988; Lund, 2004). These veins lie along the fabrics in the Johnson Creek-Profile Gap shear zone, and some mineralized veins and zones are localized in minor discrete mineralized faults and shears (Peterson, 1984; Gammons, 1988) within the larger shear zone. Most of the early deposits were overprinted by breccia-fill tungsten and (or) antimony deposits (Shenon and Ross, 1936; Peterson, 1984; Gammons, 1988; Bookstrom and others, 1998). For tungsten, huebnerite is a constituent of some precious-polymetallic quartz veins within or adjacent to roof pendants, but scheelite is the constituent mineral in the overprinting breccia-type deposits (Peterson, 1984; Gammons, 1988; Bookstrom and others, 1998). Eocene dikes and elongated stocks intruded the sheared and mineralized rocks, and these intrusions are generally fresh and only locally fractured (Shenon and Ross, 1936; Peterson, 1984; Gammons, 1988; Bookstrom and others, 1998; Lund, 2004). Limited dating indicates that early mineralizing phases are about 79–73 Ma, closely following emplacement of the Late Cretaceous granite bodies. Younger mineralization phases produced ages dating from 69 to 57 Ma, associated with brittle deformation and changes in regional tectonics but not with magmatic activity. Locally, ages as young as 52–47 Ma, coeval with shallow emplacement of Eocene dikes, are also found ($^{40}Ar/^{39}Ar$ age determinations from white mica, Gammons, 1988). Fluid-inclusion data document significant decrease in pressures at times of formation from initial mineralization settings with ductile signatures to later breccia-related settings (pressures 1.6–1.3 kilobars [kb] in early phases to 0.15–0.45 kb in brittle phases; temperatures of formation are in the 250–300 °C range; Gammons and others, 1985; Gammons, 1988). Regional geochemical data demonstrate gold-antimony-tungsten associations for these districts (Alminas, 1990; Watts and King, 1999).

The Yellow Pine district, at the southern extent of the southeastern mining district cluster, is composed of three distinct geologic settings containing deposits of different characteristics, described from west to east. Deposits of the western Yellow Pine district are hosted along the Johnson Creek-Profile Gap shear zone. Country rocks are Late Cretaceous biotite granodiorite deformed together with screens of feldspathic metasandstone and minor carbonate and biotite schist of a late Mesoproterozoic to early Neoproterozoic package (fig. 3; Lund, 2004). Early deposits are shear-zone parallel, mesothermal gold-rich silver-polymetallic accumulations in quartz veinlets and disseminated in country rock, wherein quartz exhibits plastic deformation fabrics (Peterson, 1984). Those early deposits were overprinted by a range in brittle deformation from mildly brecciated rocks (broken but not rotated) to intensely brecciated rock (rotated clasts in a matrix of crushed country rocks). Deposits with this structural style host scheelite and stibnite in the breccia matrices as well as in lesser replacement of fragments. The breccia textures and associated mineralization are part of a younger, synextensional mineralization event, indicative of shallow, epithermal mineralizing processes (Cookro, 1985; Cookro and others, 1988; Gammons, 1988; Bookstrom and others, 1998). The regional geochemical signature of the western Yellow Pine district is characterized by a gold-antimony-tungsten association (Alminas, 1990; Watts and King, 1999).

The central Yellow Pine deposits (Stibnite mining area) have been mined and extensively explored most recently, so data for these deposits are more complete. Deposits are located along the throughgoing Meadow Creek fault and along several (mostly) northeast-striking spur faults on both sides of the main fault (fig. 3). Country rocks west of and along the Meadow Creek fault zone are foliated Late Cretaceous granodiorite, whereas predominant rocks east of the fault are Neoproterozoic–Paleozoic metasedimentary rocks of the Stibnite roof pendant. Early deposits are gold-silver, base-metal bearing quartz veins and veinlets that formed between 86 Ma (rhenium-osmium [Re-Os] age determinations from molybdenum, Konyshev and Muntean, 2016) and 78 Ma ($^{40}Ar/^{39}Ar$ age determinations from white mica, Gammons, 1988) that were plastically deformed with foliated, silicified, and sericitized host granodiorite primarily along the Meadow Creek fault and its western spurs faults and are also hosted in alternating quartz-rich and carbonate-rich

metasedimentary units and structures at the western edge of the Stibnite roof pendant (Gammons, 1988; Konyshev and Muntean, 2016). Disseminated gold as well as disseminated and breccia-hosted stockwork quartz-scheelite deposits overprinted early deposits at about 65–57 Ma ($^{40}Ar/^{39}Ar$ age determinations from white mica and K-feldspar, Gammons, 1988; Gillerman and others, 2019), an age range unrelated to a magmatic event. These intermediate-age deposits are found in both granodiorite and metasedimentary rocks in the broad fault-damaged zone at the north end of the Meadow Creek fault (Yellow Pine pit area) and where fault splays intersected metasedimentary rocks in the western part of the Stibnite roof pendant (Cookro and others, 1988; Gammons, 1988; Bookstrom and others, 1998; Konyshev and Muntean, 2016; Gillerman and others, 2019). Gold-rich, epithermal, chalcedonic quartz veins overprinted both older vein types and are dated at 51–47 Ma, and scheelite is dated directly at about 45 Ma (Cookro and others, 1988; Bookstrom and others, 1998; U-Pb age determinations on scheelite, Gillerman and others, 2019); thus, this late event is coeval with Eocene magmatic activity. Both types of antimony deposits were cut by minor Eocene dikes. Fluid-inclusion data indicate pressures of formation decreased significantly between each of the mineralization phases (Gammons, 1988), with estimates of depth starting at about 5 km depth and culminating at near-surface depths (Marsh, E., and Bennett, M., 2021, U.S. Geological Survey oral commun.). Gold-antimony-tungsten geochemical associations are characteristic for this part of the district (Alminas, 1990; Watts and King, 1999).

The eastern Yellow Pine district contains gold and mercury deposits in an about 3-km wide zone hosted by Neoproterozoic to Paleozoic marble units of the Stibnite roof pendant, which overlies Cretaceous granitic rocks. Most ore zones are parallel to the strike of the marble lithologies, near the contacts between marble and quartzite, and some are in northeast-striking cross fractures (Larsen and Livingston, 1921; Schrader and Ross, 1926; Cookro and others, 1988; Bookstrom and others, 1998). Ores are in jasperoid zones and as disseminations that formed at near-surface conditions and interpreted as Eocene hot spring and chalcedonic fumarole deposits during the youngest hydrothermal activities (Larsen and Livingston, 1921; Cookro and others, 1988; Konyshev and Muntean, 2016; Gillerman and others, 2019).

Thunder Mountain deposits (near Sunnyside on figs. 2, 3) are in late-stage Eocene volcanic units preserved in a caldera collapse graben (Leonard and Marvin, 1982; Hardyman and Fisher, 1985; southern Big Creek graben, Stewart and others, 2013). These deposits from 43 Ma are hot-spring-related, disseminated gold and silver ore deposits (potassium-argon [K-Ar] dating of late-stage adularia, Adams, 1985). They are hosted in non-welded rhyolite and ash-flow tuff and in fault-juxtaposed volcaniclastic deposits (Umpleby and Livingston, 1920; Ross, 1933; Shannon and Reynolds, 1975; Adams, 1985; Parsley, 1997). Mineralizing fluids moved laterally along graben-related faults into permeable and carbon-rich layers (Shannon and Reynolds, 1975; Adams, 1985; Parsley, 1997; Bookstrom and others, 1998). The setting is similar to gold deposits of the Eocene Custer graben (30 km southeast, McIntyre and Johnson, 1985).

Metasedimentary Country-Rock Characteristics

Although epigenetic deposits in the central Idaho mineral province are of both Cretaceous and Eocene ages and associated with hosting or adjacent igneous rocks (table 2), vast expanses of identical igneous rocks in the province are not associated with mineral deposits. Geochemical signatures and different metal assemblages in different districts suggest metal endowments patterns in the mineral province that are not explained by magmatic characteristics. The inconsistent relations of igneous rocks to deposits suggest that pre-magmatic country rocks need to be considered as influencing factors in the location of deposits in the metallogenic province.

Although country rocks across the province were shown as Mesoproterozoic in two generations of state geologic maps (Ross and Forrester, 1947; Bond, 1978) and in most descriptions of mining districts, additional geologic mapping and the ability to date some units demonstrated that younger stratigraphic packages underlie large parts of the area (Lund, 1984; Lund and Esparza, 1990; Lund and others, 2003; Lund, 2004), and this change is represented on the recent state map (Lewis and others, 2012). Modern data for central Idaho country-rock packages—including their compositions, ages, provenances, facies trends, and metal endowments—help identify their basin settings and facies origins and test their potential influences on metal endowments and, consequently, on the location of mineral belts.

Mesoproterozoic Facies

The roof pendants in the many northern districts of the northwestern cluster plus the Ramey Ridge and Big Creek districts of the southern cluster are composed of fine-grained arkosic siltite and metasandstone, or gneissic equivalents of these rock types. Map units are thousands of meters thick. Based on the stratigraphic character of very thick, relatively fine-grained biotite-feldspar-quartz gneisses composing most country rocks in the northern part of the northwestern district cluster, these rocks are along-strike, western equivalents to upper parts of the Lemhi Group (fig. 3). Preserved sedimentary features in lower-metamorphic grade strata of the Big Creek district indicate large exposures of Mesoproterozoic Apple Creek and Gunsight Formations from the middle and upper parts of the Lemhi Group (Lund, 2004). A central band of rocks in the northern cluster and in the northern tip of the southeastern cluster are associated with thick calc-silicate gneiss and marble, biotite gneiss, and quartzite units that are western extensions of the Yellowjacket-Hoodoo association (fig. 3). Thus, although exposures are discontinuous because of intervening intrusions and off-setting structures, recent geologic mapping, stratigraphic studies (Lund, 2004; Lund and Tysdal, 2007; this study), and limited detrital zircon populations (Lund and others, 2008; Lewis and others, 2010, compare to Link and others, 2007; and

xenocrystic zircon ages, Gaschnig and others, 2013) outline northwest-striking belts of Mesoproterozoic Lemhi Group and Yellowjacket-Hoodoo strata across central Idaho (fig. 4).

The presence of parallel Lemhi Group and Yellowjacket-Hoodoo stratigraphic belts is strengthened by the combination of regional cobalt-copper geochemical associations (Alminas, 1990) and gold-copper-polymetallic deposits along the belt and that this facies belt includes the Blackbird gold-cobalt-copper and related deposits of east-central Idaho (Klein and Sims, 2007; Lund and Tysdal, 2007; although not all deposits bear cobalt, Johnson and others, 1998). Based on Pb-isotopic data, the source of metals for the Blackbird cobalt-copper deposits was the Apple Creek Formation (Panneerselvam and others, 2012). However, as presently constituted, deposits in this facies belt are epigenetic, associated with Late Cretaceous thrust stacking of these facies, heat from crustal thickening, and from the circulation of resultant regional-metamorphic and magmatic fluids (Lund and others, 2011).

Neoproterozoic and Paleozoic Facies

In the Yellow Pine district of the southeastern cluster (fig. 2), some metasedimentary rocks were originally interpreted to be Paleozoic based on their lithologic and thickness characteristics (Larsen and Livingston, 1921; Schrader and Ross, 1926; Shenon and Ross, 1936; White, 1945; Smitherman, 1988) as discussed in one regional interpretation (Ross, 1934), but these same rocks are shown as Mesoproterozoic Yellowjacket-Hoodoo Formations on both local (Leonard, 1962) and regional maps (Fisher and others, 1992). In the western part of the northwestern cluster of districts, metamorphosed strata, which have similar characteristics to many in the southern cluster, were also correlated to Mesoproterozoic Yellowjacket-Hoodoo Formations (Knowles and Bennett, 1978) but were reinterpreted as Neoproterozoic and early Paleozoic (Lund and Esparza, 1990). The first two state geologic maps showed central Idaho metamorphosed strata first as Mesoproterozoic Belt Supergroup formations (Ross and Forrester, 1947) and later as Mesoproterozoic Yellowjacket-Hoodoo Formations (Bond, 1978), further complicating interpretations. The recent state map (Lewis and others, 2012) corrects correlations where interpretations had been updated.

Despite the divergent interpretations for the metamorphic rocks in these particular locations, many exposures of these strata have characteristics that allow them to be distinguished from known Mesoproterozoic rocks. These strata are in discrete packages characterized by abruptly contrasting lithodemic units that have thicknesses on scales of hundreds of meters. Among exposures containing rocks with these characteristics, packages of both Neoproterozoic and Paleozoic ages are documented. The Neoproterozoic section contains some distinctive units that have been dated, but otherwise, many similar lithologies are present in both packages. The map units of similar characteristics but possibly different ages are not uniquely distinguishable in the many small, fragmented, or complexly deformed exposures; thus, in important mining districts of the province, determining age and origin of metamorphosed strata is not straightforward.

A Neoproterozoic stratigraphic package is mapped in the Gospel Peaks roof pendant between the Buffalo Hump and Florence mining districts (figs. 2, 3; Lund and Esparza, 1990). This section is dated in the Big Creek roof pendant of the Edwardsburg district. A partial section is present in the Marshall Lake-Resort district and rocks of this age may also be present in the Yellow Pine, Profile, and Warren districts (Lund, 2004). The Neoproterozoic stratigraphic section is a documented succession of distinctive metavolcanic and metadiamictite units as well as quartzite and quartz-pebble conglomerate, marble and calc-silicate gneiss, and schist units. The section, with the metavolcanic and diamictite rocks in the middle part, is estimated to be as much as 3,300 meters (m) thick (Lund, 1984; Lund and Esparza, 1990; Lund, 2004). Neoproterozoic ages are confirmed by direct dates of about 685 Ma on metavolcanic rocks in the Edwardsburg district (U-Pb ages determined from zircon, Lund and others, 2003). The characteristic stratigraphic order, lithodemic compositions, unit thicknesses, and ages provide (1) direct correlation between the rock formations of central Idaho and those of the Windermere Supergroup of northern Idaho-northwestern Washington and southeastern Idaho; the correlations support related basin development in these areas (Lund and Cheney, 2016), and (2) outline the trace of an early phase of Rodinian continental rifting. Neoproterozoic syenite-diorite suites in the Ramey Ridge and Big Creek districts intruded Mesoproterozoic metasedimentary strata (figs. 3, 4; Lund, 2004), and based on ages of about 650 Ma and geochemical characteristics, they are interpreted as a younger pulse of Rodinian rifting along the same margin as the older Neoproterozoic volcanic rocks (Lund and others, 2010).

Another package with abruptly contrasting lithodemic units, including quartzite, marble, quartzite-pebble gneiss, and biotite schist, is locally associated with the dated Neoproterozoic strata. These are interpreted as probable Paleozoic metasedimentary strata based on stratigraphic characteristics (Shenon and Ross, 1936; White, 1945; Lund, 1984, 2004; Smitherman, 1988; Lund and Esparza, 1990; shown as Mesoproterozoic in Fisher and others, 1992). They are best identified where locally identified above the dated volcanic units but, elsewhere, this package remains difficult to distinguish from the similar lithologic types of the Neoproterozoic package. Probable Paleozoic units are mapped in the Profile district and at the eastern edge of the Florence district; these units are probably present as minor components of roof rocks in the Edwardsburg and Marshall Lake-Resort districts (Lund, 2004; figs. 2, 3). Several small exposures of probable Paleozoic rocks are also located at the southeastern corner of figure 3 (for example near sample number 06KL058). The largest of these exposures is preserved in the Stibnite roof pendant (Shenon and Ross, 1936; White, 1945; Smitherman, 1988; Lund, 2004; Stewart and others, 2016).

In the Stibnite roof pendant, the possible Paleozoic metasedimentary package is estimated at 750–1,000 m thick (Lund, 2004; Stewart and others, 2016). Post-Neoproterozoic

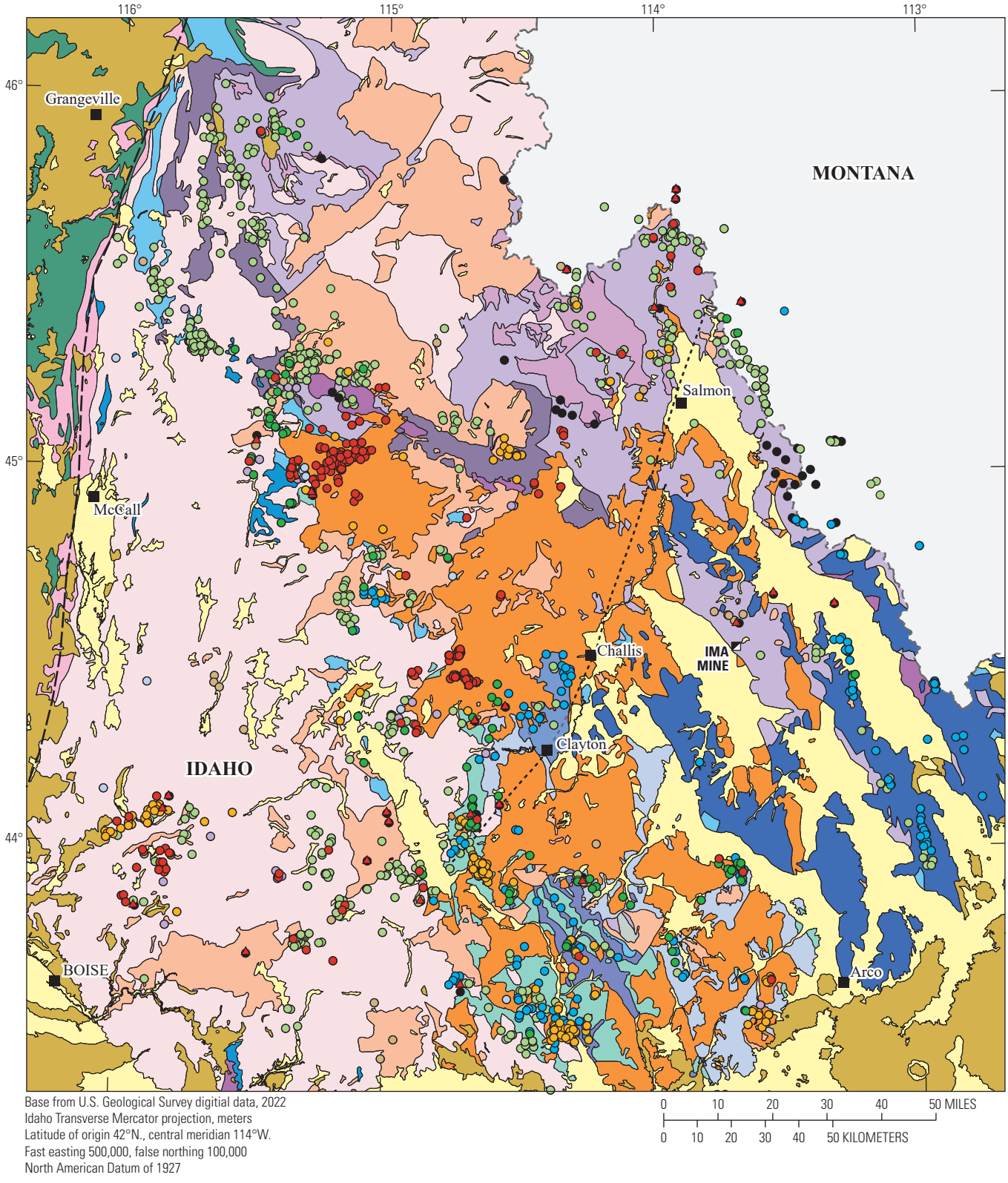

Figure 4. Generalized geologic map of south-central to central Idaho (modified from Lewis and others, 2012; Lund and others, 2016) showing location of epigenetic mineral deposits (modified from Klein and Sims, 2007). Salmon River transform is after the Salmon River lineament of Hobbs and others (1991). (Au, gold; Co, cobalt; Cu, copper; Hg, mercury; Sb, antimony; Mo, molybdenum)

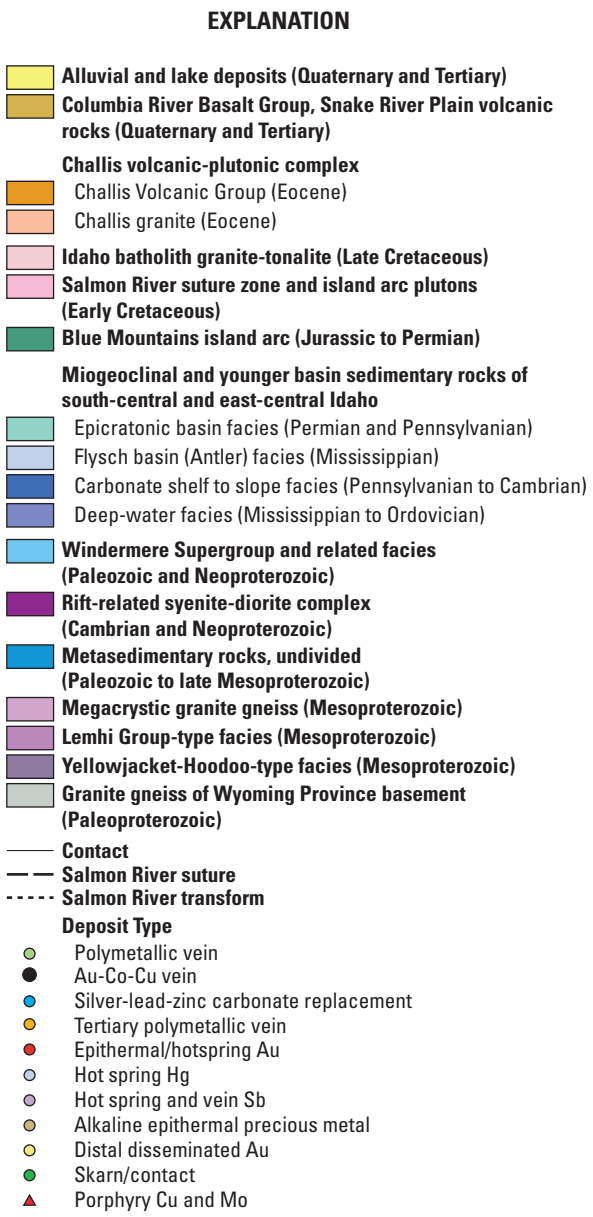

Figure 4. Generalized geologic map of south-central to central Idaho (modified from Lewis and others, 2012; Lund and others, 2016) showing location of epigenetic mineral deposits (modified from Klein and Sims, 2007). Salmon River transform is after the Salmon River lineament of Hobbs and others (1991).
(Au, gold; Co, cobalt; Cu, copper; Hg, mercury; Sb, antimony; Mo, molybdenum)—Continued

ages for some of the lithodemic units are confirmed by detrital zircon analyses (Stewart and others, 2016; Isakson, 2017). However, because there are no directly datable units and compressional structures are complex, map units have been identified in different ways in different map versions. Mapping has been attempted based on lithologies (Shenon and Ross, 1936; White, 1945), on local mine geology lithologic units (Smitherman, 1988; Stewart and others, 2016), and on regionally based characteristics of stratigraphic packages (Lund, 2004). Each of these different approaches results in different structural interpretations. Furthermore, because correlations for the package are dependent on knowing the stratigraphic order, the age range and depositional setting(s) of the package as a whole are difficult to assess.

The amphibolite facies metamorphic grade and the absence of fossils or direct ages render many traditional correlation methods unavailable for the undated Neoproterozoic and Paleozoic exposures. Thus, other criteria need to be considered to constrain interpretations of original setting and sedimentary facies of the incomplete and scattered central Idaho exposures in comparison to better documented stratigraphic sections of south- and east-central Idaho (fig. 1*B*). Such alternative approaches are described following and include comparisons to (1) distinctive characteristics of stratigraphic packages, (2) detrital zircon populations as possible constraints on ages, provenances, or depositional settings, and (3) metal endowment assemblages based on regional geochemistry and mineral deposits.

Comparison to Known-Age Sedimentary Facies of South-Central Idaho

Neoproterozoic Packages

Neoproterozoic Windermere Supergroup volcanic and diamictite strata are identified discontinuously across a broad area of central Idaho and are constrained to be about 685 Ma by dating in the Edwardsburg district (SHRIMP U-Pb ages on zircon, Lund and others, 2003). A younger volcanogenic conglomerate unit in the southern Salmon River Mountains is dated at about 654 Ma from drillcore but is not exposed at the surface (SHRIMP U-Pb ages on zircon, Lund and others, 2010). Units in this stratigraphic package are correlated regionally to sections in southeastern and northern Idaho and along the western Laurentian margin (Lund and others, 2003, 2010; Lund and Cheney, 2016). Despite the Neoproterozoic package (Windermere Supergroup) being widely distributed along the ancient margin, no strata of this age are known to be exposed in south-central or east-central Idaho.

In the southern Salmon River Mountains (fig. 1*B*; Bayhorse area southwest of Challis, fig. 4), strata in the middle levels of a folded thrust stack (Bayhorse antiform, Hobbs and others, 1991) have been recently interpreted to be Neoproterozoic based on a date of about 600 Ma from one of a number of small mafic bodies (Brennan and others, 2020). However, one of the units associated with the mafic rocks gradationally overlies a unit containing Late Cambrian to Early Ordovician

fossils (Hobbs and Hays, 1990; Hobbs and others, 1991; although this is not acknowledged by Brennan and others, 2020). Examination of the mafic exposures reveals they are in a thin zone along a contact interpreted as a thrust fault for about 22 km (Hobbs and others, 1991), suggesting that the mafic exposures are klippen from a Neoproterozoic remnant at the base of a thrust plate. The fossil evidence is compelling for the age of the strata in the core of the Bayhorse antiform, so herein the strata in the core of the Bayhorse antiform are interpreted as Cambrian–Ordovician following previous studies (Hobbs and Hays, 1990; Hobbs and others, 1991; Lund and others, 2010) and are thus discussed with other lower Paleozoic rocks. The only Neoproterozoic strata exposed in east-central Idaho and constrained by fossils and detrital zircon dating are in small exposures of upper Ediacaran and Lower Cambrian quartzite deposited on Mesoproterozoic rocks (McCandless, 1982; Carr and Link, 1999; Pearson and Link, 2021).

In the absence of known Windermere Supergroup strata exposed in south-central Idaho or in the intervening southern Salmon River Mountains, evaluation of any association between mineral deposits and the Neoproterozoic section is based on the dated stratigraphic section in central Idaho.

Paleozoic Packages

Correlating the probable Paleozoic metasedimentary rocks of central Idaho poses significant problems, given that stratigraphic successions and rock ages are largely unconstrained. The approach attempted in this study is to evaluate the probable Paleozoic metamorphosed strata of central Idaho as stratigraphic package(s) that help define potential original depositional settings. These package(s) are compared to four main Paleozoic facies belts that cross south- and east-central Idaho striking north-northwest and that were deposited in separate basinal settings. The four facies belts are numbered and described in the following paragraphs.

(1) An Ordovician to Pennsylvanian shelf facies composes the Paleozoic section in the eastern three tilt-block ranges of east-central Idaho (fig. 4). This greater than 1,500-m thick, primarily carbonate section (Ruppel and Lopez, 1988) was deposited in deepening water westward (Isaacson and others, 1983; Grader and Dehler, 1999). This facies is primarily associated with silver-lead-zinc vein and skarn deposits (fig. 4). Such a thick carbonate package with an accompanying metals assemblage is not present in central Idaho.

(2) Cambrian to Devonian shelf-break to slope strata are present in south-central Idaho but only locally exposed and found mostly southeast of Challis (these are the western extent of the facies on fig. 4). The section is composed of Cambrian to Ordovician siliciclastic rocks, Ordovician to Devonian siltstone, and Ordovician to Devonian carbonate rocks; of these, the Ordovician Kinnikinic Quartzite can be recognized from across the shelf and into this deeper water section (Isaacson and others, 1983; Hobbs and others, 1991; Grader and Dehler, 1999; Baar, 2009). The section is not associated with mineral deposits.

(3a) The Mississippian deep-sea fan turbidite (Antler flysch) facies of south-central Idaho (fig. 4) is composed of carbonaceous argillite and siltite and carbonate rocks and unconformably overlies Cambrian to Devonian shelf-break strata (facies number 2, above). (3b) Ordovician to Devonian deep-water facies rocks lie west of (and formed the highlands for) the Mississippian flysch basin and are of similar composition. Together these two different facies compose most of the Idaho "black shale belt." They are structurally juxtaposed through their central extent and, combined, are more than 4,000-m thick (Link and others, 1995). The western strata of this "black shale belt" are associated with silver-lead deposits and the eastern are associated with gold deposits (Hall and others, 1978; Hall, 1985; Soulliere and others, 1995). If metamorphosed, these facies belts would amount to a comparably thick stack of carbonaceous schist, which is not present in central Idaho.

(4) The facies exposed farthest west in south-central Idaho is 3,000 m of Pennsylvanian to Permian strata complexly alternating carbonaceous siltstone, limestone, sandy limestone, sandstone, and conglomerate that were deposited in an epicratonic onlap basin (fig. 4; Mahoney and others, 1991; Link and others, 1995). Tungsten, silver-lead-zinc-tin, and antimony deposits are associated with these units; some mineral deposits are associated with depositional contacts, but most mineral deposits occur where these units were thrust faulted over early Paleozoic deep-water facies and where either Late Cretaceous or Eocene intrusions invaded the structures (Hall and others, 1978; Cookro, 1985; Hall, 1985). The compositional variations and the scale of compositional alternation of this facies are similar to, but generally thicker than, probable Paleozoic lithodemic units in the central Idaho mineral province.

The farthest north strata with fossil control for ages of some of the rocks are part of a folded thrust fault complex in the southern Salmon River Mountains (figs. 1*B*, 4). On the west is the primarily siliciclastic-facies of the Pennsylvanian–Permian onlap facies (Mahoney and others, 1991); these rocks overlie a thrust plate of Mississippian flysch facies that includes basal thrust slivers as old as Cambrian (Hall, 1985; Hobbs and others, 1991; Link and others, 1995). These two facies packages are along strike with similar facies in south-central Idaho. Deeper in the thrust stack are incompletely dated late Neoproterozoic–Cambrian(?), Cambrian(?), and dated Ordovician successions of quartzite, quartz-pebble conglomerate, siltstone, and carbonate, which seem to represent a broad, somewhat diverse succession that was telescoped. These are faulted over Cambrian(?) and Ordovician carbonate, slate, phyllite units. This complex structural stack was folded into two large antiforms (Hobbs and Hays, 1990; Hobbs and others, 1991). The Cambrian and Ordovician rocks in this area are a mostly older, thicker, and coarser-grained siliciclastic facies than the exposed Ordovician and younger deep-water carbonaceous-predominant facies in south-central Idaho (although both are included with the Paleozoic shelf-slope strata on fig. 4). This change

in stratigraphy from south-central Idaho to the southern Salmon River Mountains reflects a transition in sedimentary successions across a north-northeast striking, syn-depositional paleostructure (fig. 4) called the "Salmon River lineament" by Hobbs and Hays (1990) and Hobbs and others (1991).

Provenance Characteristics

Another approach for evaluating the original facies of the metasedimentary rocks of central Idaho is to evaluate provenance information. Detrital zircon analyses can establish potential limits on ages but they can also provide possible matching of relative probabilities for detrital zircon populations among metasedimentary packages and some data about sources of detritus and stability of basins. Data from the mapped and dated Neoproterozoic volcanic rocks in the Edwardsburg district (Lund and others, 2003) and some map relations in the Yellow Pine district provide relative age information for some units. To provide detrital zircon population data for rocks with the best documented stratigraphic relations, five samples are analyzed in the present study (table 3, fig. 5*A*). Data for these samples are in Aleinikoff and others (2023). These data can be compared to existing detrital zircon data for other rocks of undetermined ages in this area. (fig. 5*B, C*). Similarly, data from known-age Paleozoic facies belts in south-central Idaho can be compared to undated packages in central Idaho (fig. 5*D–I*).

The Edwardsburg district contains the about 685-Ma Edwardsburg Formation of Lund and others (2003). These dated rocks and a straight section in this locality provide context for post-volcanic units which are also part of the Neoproterozoic Windermere Supergroup, as well as for several closely associated pre-volcanic units (Gospel Peaks A) which are considered to be probably Neoproterozoic but older than the Windermere Supergroup (Lund and others, 2003; Lund, 2004). Two samples of pre-volcanic (probably pre-Windermere Supergoup) units display detrital zircon populations with a broad array of provenance signatures (Placer lake and Whiskey Creek samples, fig. 5*A*) including Paleoproterozoic and Mesoproterozoic peaks similar to those of the Ordovician units in the Clayton and Bayhorse antiforms (fig. 5*D, E*) and Pennsylvanian–Permian Wood River Formation (fig. 5*F*), Paleoproterozoic and Mesoproterozoic peaks similar to those of the Mesoproterozoic Lemhi Group strata (for example, Link and others, 2007; Lund and others, 2008), an unusual peak at about 1,250 Ma, and several peaks in the 1.2–1.0 billion years (Ga) range which is similar to many of the younger rocks in this region (below).

The few Neoproterozoic Windermere Supergrpoup equivalent rocks that have been analyzed for detrital zircon are from the Edwardsburg section (Isakson, 2017; this study) and have distinctly different detrital zircon populations than Mesoproterozoic units. Several samples of this type, which depositionally overlie the Neoproterozoic Edwardsburg Formation metavolcanic units but are also correlated with the Windermere Supergroup (Lund and others, 2003; Lund, 2004), contain detrital zircon derived from the about 685 Ma metavolcanic rocks but the main peak ranges from about 1,000-1,600 Ma and samples contain some Paleoproterozoic zircon as well (Isakson, 2017). Strata that structurally overlie the 685 Ma metavolcanic units do not include zircon sourced from the volcanic rocks but only zircon of Mesoproterozoic and older ages (see McFadden Point sample, fig. 5*A*); however, based on the compositional and sedimentological features, these rocks are interpreted as post-Mesoproterozoic ages but probably pre-Windermere Supergroup (Gospel Peak A; Lund and others, 2003; Lund, 2004). There are no known Neoproterozoic strata equivalent to the Windermere Supergroup or the Gospel Peak A units exposed in south-central Idaho or in the southern Salmon River Mountains (see Neoproterozoic Packages section above) for provenance comparison.

The maximum ages from a number of lithologic types in the roof pendants of the southern cluster of districts, as provided by youngest zircon populations (Stewart and others, 2016; Isakson, 2017; table 3 and fig. 5*A, B, C*), corroborate the stratigraphic interpretations that they are post-Mesoproterozoic. The age data require that several of them are younger than the 685 Ma volcanic event and that a few are younger than Cambrian (fig. 5*B*). Many of the unknown-age samples from the Yellow Pine district contain zircon derived from the 685 Ma volcanic source or 1.2–1.0 Ga sources, although some contain evidence for both sources. Other samples from interlayered or structurally interleaved units contain only older zircon populations in the 1.7 Ga range although interpreted as probably Paleozoic units (fig. 5*C*). The lower Monumental Summit sample (figs. 5*B*) has similar zircon population to that of the Jackass Gulch sample (fig. 5*A*) which is located farther southeast (fig. *3*) and between the Stibnite roof pendant and the southern Salmon River area; these samples contain a broad range of zircon ages between about 900 and 1300 Ma and are quite similar to the structurally lower schist sample (fig. 5*C*) and Whiskey Creek sample (fig. 5*A*) that are interpreted as older than Windermere Supergroup. With the available data, the presence or absence of the Neoproterozoic or late Mesoproterozoic detrital zircon do not seem to uniquely identify the Neoproterozoic rocks or discriminate them from younger strata.

The oldest Paleozoic strata from which detrital zircon data have been acquired in south-central Idaho are the Middle Ordovician Kinnikinic Quartzite (fig. 5*I*). Samples from this unit produced consistent Paleoproterozoic detrital zircon populations with few or no younger grains. In addition to the regional correlation of rocks of this unit, its zircon population further documents a Middle Ordovician sand wedge that spread from shelf to deep-water settings across from east- to south-central Idaho and that had a characteristic provenance (Baar, 2009). Samples of Devonian deep-water (lower part of the Milligen Formation, fig. 5*G*) and shelf-break (Jefferson Formation, fig. 5*I*), plus the Mississippian flysch strata (Copper Basin Group samples, fig. 5*G*), display the same Paleoproterozoic peak as the predominant signature.

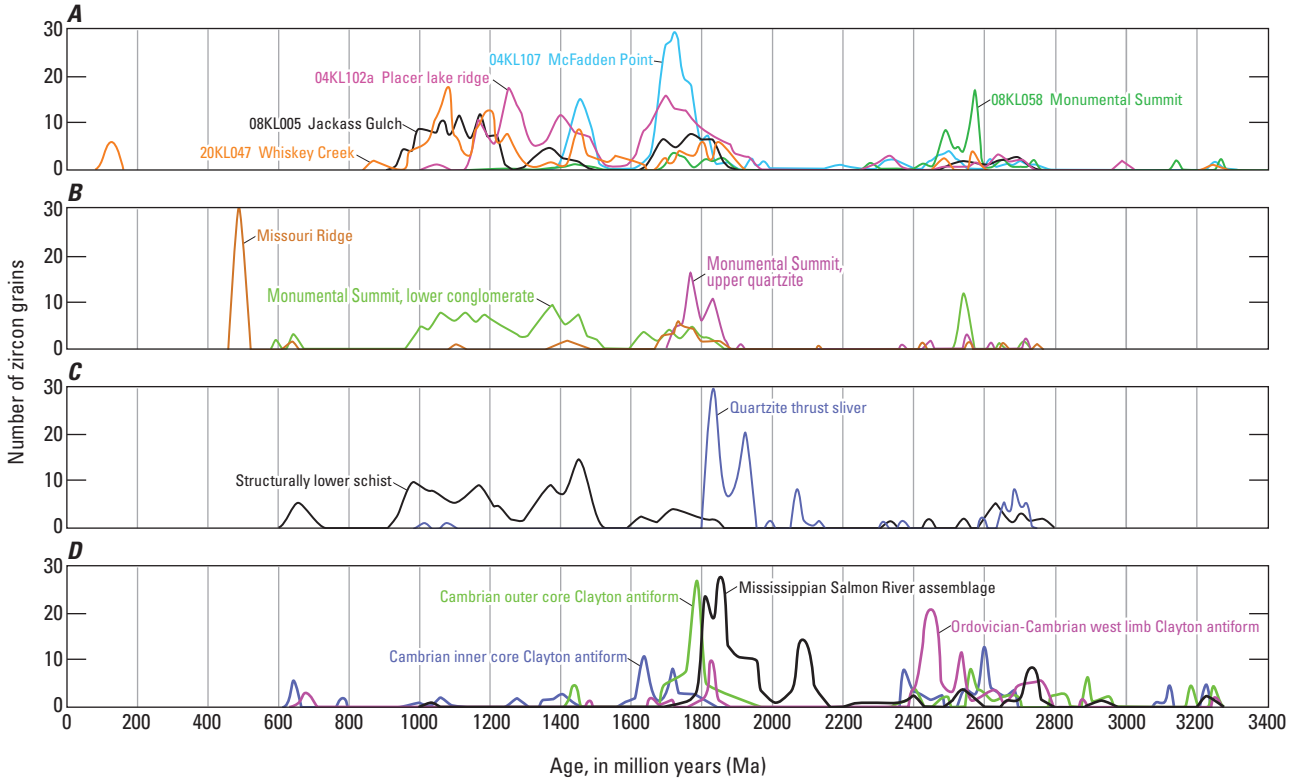

Figure 5. Detrital zircon relative probability plots for samples of probable Neoproterozoic and Paleozoic metasedimentary rocks of undetermined ages in central Idaho and of unmetamorphosed rocks of known ages in south-central Idaho. *A*, Relative probability plots for five samples of metasedimentary rocks in the central Idaho mineral province from the present study. Placer lake ridge siltite (04KL102a, "Placer lake" is informal location name used in Cater and others, 1973, fig. 73) from below dated volcanic rocks of Edwardsburg Formation (685 million years [Ma], Lund and others, 2003; Lund, 2004) from Big Creek roof pendant; Whiskey Creek metasandstone gneiss (20KL047), having angular upper contact with probable Paleozoic units, from central Stibnite roof pendant; McFadden Point quartzite (04KL107) structurally above Neoproterozoic units from Big Creek roof pendant (Lund and others, 2003); Monumental Summit metamorphosed quartz-pebble quartzite (08KL058) from southern Stibnite roof pendant; Jackass Gulch metamorphosed quartz-pebble quartzite (08KL005) from roof pendant along Middle Fork of the Salmon River 34 km east-southeast of Stibnite and without context with other strata. Locations shown on figure 3. Analytical data is presented in table 3 and available in Aleinikoff and others (2023). *B*, Relative probability plots for units in the Stibnite roof pendant including a sample from Missouri Ridge Formation of Lund (2004; named in Lund and others, 2003) in the probable youngest facies in the northern part of the roof pendant (14DS12, Stewart and others, 2016; Isakson, 2017) and two samples from the upper and lower (denoted as 12DS19 and QPC, Stewart and others, 2016) parts of the quartzite and conglomerate unit of Monumental Summit that composes about a third of the roof pendant (Lund, 2004; Stewart and others, 2016); these quartzite and conglomerate samples from the Stibnite roof pendant (Stewart and others, 2016; Isakson, 2017) are from the same map unit as Monumental Summit sample in figure 5*A*. *C*, Relative probability plots for biotite-feldspar-quartz schist that is the structurally lowest unit in the southern Stibnite roof pendant and for a quartzite unit from a thrust sliver (Lund, 2004) internal to the southern Stibnite roof pendant (14RL011a and 12DS14, respectively, from Stewart and others, 2016; Isakson, 2017). *D*, Relative probability plots for samples from the southwestern part of southern Salmon River Mountains area (fig. 1*B*) including, from west to east: Ordovician to Mississippian Salmon River assemblage at the northern extent of recognized flysch basin facies rocks (Beranek and others, 2016) in a thrust plate over three quartz-rich sandstones (8NK15, 4TA09, 3TA09, Krohe and others, 2020) which are located from structurally shallower to deeper in the west limb of Clayton antiform and have ages that may be Cambrian to Ordovician, Cambrian, and late Neoproterozoic to Cambrian, respectively (Hobbs and others, 1991).

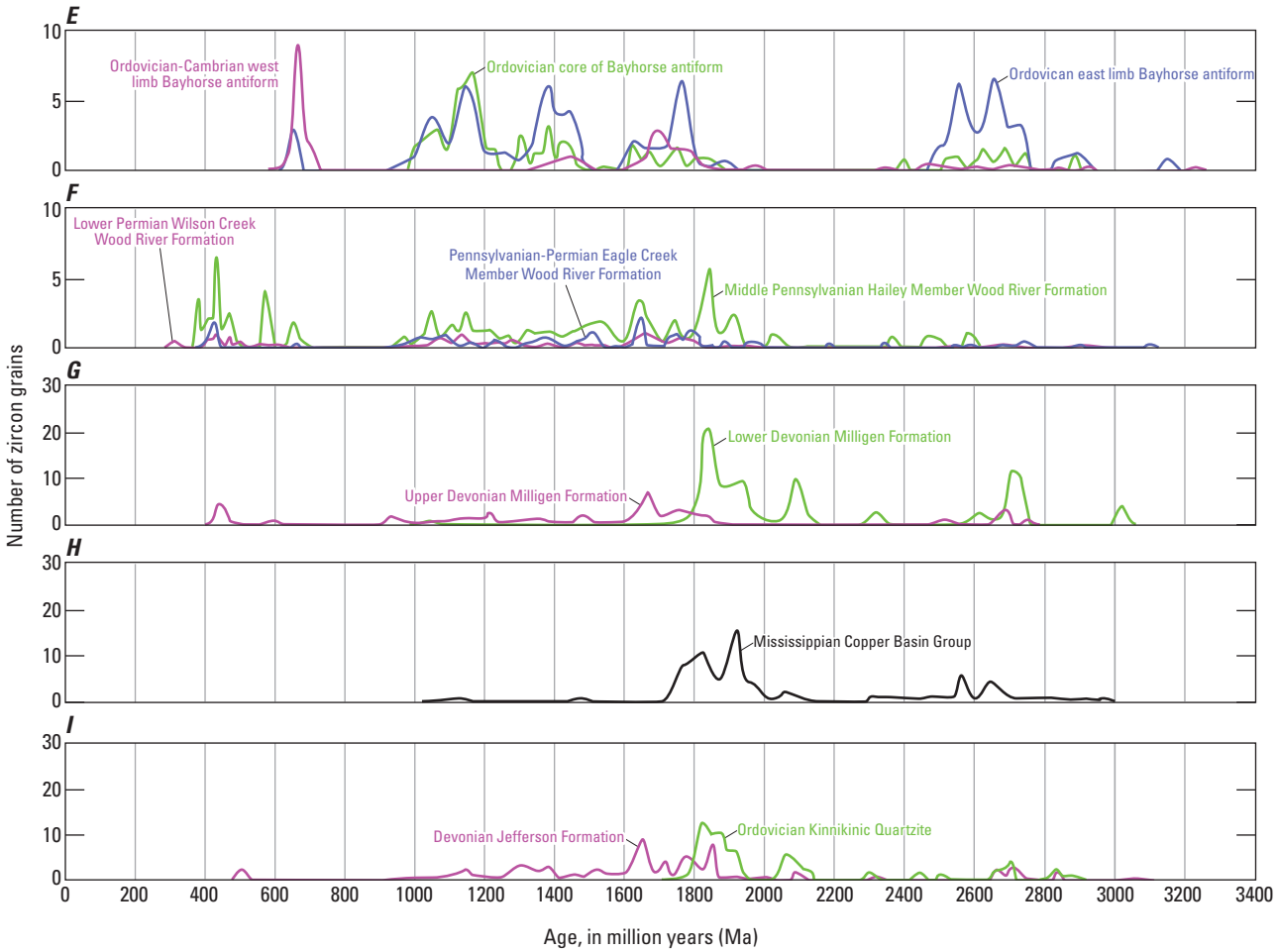

Figure 5. Detrital zircon relative probability plots for samples of probable Neoproterozoic and Paleozoic metasedimentary rocks of undetermined ages in central Idaho and of unmetamorphosed rocks of known ages in south-central Idaho. *E*, Relative probability plots from southeastern part of Salmon River Mountains area, including units on west and east limbs of Bayhorse antiform (DTB17-11 and DTB17-19, respectively, Brennan, 2020) of Ordovician or older age in the thrust sheet overlying the fold core (Hobbs and others, 1991) and in the core of Bayhorse antiform (10NK15, Krohe and others, 2020) from Ordovician slate overlying Ordovician fossil-bearing rocks (Hobbs and others, 1991). *F*, Relative probability plots for the epicratonic basin facies, Wood River Formation of the Pennsylvanian–Permian Sun Valley Group from Link and others (2014). *G*, Relative probability plots for deep-water facies, Devonian Milligen Formation from Beranek and others (2016). *H*, Relative probability plot for flysch basin facies, Mississippian Copper Basin Group from Beranek and others (2016). *I*, Relative probability plots for shelf and slope facies, Ordovician Kinnikinic Quartzite and Devonian Jefferson Formation from Beranek and others (2016).—Continued

Table 3. Uranium-thorium-lead (U-Th-Pb) data for detrital zircon from metasedimentary rock, central Idaho mineral province.

[Data are available in Aleinikoff and others (2023). Datum for latitude-longitude is World Geodetic System 1984. Propagated uncertainties include both reference material and instrumental uncertainties. Preferred ages determined according to $^{206}Pb/^{238}U$ age is used if grain is less 1,300 Ma and $^{207}Pb/^{206}Pb$ age is used if grain is more than 1,300 Ma. Discordant analyses (greater than about 10 percent discordant) are excluded from relative probability plots. ID, identification; Ma, million years; sig, sigma; abs, absolute; PDP, probability density plots]

Analysis ID	Preferred Age (Ma)	2-sig (abs)	Included in relative probability plot
04KL102A (Placer lake ridge, siltite) [latitude 45.161, longitude –115.35667]			
04KL102A-001	1697	74	Yes
04KL102A-002	1855	61	No
04KL102A-003	1414	74	Yes
04KL102A-004	1175	33	Yes
04KL102A-005	1368	90	Yes
04KL102A-006	1246	32	Yes
04KL102A-007	1849	64	Yes
04KL102A-008	1160	100	No
04KL102A-009	1585	66	Yes
04KL102A-010	1418	80	Yes
04KL102A-011	1014	33	No
04KL102A-012	1245	31	Yes
04KL102A-013	1852	64	No
04KL102A-014	2320	61	Yes
04KL102A-015	1474	65	Yes
04KL102A-016	1024	30	No
04KL102A-017	1692	68	Yes
04KL102A-018	1389	73	Yes
04KL102A-019	1475	65	Yes
04KL102A-020	1734	60	Yes
04KL102A-021	1382	71	Yes
04KL102A-022	1157	29	Yes
04KL102A-023	2305	58	Yes
04KL102A-024	1264	30	Yes
04KL102A-025	1282	29	Yes
04KL102A-026	1420	81	Yes
04KL102A-027	1259	67	Yes
04KL102A-028	1164	31	Yes
04KL102A-029	1206	32	Yes
04KL102A-030	1287	31	Yes
04KL102A-031	1785	66	Yes
04KL102A-032	1195	31	Yes
04KL102A-033	1041	42	Yes
04KL102A-034	1414	70	Yes
04KL102A-035	1259	58	No
04KL102A-036	1035	89	No
04KL102A-037	1754	66	Yes
04KL102A-038	1241	38	Yes
04KL102A-039	1336	73	Yes
04KL102A-040	871	40	No
04KL102A-041	1742	72	Yes
04KL102A-042	2506	64	Yes
04KL102A-043	1906	62	Yes
04KL102A-044	1455	73	Yes
04KL102A-045	1744	64	Yes
04KL102A-046	1667	65	Yes
04KL102A-047	1460	71	Yes
04KL102A-048	1193	66	No
04KL102A-049	1195	31	No
04KL102A-050	972	42	No
04KL102A-051	1731	71	Yes
04KL102A-052	1773	61	Yes
04KL102A-053	1457	66	Yes
04KL102A-054	520	51	No
04KL102A-055	2685	56	Yes
04KL102A-056	1187	37	Yes
04KL102A-057	730	29	No
04KL102A-058	1670	78	Yes
04KL102A-059	1740	64	Yes
04KL102A-060	1764	64	Yes
04KL102A-061	1066	19	No
04KL102A-062	1393	33	Yes
04KL102A-063	1790	32	Yes
04KL102A-064	1262	34	Yes
04KL102A-065	1260	23	Yes
04KL102A-066	1161	16	Yes
04KL102A-067	1231	17	Yes
04KL102A-068	1295	24	Yes
04KL102A-069	2633	29	Yes
04KL102A-070	1171	22	Yes
04KL102A-071	2331	27	Yes
04KL102A-072	1478	32	Yes
04KL102A-073	1297	41	Yes
04KL102A-074	2574	30	Yes
04KL102A-075	1342	40	No
04KL102A-076	1378	52	Yes
04KL102A-077	1326	47	Yes
04KL102A-078	1678	44	Yes
04KL102A-079	1708	38	Yes
04KL102A-080	1412	49	Yes
04KL102A-081	1244	27	Yes
04KL102A-082	1824	42	Yes
04KL102A-083	1745	37	Yes
04KL102A-084	1695	33	Yes
04KL102A-085	1872	33	Yes
04KL102A-086	1657	39	Yes
04KL102A-087	1732	38	Yes
04KL102A-088	1850	130	Yes
04KL102A-089	1695	43	Yes
04KL102A-090	2991	26	Yes
04KL102A-091	1398	44	Yes
04KL102A-092	1245	31	Yes
04KL102A-093	1870	46	Yes
04KL102A-094	2617	30	No
04KL102A-095	1393	34	Yes
04KL102A-096	985	97	No
04KL102A-097	1260	250	No
04KL102A-098	1687	32	Yes
04KL102A-099	1759	39	Yes
04KL102A-100	1280	26	Yes
04KL102A-101	1628	28	Yes

Table 3. Uranium-thorium-lead (U-Th-Pb) data for detrital zircon from metasedimentary rock, central Idaho mineral province. —Continued

[Data are available in Aleinikoff and others (2023). Datum for latitude-longitude is World Geodetic System 1984. Propagated uncertainties include both reference material and instrumental uncertainties. Preferred ages determined according to $^{206}Pb/^{238}U$ age is used if grain is less 1,300 Ma and $^{207}Pb/^{206}Pb$ age is used if grain is more than 1,300 Ma. Discordant analyses (greater than about 10 percent discordant) are excluded from relative probability plots. ID, identification; Ma, million years; sig, sigma; abs, absolute; PDP, probability density plots]

Analysis ID	Preferred Age (Ma)	2-sig (abs)	Included in relative probability plot
04KL102A (Placer lake ridge, siltite) [latitude 45.161, longitude –115.35667]—Continued			
04KL102A-102	87	3	No
04KL102A-103	1617	44	Yes
04KL102A-104	1672	38	Yes
04KL102A-105	2700	35	Yes
04KL102A-106	1703	26	Yes
04KL102A-107	2640	33	Yes
04KL102A-108	1250	19	Yes
04KL102A-109	1671	42	Yes
04KL102A-110	1798	35	Yes
04KL102A-111	1321	35	No
04KL102A-112	1671	59	Yes
04KL102A-113	1839	39	Yes
04KL102A-114	1640	29	Yes
04KL102A-115	1753	52	Yes
04KL102A-116	1355	44	Yes
04KL102A-117	1850	100	Yes
04KL102A-118	1447	71	Yes
04KL102A-119	1827	36	Yes
04KL102A-120	1924	29	Yes
04KL107 (McFadden Point, metaquartzite) [latitude 45.17355, longitude –115.351117]			
04KL107_001	1451	41	Yes
04KL107_002	1692	39	Yes
04KL107_003	1809	30	Yes
04KL107_004	1963	31	Yes
04KL107_005	2441	29	Yes
04KL107_006	1805	32	Yes
04KL107_007	1683	52	Yes
04KL107_008	1622	36	Yes
04KL107_009	1650	38	Yes
04KL107_010	1672	31	Yes
04KL107_011	1728	36	Yes
04KL107_012	2463	30	Yes
04KL107_013	2337	31	Yes
04KL107_014	1455	58	Yes
04KL107_015	1733	30	Yes
04KL107_016	2657	38	Yes
04KL107_017	1444	37	Yes
04KL107_018	1723	30	Yes
04KL107_019	1759	88	Yes
04KL107_020	1715	36	Yes
04KL107_021	1455	46	Yes
04KL107_022	1687	34	Yes
04KL107_023	1744	42	Yes
04KL107_024	1699	32	Yes
04KL107_025	2736	41	Yes
04KL107_026	1823	68	Yes
04KL107_027	1177	51	No
04KL107_028	1930	28	Yes
04KL107_029	1670	34	Yes
04KL107_030	1784	33	Yes
04KL107_031	1747	32	Yes
04KL107_032	1723	29	Yes
04KL107_033	1157	44	Yes
04KL107_034	2697	32	Yes
04KL107_035	1435	46	Yes
04KL107_036	2497	32	Yes
04KL107_037	1670	36	Yes
04KL107_038	1409	59	Yes
04KL107_039	1660	33	Yes
04KL107_040	1871	49	No
04KL107_041	1711	41	Yes
04KL107_042	1747	41	Yes
04KL107_043	910	23	No
04KL107_044	1747	46	Yes
04KL107_045	1469	40	Yes
04KL107_046	1627	44	Yes
04KL107_047	1687	44	Yes
04KL107_048	1720	40	Yes
04KL107_049	1756	43	Yes
04KL107_050	1721	42	Yes
04KL107_051	1419	48	Yes
04KL107_052	1860	46	Yes
04KL107_053	1712	39	Yes
04KL107_054	2611	35	Yes
04KL107_055	2312	40	Yes
04KL107_056	1445	61	Yes
04KL107_057	2187	61	Yes
04KL107_058	1443	42	Yes
04KL107_059	1762	39	Yes
04KL107_060	1690	42	Yes
04KL107_061	1804	40	Yes
04KL107_062	2362	46	Yes
04KL107_063	1712	42	Yes
04KL107_064	2494	35	Yes
04KL107_065	1670	39	Yes
04KL107_066	1685	53	Yes
04KL107_067	1707	40	Yes
04KL107_068	1701	46	Yes
04KL107_069	1720	38	Yes
04KL107_070	1412	44	Yes
04KL107_071	1721	42	Yes
04KL107_072	1718	46	Yes
04KL107_073	1469	65	Yes
04KL107_074	1698	40	Yes
04KL107_075	1719	43	Yes
04KL107_076	1767	44	Yes
04KL107_077	1771	49	No
04KL107_078	2335	40	No
04KL107_079	1767	41	Yes

Table 3. Uranium-thorium-lead (U-Th-Pb) data for detrital zircon from metasedimentary rock, central Idaho mineral province. —Continued

[Data are available in Aleinikoff and others (2023). Datum for latitude-longitude is World Geodetic System 1984. Propagated uncertainties include both reference material and instrumental uncertainties. Preferred ages determined according to $^{206}Pb/^{238}U$ age is used if grain is less 1,300 Ma and $^{207}Pb/^{206}Pb$ age is used if grain is more than 1,300 Ma. Discordant analyses (greater than about 10 percent discordant) are excluded from relative probability plots. ID, identification; Ma, million years; sig, sigma; abs, absolute; PDP, probability density plots]

Analysis ID	Preferred Age (Ma)	2-sig (abs)	Included in relative probability plot
04KL107 (McFadden Point, metaquartzite) [latitude 45.17355, longitude –115.351117]—Continued			
04KL107_080	854	22	No
04KL107_081	1749	30	Yes
04KL107_082	1469	27	Yes
04KL107_083	1675	34	Yes
04KL107_084	1799	22	Yes
04KL107_085	1480	19	Yes
04KL107_086	2519	22	Yes
04KL107_087	1697	35	Yes
04KL107_088	1682	26	Yes
04KL107_089	1436	32	Yes
04KL107_090	1694	26	Yes
04KL107_091	1449	21	Yes
04KL107_092	1717	74	Yes
04KL107_093	1717	26	Yes
04KL107_094	1463	45	Yes
04KL107_095	1742	15	Yes
04KL107_096	1693	21	Yes
04KL107_097	1694	41	Yes
04KL107_098	1436	37	Yes
04KL107_099	1673	26	Yes
04KL107_100	1468	37	Yes
04KL107_101	1703	32	Yes
04KL107_102	1730	22	Yes
04KL107_103	1711	44	Yes
04KL107_104	2476	20	Yes
04KL107_105	1412	29	Yes
04KL107_106	3247	23	Yes
04KL107_107	1690	24	Yes
04KL107_108	1739	34	Yes
04KL107_109	1683	24	Yes
04KL107_110	1771	25	Yes
04KL107_111	1457	32	Yes
04KL107_112	1425	25	Yes
04KL107_113	1744	22	Yes
04KL107_114	1755	15	Yes
04KL107_115	1446	22	Yes
04KL107_116	1766	18	Yes
04KL107_117	1690	30	Yes
04KL107_118	1767	20	Yes
04KL107_119	1686	24	Yes
08KL005 (Jackass Gulch, metamorphosed quartz-pebble conglomerate) [latitude 44.903306, longitude –115.269472]			
08KL005-001	1177	29	Yes
08KL005-002	1825	32	Yes
08KL005-003	2609	30	No
08KL005-004	2687	32	Yes
08KL005-005	1391	46	Yes
08KL005-006	1146	27	Yes
08KL005-007	1017	23	Yes
08KL005-008	1075	31	Yes
08KL005-009	832	38	No
08KL005-010	1205	26	No
08KL005-011	1117	28	Yes
08KL005-012	1376	35	Yes
08KL005-013	754	17	No
08KL005-014	432	12	No
08KL005-015	1127	62	Yes
08KL005-016	2546	28	Yes
08KL005-017	535	30	No
08KL005-018	950	25	Yes
08KL005-019	783	43	No
08KL005-020	1218	29	Yes
08KL005-021	997	28	Yes
08KL005-022	670	110	No
08KL005-023	1176	31	No
08KL005-024	2885	55	No
08KL005-025	1205	33	Yes
08KL005-026	883	34	No
08KL005-027	981	32	Yes
08KL005-028	2692	26	No
08KL005-029	1122	28	Yes
08KL005-030	587	16	No
08KL005-031	1222	33	Yes
08KL005-032	1336	45	Yes
08KL005-033	1692	47	Yes
08KL005-034	2658	26	No
08KL005-035	1159	40	No
08KL005-036	960	22	Yes
08KL005-037	1437	57	Yes
08KL005-038	1015	29	No
08KL005-039	1270	36	No
08KL005-040	1437	48	Yes
08KL005-041	504	39	No
08KL005-042	745	29	No
08KL005-043	880	110	Yes
08KL005-044	517	22	No
08KL005-045	1169	36	Yes
08KL005-046	1819	36	Yes
08KL005-047	1000	22	Yes
08KL005-048	762	30	No
08KL005-049	1771	45	No
08KL005-050	1016	31	No
08KL005-051	1771	35	Yes
08KL005-052	1348	46	Yes
08KL005-053	736	98	No
08KL005-054	963	47	No

Table 3. Uranium-thorium-lead (U-Th-Pb) data for detrital zircon from metasedimentary rock, central Idaho mineral province. —Continued

[Data are available in Aleinikoff and others (2023). Datum for latitude-longitude is World Geodetic System 1984. Propagated uncertainties include both reference material and instrumental uncertainties. Preferred ages determined according to $^{206}Pb/^{238}U$ age is used if grain is less 1,300 Ma and $^{207}Pb/^{206}Pb$ age is used if grain is more than 1,300 Ma. Discordant analyses (greater than about 10 percent discordant) are excluded from relative probability plots. ID, identification; Ma, million years; sig, sigma; abs, absolute; PDP, probability density plots]

Analysis ID	Preferred Age (Ma)	2-sig (abs)	Included in relative probability plot
08KL005 (Jackass Gulch, metamorphosed quartz-pebble conglomerate) [latitude 44.903306, longitude –115.269472]—Continued			
08KL005-055	1833	34	Yes
08KL005-056	1136	29	Yes
08KL005-057	1032	28	Yes
08KL005-058	556	18	No
08KL005-059	1057	29	Yes
08KL005-060	563	43	No
08KL005-061	1788	53	Yes
08KL005-062	551	41	No
08KL005-063	1110	20	Yes
08KL005-064	2637	42	Yes
08KL005-065	919	29	No
08KL005-066	2511	43	Yes
08KL005-067	1164	27	Yes
08KL005-068	1687	49	Yes
08KL005-069	544	13	No
08KL005-070	1766	46	Yes
08KL005-071	1197	26	Yes
08KL005-072	1773	58	No
08KL005-073	1067	21	Yes
08KL005-074	583	15	No
08KL005-075	1171	27	Yes
08KL005-076	1110	21	Yes
08KL005-077	2580	45	No
08KL005-078	2658	46	Yes
08KL005-079	1124	20	Yes
08KL005-080	955	44	No
08KL005-081	778	41	No
08KL005-082	918	15	No
08KL005-083	1171	22	Yes
08KL005-084	949	32	Yes
08KL005-085	1038	24	Yes
08KL005-086	2707	42	Yes
08KL005-087	656	18	No
08KL005-088	719	25	No
08KL005-089	1688	47	Yes
08KL005-090	876	22	Yes
08KL005-091	460	100	No
08KL005-092	1679	49	Yes
08KL005-093	2545	41	Yes
08KL005-094	1756	48	Yes
08KL005-095	1022	23	Yes
08KL005-096	1177	25	Yes
08KL005-097	1012	37	No
08KL005-098	1699	52	Yes
08KL005-099	1766	44	Yes
08KL005-100	1094	23	Yes
08KL005-101	1044	28	Yes
08KL005-102	1218	24	Yes
08KL005-103	1331	75	Yes
08KL005-104	1165	30	Yes
08KL005-105	1067	29	Yes
08KL005-106	2852	40	No
08KL005-107	1697	55	Yes
08KL005-108	1753	46	Yes
08KL005-109	1001	24	Yes
08KL005-110	1724	60	Yes
08KL005-111	1796	47	Yes
08KL005-112	1220	130	No
08KL005-113	846	21	No
08KL005-114	1069	21	Yes
08KL005-115	1363	53	Yes
08KL005-116	1850	48	Yes
08KL005-117	1097	23	Yes
08KL005-118	1797	43	Yes
08KL005-119	480	150	No
08KL005-120	2584	48	Yes
20KL047 (Whiskey Creek, metasandstone gneiss) [latitude 44.95677, longitude –115.36973]			
20KL047-001	124	6	Yes
20KL047-002	225	37	No
20KL047-003	228	33	No
20KL047-004	287	12	No
20KL047-005	289	20	No
20KL047-006	386	7	No
20KL047-007	415	33	No
20KL047-008	423	30	No
20KL047-009	433	59	No
20KL047-010	464	71	No
20KL047-011	500	53	No
20KL047-012	508	33	No
20KL047-013	557	30	No
20KL047-014	563	92	No
20KL047-015	595	14	No
20KL047-016	670	100	No
20KL047-017	708	12	No
20KL047-018	810	140	No
20KL047-019	861	19	No
20KL047-020	865	22	Yes
20KL047-021	897	31	Yes
20KL047-022	910	120	Yes
20KL047-023	975	9	Yes
20KL047-024	992	18	Yes
20KL047-025	1000	24	Yes
20KL047-026	1009	19	Yes
20KL047-027	1021	37	Yes
20KL047-028	1022	11	Yes

Table 3. Uranium-thorium-lead (U-Th-Pb) data for detrital zircon from metasedimentary rock, central Idaho mineral province. —Continued

[Data are available in Aleinikoff and others (2023). Datum for latitude-longitude is World Geodetic System 1984. Propagated uncertainties include both reference material and instrumental uncertainties. Preferred ages determined according to $^{206}Pb/^{238}U$ age is used if grain is less 1,300 Ma and $^{207}Pb/^{206}Pb$ age is used if grain is more than 1,300 Ma. Discordant analyses (greater than about 10 percent discordant) are excluded from relative probability plots. ID, identification; Ma, million years; sig, sigma; abs, absolute; PDP, probability density plots]

Analysis ID	Preferred Age (Ma)	2-sig (abs)	Included in relative probability plot
20KL047 (Whiskey Creek, metasandstone gneiss) [latitude 44.95677, longitude –115.36973]—Continued			
20KL047-029	1028	54	Yes
20KL047-030	1028	37	Yes
20KL047-031	1035	13	Yes
20KL047-032	1042	22	Yes
20KL047-033	1044	16	Yes
20KL047-034	1048	23	Yes
20KL047-035	1054	19	Yes
20KL047-036	1056	21	Yes
20KL047-037	1062	21	Yes
20KL047-038	1063	21	Yes
20KL047-039	1064	13	Yes
20KL047-040	1065	21	Yes
20KL047-041	1071	21	Yes
20KL047-042	1074	13	Yes
20KL047-043	1077	25	Yes
20KL047-044	1078	45	Yes
20KL047-045	1078	9	Yes
20KL047-046	1079	26	Yes
20KL047-047	1079	10	Yes
20KL047-048	1093	21	Yes
20KL047-049	1097	9	Yes
20KL047-050	1105	33	Yes
20KL047-051	1113	21	Yes
20KL047-052	1122	17	Yes
20KL047-053	1143	23	Yes
20KL047-054	1151	10	Yes
20KL047-055	1156	18	Yes
20KL047-056	1158	25	Yes
20KL047-057	1161	12	Yes
20KL047-058	1175	20	Yes
20KL047-059	1176	13	Yes
20KL047-060	1179	23	Yes
20KL047-061	1182	23	Yes
20KL047-062	1184	24	Yes
20KL047-063	1186	23	Yes
20KL047-064	1189	17	Yes
20KL047-065	1194	16	Yes
20KL047-066	1197	24	Yes
20KL047-067	1206	13	Yes
20KL047-068	1206	27	Yes
20KL047-069	1208	14	Yes
20KL047-070	1211	36	Yes
20KL047-071	1211	25	No
20KL047-072	1223	31	Yes
20KL047-073	1234	26	Yes
20KL047-074	1242	42	Yes
20KL047-075	1244	11	Yes
20KL047-076	1246	30	No
20KL047-077	1249	31	Yes
20KL047-078	1258	25	Yes
20KL047-079	1262	28	Yes
20KL047-080	1281	30	Yes
20KL047-081	1351	52	Yes
20KL047-082	2438	16	No
20KL047-083	1369	40	Yes
20KL047-084	1376	50	Yes
20KL047-085	1446	13	Yes
20KL047-086	1625	19	Yes
20KL047-087	1770	14	No
20KL047-088	1551	13	Yes
20KL047-089	1433	38	Yes
20KL047-090	1440	19	Yes
20KL047-091	1442	24	Yes
20KL047-092	1431	13	Yes
20KL047-093	1487	40	Yes
20KL047-094	1727	37	Yes
20KL047-095	1454	40	Yes
20KL047-096	1458	47	Yes
20KL047-097	1758	37	Yes
20KL047-098	1813	37	Yes
20KL047-099	1569	41	Yes
20KL047-100	1527	38	Yes
20KL047-101	1506	41	Yes
20KL047-102	1582	23	Yes
20KL047-103	1730	16	Yes
20KL047-104	1598	39	Yes
20KL047-105	1683	13	Yes
20KL047-106	1724	52	Yes
20KL047-107	1785	38	Yes
20KL047-108	1865	39	Yes
20KL047-109	1790	20	Yes
20KL047-110	1741	39	Yes
20KL047-111	1791	14	Yes
20KL047-112	1855	37	Yes
20KL047-113	1867	37	Yes
20KL047-114	1874	37	Yes
20KL047-115	1844	11	Yes
20KL047-116	1836	13	Yes
20KL047-117	2502	9	No
20KL047-118	2560	8	Yes
20KL047-119	2475	13	Yes
20KL047-120	3237	32	Yes

Table 3. Uranium-thorium-lead (U-Th-Pb) data for detrital zircon from metasedimentary rock, central Idaho mineral province. —Continued

[Data are available in Aleinikoff and others (2023). Datum for latitude-longitude is World Geodetic System 1984. Propagated uncertainties include both reference material and instrumental uncertainties. Preferred ages determined according to $^{206}Pb/^{238}U$ age is used if grain is less 1,300 Ma and $^{207}Pb/^{206}Pb$ age is used if grain is more than 1,300 Ma. Discordant analyses (greater than about 10 percent discordant) are excluded from relative probability plots. ID, identification; Ma, million years; sig, sigma; abs, absolute; PDP, probability density plots]

Analysis ID	Preferred Age (Ma)	2-sig (abs)	Included in relative probability plot
08KL058 (Monumental Summit, metamorphosed quartz-pebble conglomerate) [latitude 44.72394, longitude –114.966278]			
08KL058-53.1	1229	47	Yes
08KL058-49.1	1304	26	No
08KL058-18.1	1377	28	Yes
08KL058-50.1	1425	17	Yes
08KL058-9.1	1466	22	Yes
08KL058-52.1	1693	16	Yes
08KL058-30.1	1704	12	Yes
08KL058-41.1	1705	16	Yes
08KL058-40.1	1730	13	Yes
08KL058-46.1	1737	14	Yes
08KL058-8.1	1788	15	Yes
08KL058-13.1	1799	14	Yes
08KL058-44.1	1834	17	Yes
08KL058-15.1	1838	20	Yes
08KL058-11.1	1853	18	Yes
08KL058-21.1	2162	20	No
08KL058-34.1	2226	30	No
08KL058-33.1	2261	12	Yes
08KL058-7.1	2328	47	Yes
08KL058-28.1	2401	16	No
08KL058-32.1	2411	14	Yes
08KL058-29.1	2416	23	No
08KL058-56.1	2422	7	No
08KL058-5.1	2457	6	No
08KL058-16.1	2461	12	Yes
08KL058-27.1	2462	9	Yes
08KL058-2.1	2469	11	Yes
08kl058-36.1	2474	27	Yes
08KL058-54.1	2477	8	Yes
08KL058-60.1	2482	28	Yes
08KL058-4.1	2484	14	No
08KL058-22.1	2486	15	Yes
08KL058-20.1	2486	10	Yes
08KL058-6.1	2498	21	Yes
08KL058-51.1	2509	8	Yes
08KL058-12.1	2510	13	No
08KL058-24.1	2532	11	No
08KL058-23.1	2535	15	Yes
08KL058-17.1	2541	11	Yes
08KL058-39.1	2544	18	Yes
08KL058-38.1	2545	16	Yes
08KL058-47.1	2546	10	Yes
08KL058-35.1	2550	9	Yes
08KL058-58.1	2552	40	Yes
08KL058-14.1	2552	11	Yes
08KL058-45.1	2554	11	Yes
08KL058-37.1	2556	7	Yes
08KL058-10.1	2558	6	Yes
08KL058-43.1	2562	7	Yes
08KL058-1.1	2564	7	Yes
08KL058-55.1	2579	7	No
08KL058-59.1	2602	7	No
08KL058-42.1	2626	22	Yes
08KL058-31.1	2637	12	Yes
08KL058-25.1	2688	24	Yes
08KL058-19.1	2715	5	No
08KL058-26.1	2724	9	Yes
08KL058-48.1	2737	10	No
08KL058-57.1	3126	8	Yes
08KL058-3.1	3252	7	Yes

The detrital zircon age distribution for the Salmon River assemblage from the southern Salmon River Mountains (fig. 5*D*) is much the same as the Mississippian Copper Basin Group, with which it is correlated (Link and others, 1995). The thrust-sliver quartzite from the southern Stibnite roof pendant (fig. 5*C*) has a main Paleoproterozoic peak similar to this group. The upper quartzite from the Monumental Summit quartzite-conglomerate unit of the southern Stibnite roof pendant has some similar grains but also contains a larger, younger Paleoproterozoic population (fig. 5*B*) making it more similar to the Cambrian samples from the outer core of the Clayton antiform (fig. 5*D*). The Middle Pennsylvanian Hailey Member of the Wood River Formation (fig. 5*F*) contains the Paleoproterozoic detrital zircon peak similar to the Kinnikinic Quartzite but also contains significant amounts of younger zircon peaks, indicating mixed provenances (fig. 5*I*). These data indicate that a particular source terrain remained intermittently available, that sediment transport from it was active during much of the span from the Ordovician to Pennsylvanian, and that the sand wedge from it also spread westward into central Idaho.

Devonian slope-break and deep-water facies belts of south-central Idaho (fig. 4) both produced the two youngest peaks at about 500–450 Ma (Jefferson Formation [fig. 5*I*] and the upper part of the Milligen Formation [fig. 5*G*]). Samples from the Pennsylvanian–Permian epicratonic basin facies belt and from Upper Devonian deep-water facies of western south-central Idaho (fig. 4) also produced young peaks at about 500–450 Ma (fig. 5*F*). These young peaks from some of the Devonian strata—and those from the Wood River Formation—match peaks in several of the samples from the Yellow Pine district as in the Missouri Ridge, western facies sample, of the northern Stibnite roof pendant (fig. 5*B*). However, except for matching youngest grains, the overall relative-probability patterns ("barcodes") from the known-age strata of south-central Idaho and Stibnite samples are not well matched.

The Middle to Upper Devonian Jefferson and Devonian Milligen Formations (fig. 5*I*, *G*) and the Pennsylvanian–Permian Wood River Formation (fig. 5*F*) contain late Mesoproterozoic detrital zircon (about 1.2–1.0 Ga). These zircon are also present in three of the curves shown from the southern Salmon River Mountains (fig. 5*D*, *E*), in two of the curves shown from the Yellow Pine district (both the basal conglomerate of the Monumental Creek unit of the northern Stibnite roof pendant, fig. 5*B*), in the structurally lowest schist unit of the southern Stibnite roof pendant, fig. 5*C*), in the unknown-age Jackass Gulch sample from southeast of the Yellow Pine district, and in the Neoproterozoic Placer lake sample (older than the 685 Ma volcanic rocks) from the Edwardsburg district (fig. 5*A*). Many other zircon peaks from these curves differ but it is clear that through time and across this entire region, the provenance switched repeatedly such that a late Mesoproterozoic source was only intermittently included.

Samples from south-central Idaho have fairly uniform intra-facies detrital zircon populations, indicating relatively consistent provenances and sediment transport systems. However, the metasedimentary rocks from the Yellow Pine district (Stewart and others, 2016; Isakson, 2017) produced six types of relative-probability patterns from 12 samples and additional patterns from samples analyzed for the present study (fig. 5*A–C*). These data suggest that the central Idaho rocks were derived from a variety of provenances and that the sources changed markedly during the depositional history. Thus, there are strikingly different zircon populations (that is, provenance and sediment transport factors) between south-central and central Idaho samples, although the rocks are along strike and parallel to the Neoproterozoic-Paleozoic continental margin (Lund, 2008; Lund and others, 2010).

Mineral Deposit Associations

The most well documented and complete of the central Idaho Neoproterozoic sections, located in the Gospel Peak and Big Creek roof pendants, are not associated with mineral deposits. Likewise, the probable Neoproterozoic rocks in the Stibnite roof pendant do not host the mineralized zones. The only Neoproterozoic rocks in the central Idaho mineral province that host deposits are in the Marshall Lake-Resort district, where carbonate-bearing biotite schist correlated with the upper part of the Neoproterozoic section (Lund, 2004) hosts gold-silver±lead-zinc±antimony±tungsten vein deposits.

The Paleozoic miogeoclinal facies belts, which cross from east- to south-central Idaho, are linked to mineral belts in a manner that matches a generalized model (Lund, 2008), although there is added complication where middle Paleozoic flysch basin and late Paleozoic onlap basin successions were telescoped by thrust faulting onto the miogeoclinal belts. The east-central Idaho shelf to slope facies strata are associated with silver-lead-zinc deposits of Mississippi Valley Type (MVT) and Sedex types, respectively. The Ordovician–Mississippian outer shelf, deep-water facies are overlapped by Mississippian deep-sea fan, turbidite (Antler flysch) basin strata, and gold is added as a significant commodity to deposits. Farther west, mines and prospects associated with Pennsylvanian–Permian epicratonic onlap basin facies are characterized by gold-silver-tungsten-antimony enrichments (Worl and Johnson, 1995). The setting associated with the most complicated metals assemblages in western south-central Idaho is where the Ordovician–Devonian deep-water facies were depositionally or structurally overlapped by the Pennsylvanian–Permian epicratonic-basin onlap facies (fig. 4; Hall and others, 1978; Cookro, 1985; Hall, 1985; Link and others, 1995).

Farther north, the Cambrian–Ordovician package on the western side of the southern Salmon River Mountains contains a greater proportion of coarse siliciclastic strata than more southerly sections do, and it hosts silver-lead and tungsten occurrences (Hobbs, 1985; Hobbs and others, 1991). Those deposits are located where the Cambrian–Ordovician package was structurally overridden from the west by the thrust plate of Mississippian deep-water and Pennsylvanian–Permian onlap facies and where Late Cretaceous or Eocene magmas intruded along the structures (Hall and others, 1978; Cookro, 1985; Hall, 1985). Each of these facies belts is matched with associated regional geochemical anomalies for the relevant metal signatures (Erdman and others, 1995). Lower Cambrian–Middle Ordovician phyllite and dolostone in the eastern part of the southern Salmon River Mountains, which may represent a significant facies transition from (or are not exposed in) south-central Idaho, host significant silver-lead-zinc vein deposits.

The central Idaho districts in and adjacent to roof pendants that contain most of the probable Paleozoic strata are those linked to gold-antimony-tungsten geochemical associations (Alminas, 1990) and to deposits containing these metals (table 2, fig. 1). This places the central Idaho tungsten-gold deposits and their host rocks north-northwest of tungsten-endowed mineral deposits of south-central Idaho.

Neoproterozoic–Paleozoic Facies Belts Reconstruction

Although the western Laurentian rift system and developing miogeocline were geographically continuous in Idaho (Lund, 2008; Lund and others, 2010), the details (see Neoproterozoic Packages and Paleozoic Packages sections, above) present along-strike contrasts among stratigraphic packages in central Idaho (Lund, 2004; Stewart and others, 2016), the southern Salmon River Mountains (Hobbs and Hays, 1990; Brennan and others, 2020), and south-central Idaho (Isaacson and others, 1983; McFadden and others, 1988; Grader and Dehler, 1999). Information from the stratigraphic packages indicate a thick Neoproterozoic section is present in central Idaho but absent in south-central Idaho, whereas a broader, thicker, and more complete set of Paleozoic miogeoclinal facies belts is present in east- and south-central Idaho compared to central Idaho (figs. 1*B*, 4).

Available detrital zircon analyses from probable Paleozoic sections in central Idaho indicate diverse provenances and some unique populations (which can be evaluated independent of stratigraphic stacking or structural complications) in comparison to the known-age strata in south-central Idaho (compare fig. 5 *A–C* to *F–I* and *D–E*). Together, the stratigraphic and detrital zircon comparisons reveal that central Idaho had the more tectonically active Paleozoic basin histories, as shown by (1) the more abrupt changes of sedimentary character—quartz-rich siliciclastic sheets alternating with carbonate and carbonaceous-silt deposition—as well as (2) distinctly variable provenances (sediment sources).

A significant change in Paleozoic stratigraphic packages and provenances occurs in the southern Salmon River Mountains (fig. 1*B*) where Hobbs and others (1991) describe the juxtaposition of coeval stratigraphic sections with contrasting stratigraphic and compositional characteristics. Similarly, the Neoproterozoic rocks in central Idaho are a thick section that is different from the only occurrence documented in a deep drillhole in the eastern part of the southern Salmon River Mountains area (Lund and others, 2010) and from the thin upper Neoproterozoic unit locally present in east-central Idaho (McCandless, 1982; Hobbs and others, 1991). The details suggest that there was a long-lived transition zone in Neoproterozoic–Paleozoic depositional basins in this area (as suggested by Hobbs and others, 1991). This transition zone probably originated as a northeast-striking transform in the Neoproterozoic through middle Paleozoic miogeoclinal rift system(s) (for example, Lund and others, 2003, 2010) and is herein named the Salmon River transform (fig. 4; Salmon River lineament of Hobbs and Hays, 1990; Hobbs and others, 1991).

This along-paleomargin transition in the Neoproterozoic–Paleozoic sedimentary rocks frustrates correlation of units from south-central to central Idaho but also clarifies the problem. The evidence from stratigraphic, compositional, and provenances for Neoproterozoic–Paleozoic strata of central Idaho compared to south-central Idaho suggests that the Paleozoic miogeoclinal basin tectonic history diverged across the Salmon River transform, such that, for the northern Paleozoic rocks, the miogeoclinal rift basin narrowed, the stratigraphic sections thinned, and the deposits were of a coarser nature. However, there are indications of continuity for stratigraphic packages, such as the detrital zircon data that partially constrain ages and provide some indications of corresponding sediment sources, the stratigraphic characteristics (compositions and their thicknesses and alternation styles) that are similar along strike, and the presence of gold-silver-antimony-tungsten deposits. Together, continuity of these characteristics along strike of the paleomargin and across the transition suggests some continuity in the essential characteristics of sedimentary deposits and perhaps in the underlying crust. These data particularly suggest that some proportion of the metasedimentary rocks in the Yellow Pine district (and potentially to lesser degrees in the Profile, Edwardsburg, and to Marshall Lake-Resort districts) likely include northern correlatives to the western Pennsylvanian–Permian epicratonic facies and to early Paleozoic deep-water facies.

Igneous Events in Relation to Crustal and Deposit Settings

Four magmatic episodes occurred in the central Idaho mineral province, in the Mesoproterozoic, Neoproterozoic, Late Cretaceous, and Eocene. Each magmatic episode provides information on the crustal setting at the time of magma genesis and on a number of factors including intrusive histories and rock fabrics. Present settings provide details of upper-crustal structural evolution. All of these were potential drivers of mineralizing systems.

Mesoproterozoic Salmon River Mountains Orthogneiss

Mesoproterozoic foliated porphyritic granite and granodiorite and augen gneiss is discontinuously exposed in a northwest-striking belt across central Idaho. They are dated at 1380–1360 Ma (U-Pb ages determined from zircon, Evans and Zartman, 1990; Aleinikoff and others, 2012) and classified as peraluminous calc-alkalic, ferroan granitoids (du Bray and others, 2018). They intruded the middle formations of the Mesoproterozoic Lemhi Group and gneisses correlated with those strata. Gold-polymetallic vein deposits in the Orogrande, Elk City, and Dixie mining districts (fig. 2) are locally hosted in these granitoids but are also in Mesoproterozoic metasedimentary and Cretaceous granitic rocks (table 2). Although an early phase of xenotime in gold-cobalt-copper deposits of the Blackbird mining district of east-central Idaho is dated at about the same age as a structurally juxtaposed Mesoproterozoic granitoid (Aleinikoff and others, 2012), most of the datable minerals related to the deposits produced Cretaceous ages (Lund and others, 2011; Aleinikoff and others, 2012). Similarly, the deposits that are hosted in Mesoproterozoic augen gneiss of the central Idaho districts are structurally controlled, and available dates indicate mineralizing events were Cretaceous (Lund and others, 1986) and not related to the Mesoproterozoic magmatism.

Neoproterozoic Syenite-Diorite Suites of Big Creek-Beaverheads Belt

Neoproterozoic syenite-diorite suites in the Ramey Ridge and Big Creek districts (figs. 2, 3) are dated at about 650 Ma and help mark the strike and general location of a second pulse of Neoproterozoic continental rifting that followed the initial phase identified by the nearby about 685-Ma volcanic rocks (Lund and others, 2003, 2010). The syenite-diorite complexes and the Mesoproterozoic strata they intruded both host the structurally controlled mineral deposits. Those in syenite-diorite complexes are precious-metal rich, one bearing stibnite, whereas the deposits in the older country rocks are copper rich (Cater and others, 1973). Because of their structural control, deposits are presumed to be Cretaceous or possibly Eocene in age and preliminary dating of the deposits hosted in the syenite-diorite suites resulted in ages of 79–65 Ma (Lund, 2004).

Late Cretaceous Idaho Batholith

Based on geologic-map geometries and ages of intrusive units, the northern and central Atlanta lobe of the late Cretaceous Idaho batholith (which underlies the central Idaho mineral province) is interpreted to have age- and composition-defined shells (see Lund, 2004). Most mining districts in the province are located near exposures of metasedimentary roof rocks (in three dimensions) and are seldom found in similar age or similar composition plutons where those are not adjacent to the metasedimentary rocks. Our combined geologic mapping and geochronology are applied to test the geometry and veracity of the semi-concentric shells and most particularly to identify crustal depths related to fault offsets (that is, uplifted or tilted blocks) and the relative offset amounts, timing, and duration of such structural events. This is another way to test the controls for mineral deposit localization and also potentially for controls on preservation.

U-Pb Ages across Atlanta Lobe

Many of the mining districts are hosted in Late Cretaceous plutons of the Idaho batholith and the interpretation of timing, amount of offset, and sense of movement on bounding faults can only be gained through details relating to emplacement ages and geometry of plutons. Preliminary ages for Late Cretaceous granites of the northern Atlanta lobe are presented in Unruh and others (2008, TIMS U-Pb method [thermal ionization mass spectrometry] and multigrain analyses). However, many of those ages are relatively imprecise because of zircon with inherited cores or overgrowths caused by multiple events. To mitigate these problems, samples from across the Atlanta lobe, extending from adjacent to the Salmon River suture on the west to the central Yellow Pine district, are reanalyzed by the SHRIMP U-Pb method (fig. 6, table 4). Data for these samples are in Aleinikoff and others (2023). These new emplacement ages help constrain some of the mineralization and fault movement questions for the mineral province. Results complement ages for Stibnite area granitoids and for mineral deposits in the central Yellow Pine to Thunder Mountain districts (tabulated in Gillerman and others, 2019).

Methods

Zircon was extracted from samples using standard mineral-separation procedures including crushing, pulverizing, Wilfley table, magnetic separator, and heavy liquids. Pristine grains were handpicked onto double-sided tape, mounted in epoxy, ground to about half-thickness using 2500-grit sandpaper, and polished sequentially using 6 micrometer (μm) and 1 μm diamond suspensions. Zircon grains were imaged in transmitted and reflected light on a petrographic microscope, and cathodoluminescence (CL) using the JEOL 5800LV SEM at the U.S. Geological Survey, Denver, Colorado.

SHRIMP U-Pb zircon dating was accomplished using the sensitive high resolution ion microprobe-reverse geometry (SHRIMP-RG) at Stanford University. The primary oxygen beam was operated at about 6 nano-Amperes (nA), resulting in a pit about 20–25 µm in diameter. Isotopic data were collected during cycling through the mass stations five times. Measured $^{206}Pb/^{238}U$ for zircon was normalized to values for zircon standard R33 (419 Ma; Black and others, 2004). U concentrations were determined by comparison with data from standard MADDER (4,350 ppm U), thought to be accurate to about ±20 percent. SHRIMP data are reduced using Squid 2 (Ludwig, 2009) and plotted using Isoplot 3 (Ludwig, 2003). Ages are determined by calculating the weighted average of selected $^{206}Pb/^{238}U$ ages, with 2-sigma uncertainties. Data are available in Aleinikoff and others (2023).

Results

Foliated hornblende-biotite tonalite (MC13-91, Upper Payette Lake) is from the elongated exposures directly east of the Salmon River suture complex (fig. 6*A*). Zircon from this sample are euhedral, colorless to pale tan, and have length-to-width ratios (l/w) of 3–5. In CL, the grains display fine concentric oscillatory zoning and contain numerous tiny inclusions (fig. 6*A*). Isotopic data yield a $^{206}Pb/^{238}U$ weighted average age of 88.8 ± 1.4 Ma (*n*=10; fig. 6*B*). Two analyses are slightly older (approximately 110–100 Ma), perhaps due to inheritance, and one analysis is slightly younger (approximately 80 Ma). CL imaging does not show evidence of younger zircon overgrowths.

Locally foliated, biotite granodiorite (MC1-91, Paddy Flat) contains minor muscovite and several percent monazite and xenotime. Zircon from this sample are euhedral, colorless to pale tan, and have l/w of 2–4. In CL, the grains display fine concentric oscillatory zoning (fig. 6*C*). Isotopic data yield a $^{206}Pb/^{238}U$ weighted average age of 79.5±1.2 Ma (*n*=10; fig. 6*D*). Three analyses are slightly older (approximately 85 Ma), perhaps due to inheritance, and two are slightly younger (75–70 Ma). CL imaging does not show evidence of younger overgrowths.

Muscovite-biotite granites from two locations are dated. Zircon from the Warren mining district sample (MC91-28, Chimney Rock) are euhedral, colorless to pale tan, and have l/w of 2–4. In CL, the grains display fine concentric oscillatory zoning (fig. 6*E*). Isotopic data yield a $^{206}Pb/^{238}U$ weighted average age of 82.4±1.7 Ma (*n*=14; fig. 6*F*). One analysis is slightly older (approximately 100 Ma). CL imaging does not show evidence of younger zircon overgrowths. Zircon from about 20 km south of the Warren district (MC15-91, East Fork South Fork) are euhedral, colorless to pale tan, and have l/w of 3–6. In CL, many grains display concentric oscillatory-zoned cores and large, weakly-zoned to unzoned, dark gray rims (fig. 6*G*). Isotopic data from cores yield a $^{206}Pb/^{238}U$ weighted average age of 78.9 ±0.8 Ma (*n*=10; fig. 6H). Seven analyses of cores yield older ages of 95–83 Ma and six analyses of rims yield ages of 73.9±0.8 Ma.

Foliated porphyritic epidote-hornblende-biotite granodiorite (92-MC36, Johnson Creek) is from within the Johnson Creek-Profile Gap shear zone. Zircon are euhedral, pale tan to medium brown, and have l/w of 2–4. In CL, many grains display concentric oscillatory-zoned cores and thin, weakly zoned to unzoned, light gray rims (fig. 6*I*). Isotopic data from cores yield a $^{206}Pb/^{238}U$ weighted average age of 93.4±0.5 Ma (*n*=20; fig. 6*J*). Pale rims have lower U contents than cores and yield less precise age data (86.2±1.5 Ma; *n*=11). These new data indicate that the previously reported age of 90.3 Ma for this sample (U-Pb TIMS, Unruh and others, 2008) represents a mixture of cores and rims.

Foliated hornblende-biotite granodiorite (92-MC35, Pepper Creek) is from between the Johnson Creek-Profile Gap shear zone and the Stibnite mining area. Zircon are euhedral, colorless to tan, and have l/w of 3–6. In CL, both inner and outer areas of grains display unusual, irregular oscillatory zoning (fig. 6*K*). Isotopic data from inner areas yield a $^{206}Pb/^{238}U$ weighted average age of 95.3±0.5 Ma (*n*=15; fig. 6*L*), whereas data from outer areas result in an overlapping age of 96.8±1.5 Ma (*n*=8). On the basis of similar oscillatory zoning and U-Pb age data, we conclude that both the inner and outer areas of these grains are igneous in origin.

In the broader perspective, plutonic rocks west of the suture complex, which intruded allochthonous oceanic-derived gneisses, were emplaced 160–137 Ma, dating the latest magmatic events related to tectonic activity in the accreted terranes west of the Salmon River suture (U-Pb ages determined from zircon, Lund, 2004; Unruh and others, 2008). Plutonic rocks intruded the Salmon River suture itself 115–110 Ma (U-Pb ages determined from zircon, Lund, 2004; Unruh and others, 2008). Deformation in and parallel to the suture is referred to as the western Idaho shear zone (for example, Tikoff and others, 2001). The 95–79 Ma Idaho batholith plutons presented above are east of the suture zone plutons, and those older than about 88 Ma are generally foliated due to late-stage effects of regional (east-directed) deformation (Lund, 1984, 2004; Lund and Snee, 1988).

Eocene Challis Volcanic-Plutonic Complex

With the exception of the Thunder Mountain district, the central Idaho mineral province is hosted by older rocks west of exposures of Eocene Challis volcanic and plutonic rocks. Emplacement ages are not available for most central Idaho Eocene intrusive rocks (plutons, stocks, or dikes) but, regionally, cooling ages range from about 51 to 37 Ma and dates for the volcanic rocks fall in the same range (Leonard and Marvin, 1982; Fisher and others, 1992).

For the area near the northern cluster of mining districts, a large body of moderately shallowly emplaced, Eocene monzogranite plutons forms most of the Chamberlain Basin pluton east of the Bargamin Creek and Johnson Creek-Profile Gap faults (fig. 3). Closely related, shallowly intruded, epizonal granites are between the en echelon parts of the Bargamin Creek

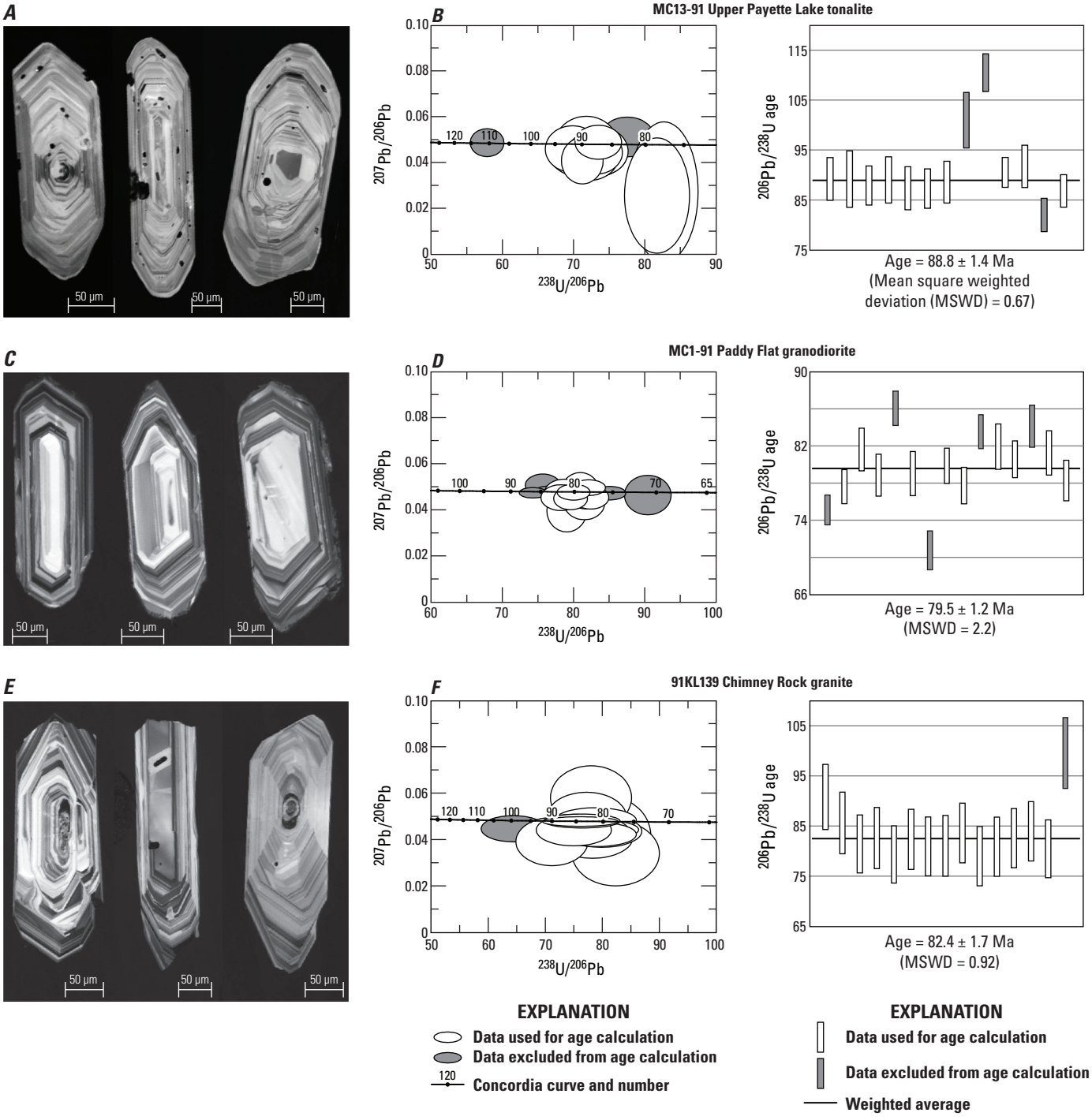

Figure 6A–L. Sensitive high resolution ion microprobe (SHRIMP) uranium-lead (U-Pb) results showing representative images of dated zircon and SHRIMP isotopic data. For each sample, representative cathodoluminescence images of three grains are shown, followed by Concordia plots showing U-Pb analyses of dated detrital zircon (two-sigma error ellipses) and weighted averages plots (two-sigma error bars). White-filled error ellipses and error bars indicate data used for age calculations; gray-filled ellipses and error bars indicate data excluded from age calculations. Data are available in Aleinikoff and others (2023). (µm, micrometers; Ma, million years; MSWD, mean squared weighted deviation)

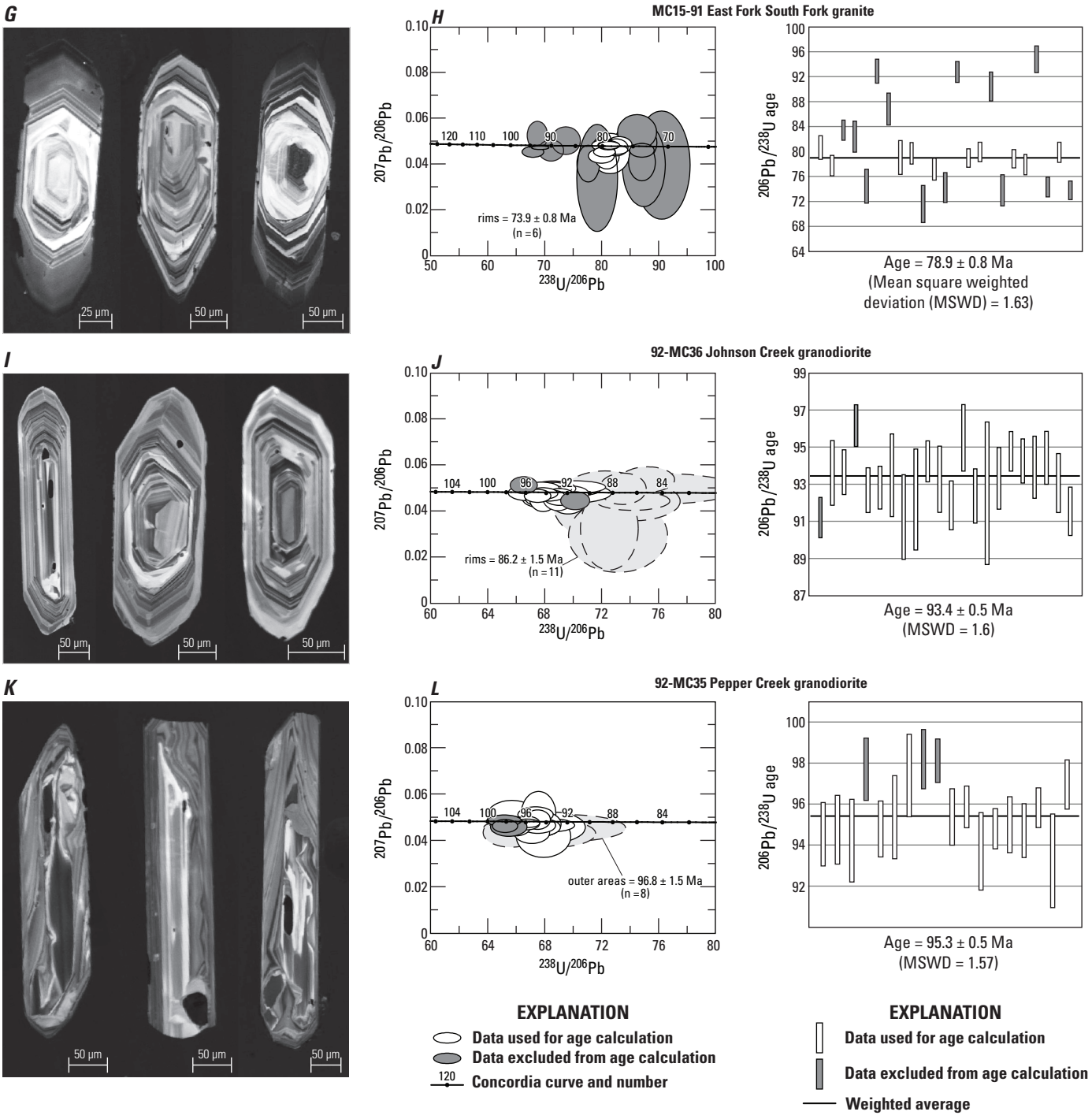

Figure 6A–L. Sensitive high resolution ion microprobe (SHRIMP) uranium-lead (U-Pb) results showing representative images of dated zircon and SHRIMP isotopic data. For each sample, representative cathodoluminescence images of three grains are shown, followed by Concordia plots showing U-Pb analyses of dated detrital zircon (two-sigma error ellipses) and weighted averages plots (two-sigma error bars). White-filled error ellipses and error bars indicate data used for age calculations; gray-filled ellipses and error bars indicate data excluded from age calculations. Data are available in Aleinikoff and others (2023). (µm, micrometers; Ma, million years; MSWD, mean squared weighted deviation)—Continued

and Johnson Creek-Profile Gap faults. Farther west between the Bargamin Creek and Dixie Meadows-Blanco Creek faults, shallowly emplaced, granite porphyry to andesite dikes intruded the older country rocks. These relations indicate stepwise changes in exposed crustal levels across the faults—deeper exposures are on the east and shallower on the west. For the southern cluster of mining districts, the Profile Gap dike swarm (Leonard and Marvin, 1982; Lund, 2004), along the central part of the Johnson Creek-Profile Gap fault zone, is composed of such a large volume of coalescing granite porphyry dikes that the country rocks are difficult to locate. These and the adjacent Savage Point granite porphyry pluton, which lies west of the shear zone, contain a significant proportion of miarolitic cavities, indicating very shallow emplacements (probably 2–4 km depth, Lund, 2004). The Pistol Creek dike swarm ranges in composition from rhyolite to diorite, extends southwest along the trace of the Thunder Mountain/Big Creek graben, and is structurally controlled (fig. 3).

The Thunder Mountain cauldron complex (Fisher and others, 1992) of the Eocene Challis Volcanic Group is exposed east of the Coin Mountain fault, a structure east of and related to the Johnson Creek-Profile Gap shear zone (figs. 3, 7). Three eruptive calderas are proposed for the main stage of volcanic activity as part of the Thunder Mountain cauldron complex (Leonard and Marvin, 1982; Stewart and others, 2016). The main units ("Tcrd, rhyolite and dacite, undifferentiated" on fig. 7) are an estimated 1,500-m thick, latite and rhyolite ash-flow tuff succession. These were overprinted by the caldera-collapse graben of the Thunder Mountain district (Leonard and Marvin, 1982; Hardyman and Fisher, 1985; named Big Creek graben at its northern extent by Stewart and others, 2013, 2016) that preserved the about 300-m thick, late-stage, rhyolite flows, tuffs, and volcanoclastic deposits ("Tcs, rhyolite tuffs and sedimentary rocks of Sunnyside" on fig. 7). These deposits in the collapse graben were erupted from a local vent, and the upper layers were interlayered with volcaniclastic conglomerate to sandstone, mudflows, volcanic breccia, and intercalated lacustrine sediments that include lignite and plant debris (the "Dewey beds"; Umpleby and Livingston, 1920; Ross, 1933; Shannon and Reynolds, 1975; Leonard and Marvin, 1982; Adams, 1985; Parsley, 1997). Ages for main phases of the Thunder Mountain cauldron complex are 49–48 Ma and for late-stage caldera-collapse units are approximately 46.7 Ma (D. John, U.S. Geological Survey, 2019, oral commun.).

The western boundary of the Eocene volcanic-plutonic Thunder Mountain cauldron complex is mapped in most places as a moderately to steeply dipping, faulted margin (Lund, 2004; Stewart and others, 2016), although younger graben structures cut the basal contact locally. The graben structures controlled and localized the deposition of younger volcanic units southwest of and outside of the main cauldron complex (figs. 3, 7; Stewart and others, 2016). Using the structures and elevation differences between highest and lowest volcanic exposures, estimates for thickness of the main volcanic deposits are a minimum thickness of about 800 m near the western margin and of about 300 m for the deposits in the graben.

Regional Normal Faults

Northern Area Faults

The northwestern cluster of mining districts is bounded on the east by a subparallel set of north-northeast-striking steep faults (fig. 2), primarily the Bargamin Creek fault zone (Weis and others, 1972; Cater and others, 1973; Greenwood and Morrison, 1973) plus the Blanco Creek (Lewis and others, 1990; 1998) and en echelon Dixie Meadows faults (named herein). West of the Bargamin Creek and northern Johnson Creek-Profile Gap faults, the country rocks are Late Cretaceous granitic rocks plus Mesoproterozoic and Neoproterozoic metasedimentary roof rocks (fig. 3). Westward from those faults, the metasedimentary rocks become progressively younger and (or) structurally higher. In the area between the Bargamin Creek and Blanco Creek-Dixie Meadows faults, the older rocks were intruded by shallowly emplaced Eocene epizonal stocks and dike-swarms. East of the Bargamin Creek fault, the Eocene Chamberlain Basin pluton is exposed to deep enough levels that no chilled upper margin, older roof rocks, or dike swarms are preserved above it. That different depths of Eocene intrusive systems are expressed across the faults, and that rocks as young as Eocene were deformed locally, indicate that faulting continued until after emplacement of the Eocene intrusive rocks.

The country-rock relations indicate down-to-the-west offsets across this set of faults. Mylonitic fabrics in Mesoproterozoic orthogneiss and in a few Eocene dikes along the Bargamin Creek fault (at about 45°30' on fig. 3) also record down-to-the-west senses of displacement. The amounts of offset across the Bargamin Creek fault after most of the Eocene offsets would be the difference between emplacement depths greater than about 6 km (below the chill-zone level) in the Chamberlain Basin pluton on the east side of the fault and emplacement of less than 2 km (very shallow) for Eocene intrusive rocks and even shallower overlying roof rocks on the west side of the fault. These provide an estimate of more than 4 km of offset across the Bargamin Creek fault. The metamorphic rocks in the Buffalo Hump roof pendant are a 600-m thick layer above the mesozonal Late Cretaceous granites that are determined to have been emplaced at about 9 km depth (Lund and others, 1986). In contrast, epizonal Eocene granites in the central zone between the Dixie Meadows-Blanco Creek and Bargamin faults were emplaced at depths of about 4 km.

These data indicate significant (about 5 km) uplift in the interval between the Late Cretaceous and Eocene. The increasing amounts of Eocene intrusive rocks east of the Dixie Meadows-Blanco Creek fault and particularly the Bargamin Creek and northern Johnson Creek-Profile Gap faults suggest that the faults exerted control on the western extent of Eocene magmatism. Further, the location of rock types across the northern part of figure 3 describe a post-middle Eocene, regional west-dipping crustal block. The mineral deposits of

the northwestern district cluster all lie west of the Bargamin Creek fault in minor fractures that are generally parallel to the main north-northeast striking structures (Chauvot, 1986; Lund and Esparza, 1990).

At its southwestern end, movement on the Bargamin Creek fault transferred into the South Fork and Smith Saddle faults (named herein; figs. 2, 3), which are both characterized by deformation fabrics in Late Cretaceous granitic rocks. Where offset of metasedimentary rocks can be determined across the South Fork fault, general movement was down to the west. Offset is not determined for the Smith Saddle fault, but because it cut and deformed Late Cretaceous granitic rocks, the time of fault movement is constrained as Late Cretaceous or younger. Here, the presence of sparse metasedimentary roof pendants on the west side of the Bargamin Creek fault compared to more widespread and generally older strata on the east side could suggest there was also activity on this part of the fault prior to Cretaceous intrusion as well as after. Motion across the Bargamin Creek fault also transferred southward to the northern extent of the regional Johnson Creek-Profile Gap shear zone (Lund, 2004). At this northern end of the Johnson Creek-Profile Gap shear zone, rocks as young as Eocene dikes locally display deformation fabrics. The relations among Mesoproterozoic roof rocks and Late Cretaceous intrusive rocks on the west and among Eocene intrusive rocks on the east indicate down-to-the-west offset of several kilometers after Eocene intrusions, similar to offsets determined for the Bargamin Creek fault.

Central Scissoring Zone

South of about 45°15', mining districts of the southeastern cluster lie within or east of the Johnson Creek-Profile Gap shear zone (fig. 2). A 3-km long segment in the western Edwardsburg district is the only part of this fault where Mesoproterozoic roof pendants, Late Cretaceous intrusive rocks, and Eocene intrusive rocks are all present on both sides. This segment was intruded by the dikes and small stocks of the Eocene Profile Gap dike swarm, and the fault segment also controlled the location of a subvolcanic complex (fig. 3; the Wolf Fang complex, Lund, 2004). The Late Cretaceous granitic rocks are intensely silicified in a more than 5-km wide zone and discrete shear zones display local, outcrop-scale, dextral ductile structures (Lund, 2004; Montz and others, 2013). North of this segment, the Johnson Creek-Profile Gap has west-side-down offset (See section Northern Area Faults, above) but, south of the segment, the fault had east-side-down offset (See section Southern Area Faults, below). That megascopic evidence indicates that this segment is a zone where dip-slip motion reversed and is thus a zone of scissoring on the fault. Rotational movement would be expected and is probably reflected by the local dextral fabrics.

The silicification and shear fabrics in Late Cretaceous granitic rocks along the fault zone indicate significant activity after emplacement of the Late Cretaceous intrusive rocks. At present, there is no known evidence from older rocks that the fault had pre-Late Cretaceous history. The emplacement of the Eocene Profile Gap dike swarm and subvolcanic complex into the fault zone indicates that the fault controlled Eocene igneous activity and was active during the Eocene.

Southern Area Faults

The southeastern cluster of districts in the central Idaho metallogenic province lies east of a set of large faults (Fisher and others, 1992; Lund, 2004). These faults are the southern extension of a large regional fault system, which includes the Bargamin Creek and related faults at the north and which extend for nearly 100 km from north to south. In the southeastern district cluster, the Johnson Creek-Profile Gap shear zone is the westernmost of the major faults and extends through the Edwardsburg, Profile, and Yellow Pine mining districts (fig. 2). In the southern part of the mineral province, the Meadow Creek and Coin Mountain faults east of the Johnson Creek-Profile Gap shear zone also control and bound mineral deposits in the Yellow Pine-Thunder Mountain districts (figs. 2, 3), which are the most recently mined and explored of the province. Faults at both regional and district scale are distinctly imaged by geophysical methods (Anderson and others, in press). The faults are described separately (see sections "Johnson Creek-Profile Gap Shear Zone", "Meadow Creek Fault Zone", and "Coin Mountain Fault")

Johnson Creek-Profile Gap Shear Zone

Southward from the Edwardsburg district, the Johnson Creek-Profile Gap shear zone is the western boundary of the southeastern cluster of mining districts. Deposits are along the shear zone itself and in the structurally complicated eastern side of the fault. Kinematic conditions in country rocks along the shear zone provide details of the fault movement and mineralization history. Directly following emplacement of the 86–78 Ma granites (Kg, fig. 7), which were cut by the fault, rocks of the study area would have been in a setting of elevated regional geothermal gradient due to the Late Cretaceous crustal thickening, heating, and melting that formed the granites. These granites and metasedimentary country rocks in the shear zone were deformed, silicified, and mineralized as early as 78 Ma (Edwardsburg district, Gammons, 1988). Thus, at 79–78 Ma, the rocks along the shear zone were under viscoplastic (frictional-brittle, see for example, Handy and others, 2007) thermal and strain conditions. Such conditions resulted in foliation of country rocks and plastic deformation of quartz in country rock and early veins (Peterson, 1984) but those conditions also alternated with rock rupture allowing invasion of fluids and formation of veins. These details could indicate depths near the brittle-ductile transition (generally mid-crustal and considered to be at about 10–15 km depths, see for example, Evans and others, 1990) but, given shear zone conditions and regionally elevated geothermal gradient,

Table 4. Sensitive high resolution ion microprobe (SHRIMP) uranium-thorium-lead (U-Th-Pb) data for zircon from intrusive rocks, west-central Idaho.

[Data are available in Aleinikoff and others (2023). Datum for latitude-longitude is WGS 84%, percent; ppm, parts per million; Ma, million years; err, error; ---, no data]

sample*	measured $^{204}Pb/^{206}Pb$	measured $^{207}Pb/^{206}Pb$	% common ^{206}Pb	U (ppm)	Th/U (ppm)	$^{206}Pb^{\dagger}/^{238}U$ (Ma)	err§(Ma)	$^{238}U^{\dagger}/^{206}Pb$	err§(%)	$^{207}Pb^{\dagger}/^{206}Pb$	err§(%)
MC13-91 (Upper Payette Lake foliated hornblende-biotite tonalite) [latitude 45.1040, longitude –116.0316]											
MC13-1.1	---	0.0427	−0.64	246	0.36	88.7	2.1	72.16	2.3	0.0427	9.6
MC13-2.1	---	0.044	−0.48	237	0.43	88.8	2.8	72.06	3.1	0.044	9.6
MC13-3.1	---	0.0447	−0.38	310	0.25	87.6	1.9	73.05	2.2	0.0447	8.6
MC13-4.1	---	0.0483	0.06	188	0.42	89.2	2.2	71.81	2.5	0.0483	10.3
MC13-5.1	---	0.0453	−0.31	232	0.39	87.2	2.1	73.43	2.4	0.0453	9.6
MC13-6.1	0.001526	0.0508	0.39	308	0.38	85.2	2.2	75.13	2.6	0.0278	44.5
MC13-7.1	0.001947	0.0556	0.99	254	0.42	86.3	2.2	74.17	2.5	0.0261	38.9
MC13-8.1	0.002608	0.0501	0.25	203	0.53	96.4	3.6	66.38	3.8	---	---
MC13-9.1	---	0.049	0.1	587	0.16	110.6	1.8	57.81	1.7	0.049	5
MC13-10.1	0.000472	0.0482	0.05	907	0.52	89.9	1.5	71.23	1.7	0.0412	10
MC13-11.1	---	0.0462	−0.20	294	0.26	91.6	2	69.87	2.2	0.0462	8.9
MC13-12.1	---	0.0515	0.48	364	0.2	82.5	1.6	77.6	2	0.0515	6.8
MC13-13.1	---	0.0492	0.18	573	0.15	87.1	1.6	73.49	1.8	0.0492	6.1
MC1-91 (Paddy Flat locally foliated, biotite granodiorite) [latitude 44.7844, longitude –115.8744]											
MC1-1	0.000079	0.0487	0.15	2582	0.67	75.1	0.8	85.32	1.1	0.0476	2.5
MC1-2	---	0.0499	0.3	934	0.27	77.8	0.9	82.33	1.2	0.0499	2.8
MC1-3	0.000459	0.0469	−0.09	372	0.31	80.8	1.2	79.27	1.4	0.0401	9.3
MC1-4	0.00026	0.047	−0.07	391	0.81	78.4	1.1	81.72	1.4	0.0431	6.6
MC1-5	0.000053	0.0485	0.1	2592	0.73	86	0.9	74.46	1.1	0.0477	1.9
MC1-6	---	0.0472	−0.05	349	0.87	79	1.1	81.14	1.4	0.0472	7.9
MC1-7	0.000367	0.0521	0.6	360	0.94	70.7	1	90.67	1.5	0.0467	7.4
MC1-8	---	0.048	0.04	858	0.34	79.9	0.9	80.23	1.2	0.048	2.9
MC1-9	0.000158	0.0481	0.06	655	0.19	77.5	1	82.64	1.3	0.0457	4.4
MC1-10	0.000061	0.0489	0.15	1983	0.73	83.5	0.9	76.69	1.1	0.048	2.2
MC1-11	---	0.0457	−0.25	389	0.64	81.7	1.2	78.42	1.5	0.0457	5
MC1-12	0.000155	0.0475	−0.02	801	0.11	80.3	1	79.78	1.2	0.0452	4.3
MC1-13	---	0.0509	0.41	447	0.2	84.4	1.1	75.87	1.3	0.0509	3.9
MC1-14	---	0.0477	0.01	385	0.72	81.2	1.2	78.87	1.4	0.0477	5
MC1-15	---	0.0458	−0.22	446	1.55	78.1	1.1	82.05	1.4	0.0458	4.4
91KL139 (Chimney Rock muscovite-biotite granite) [latitude 45.3328, longitude –115.7778]											
91KL139-1.1	0.000783	0.0514	0.45	807	0.25	90.4	3.2	71.21	3.6	0.0397	10.6
91KL 139-2.1	0.000316	0.0493	0.2	803	0.17	85.8	3	75.03	3.6	0.0446	6.2
91KL 139-3.1	0.000351	0.0479	0.04	1808	0.11	81.5	2.9	79.06	3.5	0.0427	4.9
91KL 139-4.1	0.000487	0.057	1.18	387	0.27	83.4	3.1	77.23	3.7	0.0499	8.9
91KL 139-5.1	0.001567	0.0656	2.27	1219	0.16	79.5	2.9	81.17	3.7	0.0423	15.8
91KL 139-6.1	0.000466	0.0484	0.09	497	0.17	82.3	3	78.29	3.6	0.0415	8.7
91KL 139-7.1	---	0.0448	−0.36	600	0.55	81.2	2.9	79.31	3.6	0.0448	3.8
91KL 139-8.1	---	0.0488	0.15	410	0.45	81.8	3	78.79	3.7	0.0488	4.4
91KL 139-9.1	---	0.0485	0.1	1558	0.13	84.2	3	76.45	3.5	0.0485	2.5
91KL 139-10.1	0.000646	0.0443	−0.41	294	0.68	78.3	2.9	82.31	3.8	0.0346	16.3
91KL 139-11.1	-0.000532	0.0507	0.38	474	0.28	82.5	3	78.02	3.7	0.0584	9.5
91KL 139-12.1	0.000337	0.0495	0.23	1114	0.11	82.8	2.9	77.79	3.6	0.0445	5.4
91KL 139-13.1	-0.000017	0.048	0.04	2549	0.05	84.6	3	76.16	3.5	0.0483	1.7
91KL 139-14.1	0.000337	0.0491	0.19	860	0.49	80.7	2.9	79.86	3.6	0.0441	6.3
91KL 139-15.1	0.000328	0.0501	0.26	1376	0.26	99.8	3.5	64.49	3.5	0.0452	5.1

Table 4. Sensitive high resolution ion microprobe (SHRIMP) uranium-thorium-lead (U-Th-Pb) data for zircon from intrusive rocks, west-central Idaho.—Continued

[Data are available in Aleinikoff and others (2023). Datum for latitude-longitude is WGS 84%, percent; ppm, parts per million; Ma, million years; err, error; ---, no data]

sample*	measured $^{204}Pb/^{206}Pb$	measured $^{207}Pb/^{206}Pb$	% common ^{206}Pb	U (ppm)	Th/U (ppm)	$^{206}Pb^{\dagger}/^{238}U$ (Ma)	err§(Ma)	$^{238}U^{\dagger}/^{206}Pb$	err§(%)	$^{207}Pb^{\dagger}/^{206}Pb$	err§(%)
MC15-91 (East Fork South Fork muscovite-biotite granite) [latitude 45.0056, longitude –115.7444]											
MC15-1.1	0.000153	0.0459	−0.22	1272	0.26	80.2	0.9	79.88	1.2	0.0436	3
MC15-2.1	0.000127	0.0491	0.2	1087	0.15	77.7	0.8	82.44	1	0.0472	3.2
MC15-3.1	0.000581	0.0488	0.14	2043	1.35	82.6	0.9	77.56	1	0.0402	8.1
MC15-4.1	0.001108	0.0506	0.37	214	0.28	81	1.5	79.12	1.8	0.034	28
MC15-5.1	---	0.0492	0.22	139	0.33	74.6	1.3	85.89	1.8	0.0492	7.2
MC15-6.1	−0.000269	0.0485	0.08	1008	0.11	93.3	1	68.59	1.1	0.0525	4.8
MC15-7.1	---	0.0502	0.31	216	0.24	87	1.2	73.6	1.4	0.0502	4.9
MC15-8.1	0.000373	0.0501	0.32	297	0.4	78.7	1.4	81.39	1.7	0.0446	8.1
MC15-9.1	0.000279	0.0475	−0.01	876	0.71	79.3	0.9	80.83	1.1	0.0434	5.2
MC15-10.1	0.001145	0.0566	1.15	97	0.38	70.9	1.6	90.48	2.3	0.0395	24.3
MC15-11.1	---	0.0483	0.1	604	0.47	77.2	0.9	82.98	1.1	0.0483	3.1
MC15-12.1	0.000835	0.0522	0.59	186	0.22	73.4	1.3	87.34	1.8	0.0398	18.8
MC15-13.1	0.000026	0.0475	−0.04	14579	0	92.6	0.8	69.13	0.9	0.0471	0.7
MC15-14.1	0.000065	0.0492	0.2	4060	0.08	79	0.7	81.1	0.9	0.0482	1.7
MC15-15.1	0.000119	0.047	−0.07	2072	0.04	79.7	0.8	80.41	1	0.0453	1.9
MC15-16.1	---	0.0459	−0.24	309	0.21	90.1	1.1	71.01	1.3	0.0459	4.1
MC15-17.1	---	0.0539	0.8	163	0.57	74.4	1.2	86.15	1.6	0.0539	5.8
MC15-18.1	---	0.0481	0.07	2495	0.1	78.9	0.7	81.22	0.9	0.0481	1.4
MC15-19.1	0.000068	0.0472	−0.05	2637	0.11	77.8	0.8	82.39	1	0.0462	1.8
MC15-19.2	0.000076	0.0465	−0.18	1957	0.28	94.4	1.1	67.82	1.1	0.0454	2.2
MC15-20.1	0.000478	0.0479	0.06	859	0.22	73.7	0.8	86.99	1.1	0.0408	8.1
MC15-20.2	---	0.1771	6.95	348	0.06	2023	18.2	2.71	1	0.1771	0.4
MC15-21.10	---	0.0482	0.07	2110	0.19	79.9	0.8	80.16	1	0.0482	2.1
MC15-22.10	0.000083	0.0472	−0.03	1201	0.4	73.7	0.7	86.99	1	0.046	2.6
MC92-36 (Johnson Creek foliated porphyritic epidote-hornblende-biotite granodiorite) [latitude 44.7861, longitude –115.5285]											
MC92-36-2.1	---	0.0497	0	715	0.39	93.6	0.9	68.4	0.9	0.0497	2.2
MC92-36-3.1	0	0.0467	0	887	0.56	93.7	0.6	68.3	0.6	0.0467	2.1
MC92-36-5.1	0.000141	0.0481	0.26	845	0.61	92.7	0.6	69	0.7	0.0461	3.2
MC92-36-6.1	0.000257	0.0492	0.48	600	0.43	92.8	0.6	68.9	0.6	0.0454	4.7
MC92-36-7.1	0.000308	0.0498	0.57	803	0.5	93.5	1.1	68.4	1.2	0.0452	4.1
MC92-36-8.1	---	0.0504	0	790	0.53	91.3	1.1	70.1	1.2	0.0504	2.2
MC92-36-9.1	0.000035	0.0495	0.07	875	0.53	92.2	1.3	69.4	1.5	0.049	2.4
MC92-36-10.1	0.000206	0.0487	0.38	746	0.48	94.2	0.5	67.9	0.6	0.0456	5.3
MC92-36-11.1	−0.000039	0.0491	−0.07	759	0.47	93.3	0.9	68.6	1	0.0497	2.7
MC92-36-12.1	0.000316	0.0483	0.59	778	0.43	91.9	0.7	69.7	0.7	0.0436	4.6
MC92-36-13.1	0.000062	0.0487	0.12	1359	1.03	95.5	0.9	67	0.9	0.0478	3
MC92-36-14.1	0.000215	0.0483	0.4	856	0.55	92.4	0.7	69.3	0.8	0.0451	3.7
MC92-36-15.1	0.000159	0.0499	0.3	592	0.46	92.5	1.9	69.2	2.1	0.0476	4
MC92-36-16.1	0.000112	0.0486	0.21	830	0.4	93.3	0.8	68.6	0.9	0.0469	3.1
MC92-36-17.1	0.000061	0.0475	0.11	969	0.49	94.8	0.5	67.5	0.6	0.0466	2.5
MC92-36-18.1	0.000029	0.048	0.05	1044	0.42	94.3	0.6	67.9	0.6	0.0475	2.2
MC92-36-19.1	0.000184	0.048	0.34	1026	0.35	93.9	0.8	68.1	0.9	0.0452	3.2
MC92-36-20.1	−0.000051	0.0492	−0.09	1142	0.68	94.4	0.7	67.8	0.8	0.0499	2.1
MC92-36-21.1	0.000178	0.0481	0.33	867	0.55	93.1	0.8	68.8	0.9	0.0454	3.5

Table 4. Sensitive high resolution ion microprobe (SHRIMP) uranium-thorium-lead (U-Th-Pb) data for zircon from intrusive rocks, west-central Idaho.—Continued

[Data are available in Aleinikoff and others (2023). Datum for latitude-longitude is WGS 84%, percent; ppm, parts per million; Ma, million years; err, error; ---, no data]

sample*	measured $^{204}Pb/^{206}Pb$	measured $^{207}Pb/^{206}Pb$	% common ^{206}Pb	U (ppm)	Th/U (ppm)	$^{206}Pb^{\dagger}/^{238}U$ (Ma)	err§(Ma)	$^{238}U^{\dagger}/^{206}Pb$	err§(%)	$^{207}Pb^{\dagger}/^{206}Pb$	err§(%)
MC92-36 (Johnson Creek foliated porphyritic epidote-hornblende-biotite granodiorite) [latitude 44.7861, longitude –115.5285]—Continued											
MC92-36-22.1	0.000128	0.0493	0.24	960	0.66	91.6	0.6	69.9	0.7	0.0474	2.9
MC92-36-1.1r	0.000072	0.0457	0.134	582	0.18	86.4	1.2	74.1	1.4	0.0446	3.7
MC92-36-2.1r	0.001107	0.0494	2.055	292	0.24	88.3	1	72.5	1.1	0.0328	22.1
MC92-36-3.1r	0.001524	0.0652	2.83	560	0.18	88.7	1.8	72.2	2.1	0.0426	14.3
MC92-36-4.1r	0.00008	0.051	0.149	515	0.18	87.2	0.8	73.5	0.9	0.0499	5.5
MC92-36-5.1r	0.002055	0.0505	3.817	324	0.26	83.5	1.6	76.7	2	0.0192	48.4
MC92-36-6.1r	0.001197	0.0478	2.224	410	0.17	87.6	1.7	73.1	1.9	0.0298	21.5
MC92-36-8.1r	0.000458	0.0512	0.851	519	0.18	86.4	1.6	74.1	1.9	0.0444	7.7
MC92-36-10.1r	0.000101	0.0553	0.188	370	0.39	85.2	0.9	75.2	1	0.0538	4.2
MC92-36-11.1r	0.002719	0.0614	5.053	176	0.3	80.8	2.1	79.2	2.6	0.0199	69.3
MC92-36-13.1r	0.000301	0.0543	0.559	563	0.19	84	2.4	76.2	2.8	0.0499	5.3
MC92-36-14.1r	0.003755	0.0567	6.976	365	0.18	81.5	1.9	78.6	2.4	0.0021	559.1
MC92-35 (Pepper Creek foliated hornblende-biotite granodiorite) [latitude 44.9019, longitude –115.3910]											
MC92-35-1.1i	0.000058	0.0458	0.11	917	0.21	95.1	0.5	67.3	0.6	0.0449	2.5
MC92-35-2.1i	0.000267	0.0514	0.5	537	0.11	94.6	0.8	67.7	0.9	0.0475	4.7
MC92-35-3.1i	0.000098	0.0475	0.18	586	0.14	94.8	0.9	67.5	0.9	0.0461	3.4
MC92-35-4.1i	0.000236	0.0457	0.44	492	0.12	94.2	1.1	67.9	1.1	0.0421	8.7
MC92-35-5.1i	0.000268	0.0502	0.5	962	0.17	97.7	0.8	65.5	0.8	0.0462	3.6
MC92-35-6.1i	0.000108	0.0484	0.2	816	0.86	94.8	0.7	67.5	0.8	0.0468	3
MC92-35-7.1i	0.000057	0.0458	0.11	1007	0.24	95.4	1.1	67.1	1.1	0.0449	2.6
MC92-35-9.1i	−0.000092	0.0496	−0.17	949	0.17	97.4	1	65.7	1.1	0.051	5.3
MC92-35-10.1i	0.000064	0.0498	0.12	1320	0.28	98.2	0.7	65.2	0.8	0.0489	2
MC92-35-11.1i	0.000147	0.0488	0.27	1359	0.17	98.1	0.5	65.2	0.6	0.0466	2.5
MC92-35-12.1i	0.000371	0.0492	0.69	958	0.22	95.4	0.7	67.1	0.8	0.0438	4.3
MC92-35-13.1i	−0.000063	0.0469	−0.12	951	0.07	95.9	0.5	66.7	0.6	0.0479	2.4
MC92-35-14.1i	---	0.0469	0	620	0.1	93.7	1	68.3	1.1	0.0469	2.5
MC92-35-16.1i	0.000028	0.0497	0.05	1018	0.19	94.8	0.5	67.5	0.5	0.0493	3.4
MC92-35-17.1i	−0.000126	0.0496	−0.23	943	0.14	95	0.7	67.3	0.8	0.0515	2.6
MC92-35-18.1i	−0.000212	0.0486	−0.39	283	1.32	94.7	0.7	67.6	0.7	0.0517	7.6
MC92-35-19.1i	0	0.0478	0	1663	0.01	95.8	0.5	66.8	0.5	0.0478	1.5
MC92-35-20.1i	0.000122	0.0479	0.23	244	0.85	93.3	1.2	68.6	1.3	0.0461	5.8
MC92-35-21.1i	0.0001	0.0479	0.19	1245	0.11	97	0.6	66	0.6	0.0465	3.6
MC92-35-3.1o	---	0.0461	0	829	0.19	97.7	1.1	65.5	1.1	0.0461	2.1
MC92-35-6.1o	0.000039	0.0476	0.072	932	0.18	96.9	1.3	66	1.3	0.047	2.4
MC92-35-7.1o	−0.000026	0.0485	−0.049	1335	0.26	95.9	0.7	66.7	0.7	0.0489	3.4
MC92-35-8.1o	0.000466	0.0526	0.865	880	0.12	92	2.2	69.5	2.4	0.0457	5.1
MC92-35-9.1o	0.000181	0.046	0.336	444	0.12	93.3	1.6	68.6	1.7	0.0433	5.5
MC92-35-10.1o	0.000049	0.0475	0.091	1228	0.26	98.1	0.6	65.2	0.7	0.0468	1.9
MC92-35-11.1o	0.000163	0.0514	0.302	983	0.19	96.1	1.3	66.6	1.4	0.049	2.9
MC92-35-13.1o	0.00054	0.0518	1.002	835	0.16	97.5	1.2	65.6	1.2	0.0438	5.9

*Analytical sessions: All samples analyzed on the USGS/Stanford SHRIMP-Reverse Geometry. Dates of isotopic measurements: MC13-91 (3/2002), MC1-91 (1/2001), MC91-28 and MC15-91 (10/2002), MC92-36 and MC92-35 cores (10/2017), MC92-36 and MC92-35 rims (12/2017). Sample names abbreviations: r (rim), i (inner area), o (outer area); all other data obtained from analyses of cores.

†Corrected for common Pb using the ^{204}Pb-correction method.

§1-sigma error.

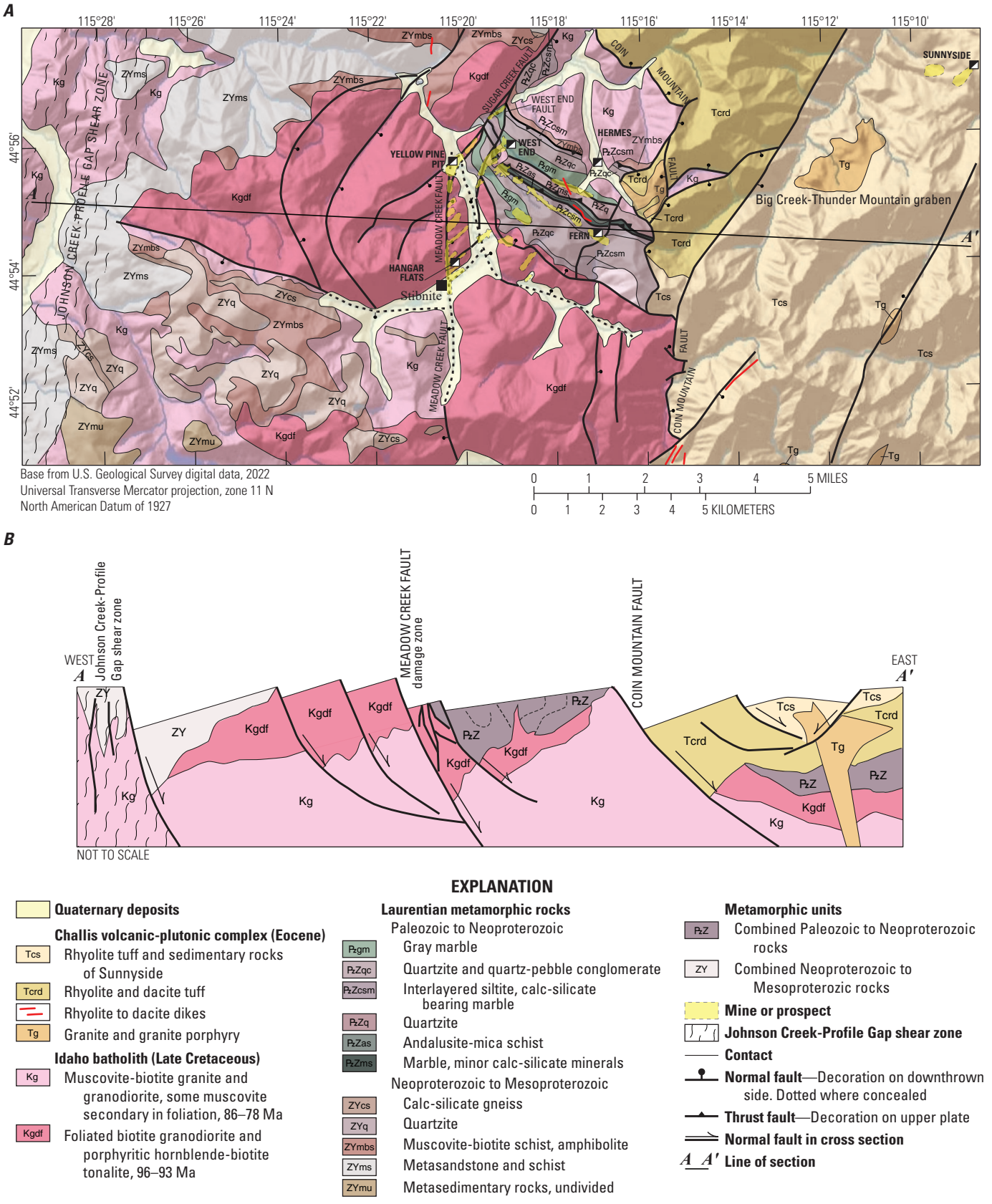

Figure 7. Geologic map of Yellow Pine-Thunder Mountain mining districts. *A*, Geologic map showing new mapping, this study, and modified from Lund (2004; Stewart and others, 2016); *B*, Interpretative section across the map (not to scale). (Ma, million years)

the brittle-ductile transition in these rocks was probably at shallower crustal levels relative to what is expected from the general case. As an analogy, granites that host similar vein deposits in the Buffalo Hump district (figs. 2, 3) formed at depths of less than 9 km and the vein systems formed at between 9 and 4 km based on cooling studies of both the host granites and the precious metal-polymetallic quartz veins (Lund and others, 1986). A similar range of crustal depths are reasonable for initial mineralization along the Johnson Creek-Profile Gap shear zone.

The best evidence for constraining the time for change from viscoplastic to brittle deformational conditions on this shear zone is in the Profile district (fig. 2). There, the country rocks (both metasedimentary and 86–79 Ma granite-granodiorite intrusive rocks) and mineralized quartz veins were deformed in a ductile manner before about 78 Ma and brecciated before emplacement of the about 51 Ma Eocene dikes, indicating that shear zone conditions changed from viscoplastic to brittle between 78 and 51 Ma. Other evidence comes from the antimony and tungsten occurrences along the shear zone, which are breccia replacement and fill deposits that overprinted the earlier quartz-vein related mineralized zones.

The mineralization history substantiates the change from ductile to brittle crustal conditions (Cookro, 1985; Cookro and others, 1988; Gammons, 1988; Bookstrom and others, 1998). Quench textures in the 51 to 45 Ma Eocene dikes indicate they were emplaced at or above 4 km. Some dikes were brecciated, indicating that minor brittle faulting continued after the 51–45 Ma interval (Lund, 2004). Combining depth estimates for mineral deposit formation (previous paragraph) and depths of emplacement for plutonic rocks plus changes in deformation types suggest that a minimum of 5 km of uplift occurred in the fault zone in the 78–45 Ma interval. These are similar to the general conditions found for the southern Atlanta lobe of the Idaho batholith (Fayon and others, 2017). Those approaches for determining fault zone kinematic conditions and crustal depths provide data on changing conditions of country rocks and mineral deposits in the shear zone but do not particularly elucidate contrasting conditions across the zone. Two other lines of evidence provide general estimates of magnitudes for offsets and relative senses of movement.

Our crystallization ages for Atlanta lobe granitic rocks corroborate the presence of rudimentary concentric pluton geometries: older deformed tonalite-granodiorite (96–88 Ma) in outer shells and younger, muscovite-bearing granodiorite and granite (86–78 Ma) as inner zones (fig. 3). The geometry is disrupted across the Johnson Creek-Profile Gap shear zone where a thin roof pendant of the outer shell of foliated 93 Ma porphyritic hornblende-biotite-tonalite is preserved on the west side, whereas that tonalite and 96 Ma foliated granodiorite (combined as Kgdf, fig. 7) are present in thick exposures below metasedimentary roof rocks on the east side. Different elevations at the base of the outer shell suggest different elevations of more than 600 m across the shear zone (figs. 3, 7). The disposition of roof rocks provides another way to estimate post-Cretaceous fault history. There are only a few very small exposures of roof rocks in the western side of the fault but a large amount of metasedimentary rocks compose most of the eastern side (fig. 3). A minimum difference in elevations for the base of the roof rocks across the fault zone is about 1 km. Like the estimate of offset based on concentric shells in the Late Cretaceous granitic rocks, this is a minimum estimate for down-to-the-east offset after about 80 Ma.

Meadow Creek Fault Zone

East of and in the hanging wall of the Johnson Creek-Profile Gap shear zone, the Meadow Creek fault (Shenon and Ross, 1936; White, 1945; Lund, 2004; Stewart and others, 2016) is the key mineral-deposit hosting fault of the Stibnite mining area (figs. 3, 7).

Fault History and Kinematics

On most maps, the Meadow Creek fault is mapped as a continuous structure with a bend from north-striking south of the Yellow Pine pit to northeast-striking northeast of the pit. An early study by Currier (1935; Cooper, 1951) suggested dextral transcurrent movement on the fault based on the change from northwest strikes in metasedimentary rocks south of the Sugar Creek drainage to north strikes along the drainage (fig. 7). Modern mapping shows the fault alternatively as a curved right-lateral strike-slip fault (Stewart and others, 2016) or as a down-to-the-southeast normal fault (Lund, 2004). Because the faults primarily cut plutonic rocks, the kinematic evidence for strike-slip offset was from underground or drillcore offsets of veinlets or dikes or from slickensides (for example, Cooper, 1951), but these minor and rare kinematic indicators could only represent late-stage activity on local fractures.

The foremost argument for the fault segments to be a single right-lateral strike-slip fault is the apparent separation of metasedimentary rocks across Sugar Creek (Stewart and others, 2016). However, mapping and structural interpretations for the present study find that the two-dimensional interpretations using fault separation to determine fault movement and control of mineral deposits are not substantiated in three dimensions, by changes in crustal conditions through time, by stratigraphic details or structures in the roof rocks, or by the near-complete lack of mineral deposits in the similar rocks north or west of the faults. To investigate the role of faulting in the mineralization history more fully, fault segments are described separately in the following paragraph. The Meadow Creek fault is described as the segment that strikes north into the Yellow Pine pit area, the Sugar Creek fault is the northeast-striking fault segment along Sugar Creek, and an aligned unnamed creek southwest of the Yellow Pine pit, and the Yellow Pine pit is in the complex area of fault junctions (fig. 7).

Based on exploration drilling and mine openings (deepest vertical depths of about 250 m), the north-striking Meadow Creek fault is described as steeply west dipping in the Yellow Pine pit, sinuous in some areas to the south, and vertical near the Hangar Flats deposit (Cooper, 1951; Huss and others, 2019). Its deformation zone is 75–300-m wide and locally includes discrete faults, many of which are subparallel, dip steeply east, and are younger than the broad shear zone based on cross-cutting relations (Cooper, 1951). The fault cuts Late Cretaceous granitic rocks along its length. North of Stibnite (fig. 7), the Stibnite roof pendant lies east of the Meadow Creek fault and only granitic rocks are west of the fault (no metasedimentary rocks are preserved above the granitic rocks in this area); these relations indicate significant down-to-the-east fault offset. South of Stibnite, roof pendants are west of the fault, and only granitic rocks are east of the fault; here, the relations indicate down-to-the-west offset. Directly south of Stibnite, the Meadow Creek fault was intersected from the west by a down-to-the-south fault paralleling upper Meadow Creek, and the west-striking fault together with the north-striking Meadow Creek fault bound a down-to-the-west fault block on the west side of the Meadow Creek fault and southwest of Stibnite. This downthrown block southwest of Stibnite is the opposite sense of offset from the downthrown block to the northeast that preserved the southern Stibnite roof pendant (fig. 7). Combined, these relations along the fault indicate that the Meadow Creek fault reversed sense of motion at about Stibnite, and was thus a normal fault with scissored offsets.

The Stibnite roof pendant lies on both sides of the Sugar Creek fault. Late Cretaceous granitic rocks are northwest of the fault but are mostly not present southeast of it. The Stibnite roof pendant northwest of the fault includes large exposures of metasedimentary rocks that are not present in the southern part of the roof pendant southeast of the fault. Additionally, the base of the roof rocks is more than 500 m higher north of the fault than south of it. These details reveal that offset on the Sugar Creek fault after emplacement of the Late Cretaceous granitic rocks was down-to-the-southeast and involved primarily dip-slip, normal sense of movement.

Many secondary faults splay from the east side of the Meadow Creek fault; these include the West End fault and a number of short faults, some illustrated as prospects (fig. 7; White, 1945; Smitherman, 1988; Lund, 2004; Stewart and others, 2016). The West End fault cut off the corner of the Meadow Creek and Sugar Creek faults junction, and the other splays extend from the Meadow Creek fault into its hanging wall. Several more faults east of the Meadow Creek fault bound the southwest side of the Stibnite roof pendant, strike northwest at shallow east dips, and are associated with a zone of foliated granodiorite which commonly also contain secondary-muscovite fabrics. Many dilational fractures with similar northwest strikes cut the main faults in the Yellow Pine pit (Huss and others, 2019) where the Meadow Creek and Sugar Creek faults intersect, suggesting that this orientation may be somewhat younger. Together the northeast-striking splay faults and the northwest-striking faults and related fracture systems accomplished significant extensional foundering of the hanging wall block east and southeast of the two main faults.

The amount of offset for the fault system can be estimated in a general way using details about the Stibnite roof pendant. The elevation difference between the base of the Stibnite roof pendant north of Sugar Creek compared to south of the creek across the Sugar Creek fault is more than 600 m. This 600 m offset would be a minimum amount of down-to-the-southeast offset on the Sugar Creek fault. The southern Stibnite roof pendant on the east side of the Meadow Creek fault is 350–700 m thick (determined from drillhole and map data, Cookro and others, 1988; Stewart and others, 2016). Because there are only granitic rocks without preserved overlying roof pendant rocks west of the Meadow Creek fault, the thickness of the roof pendant across the fault provides a 350–700 m minimum offset for that fault segment. Together, these suggest a minimum amount of normal-sense, down-to-the-southwest offset across the Meadow Creek-Sugar Creek fault system. The other hanging-wall faults cutting granodiorite add an undetermined amount of offset to the total. Additionally, the general sense of southwest dip of strata in the southern Stibnite roof pendant compared to the northeast general direction of younging for strata in the northern part of the pendant, as well as the scissored character of the Meadow Creek fault, suggest rotational motion of the hanging wall block. This motion accounts for the observations of small amounts of late-stage, dextral offsets in veinlets along the Meadow Creek fault zone from mine exposures, as described in the first paragraph this section.

The previous interpretation of dextral strike-slip faulting based on the two-dimensional map offset of parts of the Stibnite roof pendant is further refuted by several additional details. The roof pendant rocks north and south of the Sugar Creek fault are poorly matched (fig. 3; Lund, 2004; Stewart and others, 2016, 2017). The differences between parts of the pendant include: (1) the northern roof pendant includes a broader range in ages of strata, especially due to the thick, older units at the base of the northern part of the roof pendant (north of Sugar Creek) that are absent in the southern part of the roof pendant; (2) the order of map units is different from northern to southern parts of the roof pendant; (3) the structures are not continuous (as demonstrated on both existing geologic maps, Lund, 2004; Stewart and others, 2016) and possibly do not indicate the same sense of fold or thrust-fault vergence. These differences in stratigraphic sections and structure are significant and cannot be reconstructed by retrodeformation of strike-slip translation after Late Cretaceous intrusions or by any conventional structural interpretation involving dipping units. The differences between the northern and southern part of the roof pendant must be due to Late Cretaceous compressional deformation, possibly a tear fault (not necessarily dextral) between different compressional structures. This implied tear zone was subsequently intruded by the Late Cretaceous granitic rocks and reactivated by the presently mappable faults.

Relations between Fault Activity and Mineralizing Phases

Both the Meadow Creek and Sugar Creek faults, plus most of the splay faults associated with the Meadow Creek fault cut foliated granodiorite (96–93 Ma Kgdf, fig. 7) and granite-granodiorite (Kg, fig. 7; as old as 86 Ma, Stewart and others, 2016), indicating that significant fault movements occurred after 86 Ma. As with the Johnson Creek-Profile Gap shear zone, structural preparation for Stibnite area deposits, which lie along or adjacent to the Meadow Creek fault zone, initiated under regionally elevated thermal conditions following granite formation and at crustal depths consistent with post-emplacement viscoplastic deformation (possibly about 9 km depth, see section "Johnson Creek-Profile Gap Shear Zone"). Stibnite area host rocks subsequently shallowed and cooled to brittle conditions (an estimated uplift and [or] erosion of more than 5 km).

This uplift history is linked in progression to protracted mineralization events starting with 86–78 Ma mesothermal vein and disseminated gold deposits (Gammons, 1988; Konyshev and Muntean, 2016), 57 Ma and younger breccia-hosted tungsten and antimony deposits (Lewis, 1984; Cookro and others, 1988; Bookstrom and others, 1998; Gillerman and others, 2019), and 51–45 Ma post-mineral epizonal dikes (White, 1940; Cooper, 1951; Gillerman and others, 2019). The sequence and timing of mineralizing events substantiates the observed sequence of structural phases in the Meadow Creek fault damage zone with its many splays and sets of cross structures. The links between structure and mineralization are especially apparent at the Yellow Pine pit, where the junction between the Meadow Creek and Sugar Creek faults is intensely mineralized, and near splay faults that acted as structural controls for other mineralized zones (fig. 7).

Mercury deposits of the eastern Yellow Pine district are in the Stibnite roof pendant between the mineralized, hanging-wall damage zone of the Meadow Creek-Sugar Creek faults and the Coin Mountain fault. This places the mercury deposits in the eastern mining area higher in the hanging wall, at a shallower structural setting, compared to gold-antimony-tungsten deposits in the adjacent Stibnite mining area. Similarly, mercury mineralization is interpreted and dated as a late-stage assemblage (Schrader and Ross, 1926; Gammons, 1988; Gillerman and others, 2019), possibly related to the Coin Mountain fault and the cauldron complex in its hanging wall.

Coin Mountain Fault

The northwest-striking Coin Mountain fault (figs. 3, 7) juxtaposed Neoproterozoic–Paleozoic roof rocks and Late Cretaceous granite on the west against 49–48 Ma main phases of the Thunder Mountain cauldron complex (John, D., U.S. Geological Survey, 2019, oral commun.) on the east and forms the long southwestern boundary of the cauldron complex (Leonard and Marvin, 1982; Ekren, 1985; Fisher and others, 1992; Lund, 2004; Stewart and others, 2013). The faulted margin is moderately to steeply northeast dipping and experienced enough relative offset that no volcanic deposits are preserved outside (west) of this boundary fault. The map and age relations indicate that most activity on the Coin Mountain fault occurred after eruption of the main, older units of the cauldron complex, thus by about 48 Ma. The Coin Mountain fault was cut by the north-northeast-striking faults, which constrained exposures of the 46.7 Ma younger volcanic deposits and formed the cauldron collapse graben (Hairpin and Thunder Mountain faults, Adams, 1985; southern extent of the Big Creek graben, Stewart and others, 2013) and which extend to the southwest as control for the Pistol Creek dike swarm (fig. 3). Thus, the caldera collapse graben and younger volcanic deposits of the Thunder Mountain district as well as the Pistol Creek dike swarm are coeval features.

Near the eastern margin of the Yellow Pine district, a fault related to, but outside (west) of the graben cut the Coin Mountain fault and exposed a shallowly dipping depositional contact on which older volcanic succession rocks overlie Late Cretaceous granitic rocks (fig. 7; Stewart and others, 2016). This exposure provides evidence for geometries of the Coin Mountain fault and the younger graben as well as the information that the pre-volcanic rocks underlie the older volcanic rocks below the fault and at depths of 350–600 m below most present exposures. The cauldron collapse graben contains more than 900 m of volcanic and volcaniclastic deposits based on elevation differences. These volcanic and pre-volcanic exposures provide a minimum fault offset of about 900 m on the Coin Mountain fault after cessation of volcanic activity.

The Coin Mountain fault localized a rare earth element prospect about 7 km east of Stibnite (Adams, 1968; Cater and others, 1973). These rare-earth-element occurrences are in the fault where Eocene volcanic rocks are in contact with Neoproterozoic–Paleozoic marble and the occurrences extend into the older marble for about 1 km. In this area, the Coin Mountain fault may have reactivated an earlier fault, as evidenced by minor footwall structures that served as the fluid conduits and host sites for mineral deposits, including small copper-rich prospects about 10 km northeast of Stibnite (Shenon and Ross, 1936; Bookstrom and others, 1998) in Neoproterozoic–Paleozoic rocks adjacent to the Coin Mountain fault (Lund, 2004). The 46.7 Ma non-welded rhyolite ash-flow tuff ($^{40}Ar/^{39}Ar$ ages determined on whole rock, John, D., U.S. Geological Survey, 2019, oral commun.) and volcaniclastic units of the central, cauldron-collapse phase host the 43 Ma disseminated gold and silver ore deposits of the Thunder Mountain district ($^{40}Ar/^{39}Ar$ ages determined on adularia; Adams, 1985). Most deposits are in fault-juxtaposed volcaniclastic deposits where the graben-related faults served as conduits for mineralizing fluids that moved laterally into permeable and carbon-rich volcaniclastic layers (Shannon and Reynolds, 1975; Adams, 1985; Parsley, 1997; Bookstrom and others, 1998).

Discussion

The new mapping and geochronologic studies in the region can be combined to provide a more comprehensive picture of individual mining districts, such as the Yellow Pine-Thunder Mountain districts, and provide a region-wide model for location and preservation of districts in the central Idaho mineral province.

Yellow Pine and Thunder Mountain Districts Structural Model

Leonard (1985; Leonard and Christian, 1987) presents a structural and mineral deposit model for southeastern districts in which the mineral-hosting major structures (including Johnson Creek-Profile Gap shear zone and Meadow Creek fault system) are interpreted as Eocene "extra-caldera" subsidence features (ring fractures), although those authors acknowledge deposits are not zoned outward from proposed source calderas. That model is abandoned because the mineral-deposit-hosting faults of the Yellow Pine and Profile districts all display evidence of ductile deformation preceding and associated with 79–78 Ma silicification, alteration, and mineralization activities—significantly prior to the about 49 Ma onset of Eocene volcanism. In another model, Cookro and others (1988) interpret the faults as part of a dextral transcurrent system and identify the Meadow Creek fault as a dextral strike-slip fault along which Stibnite area deposits were localized at an extensional jog. However, details from the metasedimentary roof rocks do not support strike-slip offset. Furthermore, observations that specific mineral deposit types formed at different crustal depths (Cooper, 1951) and that younger, epithermal deposit types overprinted older, mesothermal types (Cookro and others, 1988) cannot be explained by strike-slip faulting.

Observed progressions from viscoplastic to brittle structural conditions, and from deep-seated to shallow ore formation conditions in the mineralized rocks at the same locations, are best explained by normal offset on the bounding structural systems for the following reasons:

1. Aggregate minimum down-to-the east offset for the three major faults of the Yellow Pine-Thunder Mountain districts, as based on map relations, is greater than 1,825 m but there is a more than 5 km difference (possibly up to a 9 km difference) between the original crustal depth of rocks on the west compared to subaerial volcanic rocks on the east. Across the districts, significantly different original crustal levels are juxtaposed across faults and now occur at essentially the same elevations. Thus, Yellow Pine-Thunder Mountain districts extend across listric(?) normal-fault, domino-style blocks, which together form a large, east-tilted crustal block (fig. 7 block model).
2. Overprinted viscoplastic to brittle deformation styles in the Johnson Creek-Profile Gap shear zone and Meadow Creek fault and in related hanging wall domains were caused by (1) initial residence of faulted rocks at depth under viscoplastic conditions and (2) subsequent extensional-fault related changes to shallow crustal levels and brittle conditions.
3. The western and central Yellow Pine mining areas experienced the most prolonged structural activity and display successive overprinted textures, mineralogies, and metal endowments—older mesothermal precious-polymetallic vein deposits overprinted by epithermal gold, antimony, and (or) tungsten deposits in breccia openings in a progression as uplift occurred in those areas. In contrast, the eastern Yellow Pine district manifests simpler and shallower settings in the near-surface hot-springs mercury deposits, and the Thunder Mountain district contains only the Eocene hot-springs gold-silver in near-surface structure- and rock permeability-controlled settings. Thus, mineral-deposit history was influenced by both (1) the kinematic histories displayed in each fault zone (Johnson Creek-Profile Gap shear zone, Meadow Creek fault and related damage zone, Coin Mountain fault, and graben-related faults of the Thunder Mountain district) and (2) the range in crustal depths (that is, crustal conditions) through which each hanging-wall domain progressed during the structural development.
4. A test of the fault geometry interpretation is that similar roof pendant and igneous rocks in the part of the Stibnite roof pendant north of the structures did not experience the structural collapse that formed the tilted crustal block to the south in the Stibnite mining area. That northern area did not experience significant mineralization activities in comparison to the long duration and multiple phases of mineralization that affected the structural block to the south.

Facies Belt Reconstruction as Potential Metallogenic Influences

In the central Idaho mineral province, different lines of evidence reveal linkages between country rock facies belts and metals endowments in ore deposits, allowing the regional distribution of both to be assessed. For Mesoproterozoic strata (Lemhi basin), exposures trace northwest from the east-central Idaho gold±cobalt±copper deposits through the Big Creek and Ramey Ridge districts (southeastern cluster), maintain the northwest strike between the Johnson Creek-Profile Gap shear zone and the Smith Saddle fault although the exposure has a north trending extent, and maintain the northwest strike into districts in the Elk City area west of the Bargamin Creek fault (northwestern cluster, figs. 3, 8). The Neoproterozoic–Paleozoic facies belts are parallel to but lie south of (above)

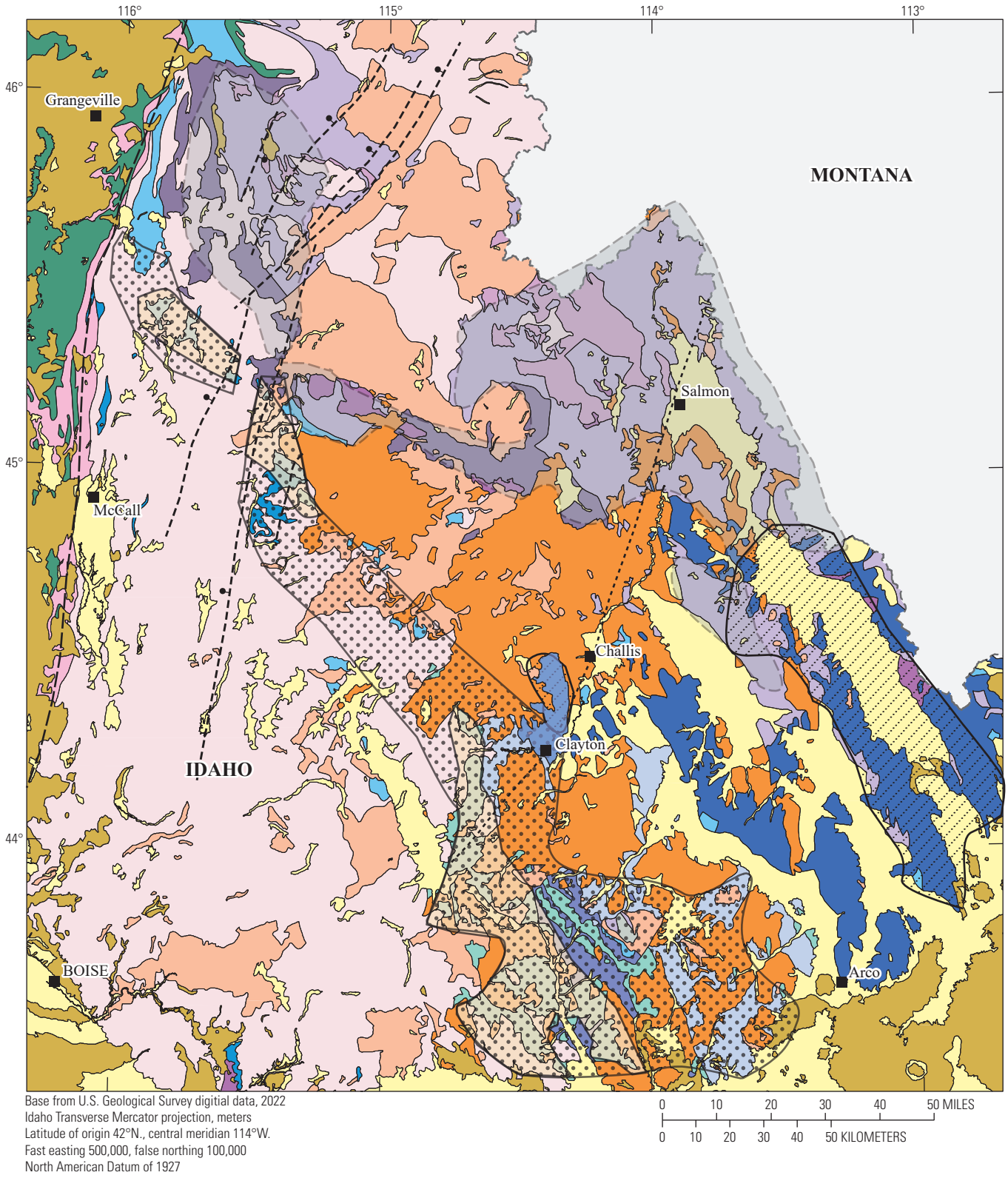

Figure 8. Generalized geologic map of south-central to central Idaho (modified from Lewis and others, 2012; Lund and others, 2016) showing mineral deposit belts.

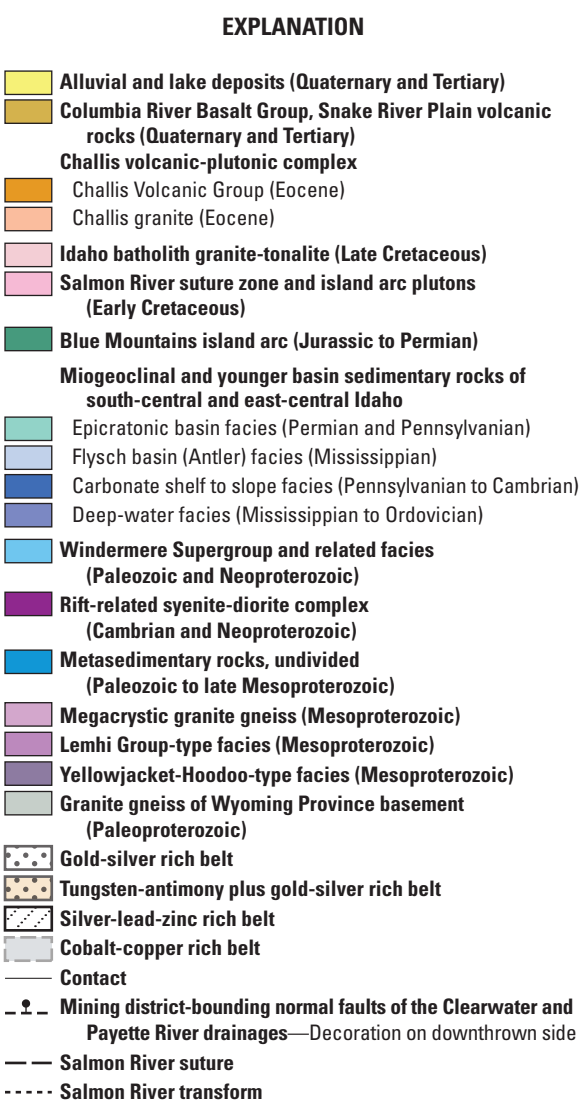

Figure 8. Generalized geologic map of south-central to central Idaho (modified from Lewis and others, 2012; Lund and others, 2016) showing mineral deposit belts.—Continued

the Mesoproterozoic belts. The Neoproterozoic facies belt contains gold-silver±lead-zinc±antimony±tungsten deposits in the Marshall Lake-Resort district but otherwise does not seem to be correlated with mineral deposits. The Paleozoic facies belts of the shelf to slope—which are characterized primarily by carbonate rocks and by lead-zinc deposits in a broad, northwest-striking belt in east-central Idaho—are apparently absent along strike in central Idaho. The stratigraphic and detrital zircon data indicate that parts of the central and western Paleozoic facies belts of south-central Idaho (the deep-water slope, orogenic-basin, and epicratonic-basin strata) are locally present along strike into central Idaho.

At that northwestern extent of central Idaho, the successions may be much thinner, belts much narrowed, and structures complicated but, as with the deep-water slope, orogenic-basin, and epicratonic-basin strata of western south-central Idaho, the central Idaho correlatives are characterized by gold-silver, antimony, and tungsten deposits. From the Yellow Pine and Profiles districts, some parts of these facies belts with their associated metals assemblages trace north to the Edwardsburg district along the Johnson Creek-Profile Gap shear zone and, from where the fault displacement reverses in the Edwardsburg district, rocks that are probably part of this facies belt trace northwest through the Warren and Marshall Lake-Resort districts on the west side of the fault system. The belt apparently terminated at the Salmon River suture as it is not present in the Gospel Peaks roof pendant.

Evidence from deposits in western south-central Idaho indicates that sulfur and metals were sourced from the Pennsylvanian–Permian epicratonic-basin onlap facies in the presence of regional thrust faults that initially juxtaposed those units over the Ordovician–Devonian deep-water facies and that secondarily provided plumbing during successive younger magmatic-hydrothermal events (Hall and others, 1978). Similar genetic linkages seem evident in central Idaho. In addition to equivalent facies and crustal conditions, additional geologic elements are associated with mineral deposits in south-central Idaho. These are northwest-striking synsedimentary basin-deepening structures and Cretaceous thrust faults that juxtaposed facies belts (Hall and others, 1978; Hall, 1985; Hobbs, 1985; Lund and others, 2016). Both of these structural elements probably extend along strike and across the Salmon River transform among the discontinuous exposures into central Idaho (fig. 8), although individual structures would be expected to differ across the transform. Linkages of northwest-striking linear arrays of structures and specific metal endowments with associated facies belts, particularly the belt of gold-antimony-tungsten deposits, support a significant mineral belt from south-central Idaho and diagonally across central Idaho, albeit across the depositional basin and structure transition (transform) at the southern Salmon River Mountains (fig. 8).

The combined lines of evidence about the central Idaho deposits and their host rocks place them at the northwestern extent of a north-northwest striking linear

array of tungsten-endowed mineral deposits. Based on the locations of metals-deposit occurrences (but not necessarily on geologic factors), this trend was previously proposed as a "tungsten belt" by Cook (1956; Savage, 1970; the single significant tungsten occurrence east of the identified tungsten belt, the Ima mine [fig. 4; Anderson, 1948; Cook, 1956] is in the area of Paleozoic-basin deepening faults [Lund and others, 2016]). The presence of tungsten endowments in this trend is strengthened by more recent mineral exploration, regional geochemical data, and mineral-deposit research (Peterson, 1984; Cookro, 1985; Hall, 1985; Hobbs, 1985; Cookro and others, 1988; Gammons, 1988; Skipp and others, 1989; Fisher and others, 1992; Link and others, 1995; Chang and Meinert, 2008; Skipp and Kuntz, 2009). However, at the time that the "tungsten belt" was proposed, the metasedimentary rocks across central Idaho were all mapped as Mesoproterozoic (Ross and Forrester, 1947; Bond, 1978). As presented herein, the newer geologic mapping, dating, and detrital zircon constraints allow the identification of discrete stratigraphic belts of discretely different ages and (or) settings. These facies belts directly correspond to the tungsten belt trend as well as to other types of metals belts that cross the central Idaho mineral province (fig. 8).

In the central Idaho mineral province, the combined Mesoproterozoic through Paleozoic facies belts themselves are southwest dipping (the facies packages young to the southwest; fig. 3). Along the regional-scale Johnson Creek-Profile Gap/Bargamin Creek fault system, the facies belts display a northward step in the area of the reversal of movement on the Johnson Creek-Profile Gap fault. This northward separation could have resulted from some transcurrent displacement prior to Late Cretaceous plutonism, but direct evidence for that is absent. Most, if not all, of the separation across the fault system can be attributed to the large amounts of dip-slip displacement of a thick, southwest-tilted set of the several-aged facies belts across the normal faults.

Role of Regional Faults in Mining District Distribution

The mining districts of central Idaho are linked by the nearly 200-km long, broad zone of subparallel, north-northeast-striking, steep normal faults (primarily the Bargamin Creek and Johnson Creek-Profile Gap faults), which mostly had opposite offsets (figs. 2, 3, 4). Without exception, northern mining districts are located west of the large normal faults, but southern districts are located both within and east of the southern faults.

The timing and magnitudes of faulting affected the ages and styles of mineralization in hanging-wall settings and may have influenced whether the fault zones themselves were mineralized or barren. In the southern part of the mineral province, deposits formed during multiple Late Cretaceous to Eocene structural openings and fluxes of mineralizing fluids related to the Johnson Creek-Profile Gap, and Meadow Creek, and Coin Mountain faults; the continued fault activity also preserved the Thunder Mountain cauldron complex, subvolcanic plutonic rocks, and Eocene gold deposits at near-surface crustal levels in the easternmost hanging-wall fault domino.

In contrast, in the northern part of the province, the Bargamin Creek and linked faults are related to significant Late Cretaceous mineralizing activity and only minor Eocene mineralizing activity but are related to significant gold placer development in Miocene–Holocene fault basins; all placers are in hanging-wall settings. Along with their roles in siting mineral deposits, the regional-scale, steep, Johnson Creek-Profile Gap and Bargamin Creek normal-fault systems controlled the regional positions for stratigraphic facies and mineral belts of central Idaho. Furthermore, these faults controlled the uplift and erosion of deep rocks versus the preservation of shallow crustal levels and, thus, controlled the presence or absence of Late Cretaceous plutonic roof zones and related ore deposits. The offsets of facies belts, localization of associated mineral deposits, and controls of exposed crustal depths across this regional fault system provide guidance for future mineral resource assessments and for exploration of specific metal endowments, whether in igneous or metasedimentary rocks.

The distribution of placer districts with respect to the faults is dissimilar between the two district clusters (compare details of the northwestern and southeastern mining districts in table 2). Large and historically important gold placer districts are a significant characteristic of the hanging wall west of the northern part of the normal-fault system. The gold placers in the Elk City, Newsome-Tenmile, Orogrande, Dixie, Florence, Marshall Lake-Resort, and Warren districts, plus heavy-mineral placers in the Warren and Marshall Lake-Resort districts, all lie west of the down-to-the-west Bargamin Creek-Dixie Meadows-Blanco Creek-Smith Saddle-South Fork faults and the northern part of Johnson Creek-Profile Gap shear zone. Although shallow, near-surface, mostly Eocene deposits are present in the eastern Yellow Pine and Thunder Mountain districts, there are no significant placers associated with the hanging-wall (eastern) side of the down-to-the-east Johnson Creek-Profile Gap, Meadow Creek, and Coin Mountain faults. Farther east, several gold placer districts were historically significant, and these are along a northeast-striking swath near the Salmon River transform. The placer districts in the northwestern district cluster are locally as old as Pleistocene but mostly Holocene. The ages of the placer deposits indicate that structural activity on the northern part of the normal-fault system, including uplift with erosion on one side and basin formation with deposition on the other side, continued into the Holocene. The absence of placer basins east of the southern normal-fault system may reflect that significant fault activity in the southeastern cluster of districts mostly ended in the Eocene.

Conclusions

The fifteen mining districts of the central Idaho mineral province include multiple deposit types of several ages. The presentation of new geologic mapping and geochronology together with evaluation of the geologic settings of mineral deposits identifies common structural, host rock, and age criteria that identify common genetic factors among districts. The derived geologic context for the province provides a new framework to be tested in future resource assessments in this mineral-rich province.

- The many productive active and historic mining districts of the central Idaho metallogenic province are distributed about a nearly 200-kilometer (km) long set of normal faults. The province is segmented into northwestern and southeastern district clusters due to reversal of fault offset along trend.

- Northwestern districts (Elk City, Newsome, Dixie, Buffalo Hump, Florence, Marshall Mountain, Warren) are in hanging-wall settings west of the multiply reactivated Late Cretaceous–Eocene Bargamin Creek and related normal faults. These hanging-wall districts include (1) Late Cretaceous fracture-hosted epigenetic deposits at upper levels of Late Cretaceous muscovite-biotite granite and in metamorphic roof rocks and (2) derivative gold and local heavy-mineral placers in Miocene–Holocene fault basins.

- Southeastern districts are along the Johnson Creek-Profile Gap shear zone (Edwardsburg, Profile, western Yellow Pine) and in hanging-wall settings to the east (Ramey Ridge, Big Creek, eastern Yellow Pine including Stibnite area, Thunder Mountain). Yellow Pine and Thunder Mountain districts are in hanging-wall dominoes that form a large east-tilted crustal block. Deep-seated, 96-million year hornblende granodiorite in the western domino, Stibnite roof pendant in the central domino, and Eocene Thunder Mountain cauldron complex in the eastern domino are all now at similar elevations, with greater than 5 km of difference in original crustal settings (from west to east) and a minimum of 1.8 km of aggregate down-to-east offset across bounding faults.

  - In the western and central Yellow Pine district, a progression from viscoplastic to brittle structural conditions in fault-zone host rocks paralleled changes from mesothermal gold-silver-polymetallic veins to overprinted open-space disseminated gold and to epithermal breccia-fill tungsten-antimony deposits. The eastern Yellow Pine district contains hot springs mercury deposits and, farther east, the Thunder Mountain district contains near-surface epithermal gold deposits.

  - The earliest mesothermal mineralization phase followed closely on the end of Late Cretaceous Idaho batholith magmatism, and the youngest epithermal phases overlapped the onset of shallow Eocene magmatism. Intermediate-aged deposit-forming fluid pulses were amagmatic, coeval with brittle structural events, and probably related to changes in crustal-plate motion.

- Remnants of pre-magmatic country rock—as structurally complex metasedimentary roof pendants in Late Cretaceous plutons—are closely associated with both district clusters. A northern belt of Mesoproterozoic roof pendants and a southern belt of Neoproterozoic–Paleozoic roof pendants characterize each cluster. These paired belts of metamorphic rocks both strike northwest but are offset by, and sheared into, the regional fault system.

  - The northern belt in each district cluster is mapped herein as thrust stacks of Mesoproterozoic Lemhi basin rocks and is associated with gold-silver-copper±cobalt deposits and geochemical associations. This facies belt extends discontinuously from east-central to western Idaho, and this interpretation triples the length of the “Idaho cobalt belt.”

  - The southern belt in each cluster is composed of Neoproterozoic–Paleozoic rocks of the Rodinian rift-related miogeoclinal basin(s). Neoproterozoic Windermere Supergroup rocks are directly dated and can be correlated regionally but are not closely associated with mineral deposits. Youngest Neoproterozoic and Paleozoic rocks are locally identified by mapping characteristics or by detrital zircon data, but are not directly dated, so correlations between pendants cannot be confirmed. Some of the Paleozoic rocks are associated with gold-silver±tungsten±antimony and mercury deposits as well as similar regional geochemical anomalies.

- Paleozoic strata in central Idaho form a relatively narrow belt that consists of metamorphosed sandstone, carbonate, conglomerate, and minor shale protoliths. Both stratigraphic and detrital zircon characteristics demonstrate tectonically active basin settings and variable provenances.

  - The central Idaho segment of the miogeocline apparently lacks thick, early Paleozoic shelf and slope carbonate facies belts and the lead-zinc-silver deposits related to them. It also probably lacks Mississippian flysch-basin carbonaceous facies belt and the gold-rich deposits found in that facies belt. Thus, central Idaho lacks the more complete systematic variation in metals endowments associated with the more complete Paleozoic set of facies in the broad miogeoclinal belt and in the younger orogenic onlap (epicratonic-basin) facies across south-central Idaho districts.

  - The most probable units with similar stratigraphic, detrital zircon, and metal endowment characteristics are wide-spread Ordovician siliciclastic facies and Pennsylvanian–Permian epicratonic-basin facies of western south-central Idaho.

- Contrasts between central Idaho and east- to south-central Idaho reflect segmentation of the miogeoclinal margin across the Salmon River transform. This segmentation provides geologic context for (1) the absence of thick Paleozoic shelf carbonate and deep-water carbonaceous strata with significant lead-zinc-silver deposits in central Idaho but also (2) the continuity of several Paleozoic facies belts (although not discrete geologic units) in association with a region-wide gold-silver-tungsten-antimony mineral belt.

- The central Idaho normal-fault system produced a mapped Z-shape in Mesoproterozoic to Paleozoic metasedimentary facies belts. Along-strike reversal of fault displacement changed the sense of preservation on one side of the fault system and erosional stripping on the other side, such that the location of deeper-seated plutons versus metasedimentary roof pendants or the location of surficial deposits (including volcanic rocks) switches along trend. Fundamentally, the fault system segmented discrete ore-hosting environments and controlled present mineral deposit locations in the central Idaho metallogenic province.

References Cited

Adams, J.W., 1968, Rhabdophane from a rare-earth occurrence, Valley County Idaho, *in* Geological Survey Research 1968: U.S. Geological Survey Professional Paper 600–B, p. B48–B51. [Also available at https://doi.org/10.3133/pp600B.]

Adams, O.F., 1985, Geology and ore deposits of the Thunder Mountain mining district, Valley County, Idaho: Reno, Nev., University of Nevada of Reno, M.S. thesis, 104 p.

Aleinikoff, J.N., Slack, J.F., Lund, K., Evans, K.V., Fanning, C.M., Mazdab, F.K., Wooden, J.L., and Pillers, R.M., 2012, Constraints on the timing of Co-Cu ± Au mineralization in the Blackbird district, Idaho, using SHRIMP U-Pb ages of monazite and xenotime plus zircon ages of related Mesoproterozoic orthogneisses and metasedimentary rocks: Economic Geology, v. 107, no. 6, p. 1143–1175. [Also available at https://doi.org/10.2113/econgeo.107.6.1143.]

Aleinikoff, J.N., Holm-Denoma, C.S., and Lund, K., 2023, SHRIMP U-Pb and LA-ICPMS U-Pb geochronologic data for igneous and metasedimentary rocks in central Idaho mineral province, U.S.A., 2023: U.S. Geological Survey Data Release, https://doi.org/10.5066/P931I3A3.

Alminas, H.V., 1990, Geochemistry of the Elk City 1° × 2° quadrangle, *in* Lund, K., Alminas, H.V., Kleinkopf, M.D., Ehmann, W.J., and Bliss, J.D., eds., Preliminary mineral resource assessment of the Elk City 1° × 2° quadrangle, Idaho and Montana—Compilation of geologic, geochemical, geophysical, and mineral deposits information: U.S. Geological Survey Open-File Report 89–16, 118 p., 14 plates, scale 1:100,000. [Also available at https://doi.org/10.3133/ofr8916.]

Anderson, A.L., 1948, Tungsten mineralization at the Ima mine, Blue Wing district, Lemhi County, Idaho: Economic Geology, v. 43, no. 3, p. 181–206. [Also available at https://doi.org/10.2113/gsecongeo.43.3.181.]

Anderson, A.L., 1951, Metallogenic epochs in Idaho: Economic Geology, v. 46, no. 6, p. 592–607. [Also available at https://doi.org/10.2113/gsecongeo.46.6.592.]

Anderson, E.D., Rodriguez, B.D., Lund, K., Dail, C., and Breen, B., in press, Aeromagnetic and magnetotelluric imaging of west-central Idaho and the Stibnite-Yellow Pine mining district—A regional to district perspective: Economic Geology.

Armstrong, R.L., Hollister, V.F., and Harakel, J., 1978, K-Ar dates for mineralization in the White Cloud–Cannivan porphyry molybdenum belt of Idaho and Montana: Economic Geology, v. 73, no. 1, p. 94–96. [Also available at https://doi.org/10.2113/gsecongeo.73.1.94.]

Baar, E.E., 2009, Determining the regional-scale detrital zircon provenance of the Middle–Late Ordovician Kinnikinic (Eureka) Quartzite, east-central Idaho, U.S.: Pullman, Wash., Washington State University, M.S. thesis, 134 p.

Beckwith, R.H., 1928, The geology and ore deposits of the Buffalo Hump district: Annals of the New York Academy of Sciences, v. 30, no. 1, p. 263–296. [Also available at https://doi.org/10.1111/j.1749-6632.1927.tb55362.x.]

Bennett, E.H., 1980, Granitic rocks of Tertiary age in the Idaho batholith and their relationship to mineralization: Economic Geology, v. 75, no. 2, p. 278–288. [Also available at https://doi.org/10.2113/gsecongeo.75.2.278.]

Beranek, L.P., Link, P.K., and Fanning, C.M., 2016, Detrital zircon record of mid-Paleozoic convergent margin activity in the northern U.S. Rocky Mountains—Implications for the Antler orogeny and early evolution of the North American Cordillera: Lithosphere, v. 8, no. 5, p. 533–550, accessed March 23, 2021, at https://doi.org/10.1130/L557.1.

Black, L.P., Kamo, S.L., Allen, C.M., Davis, D.W., Aleinikoff, J.N., Valley, J.W., Mundil, R., Campbell, I.H., Korsch, R.J., Williams, I.S., and Foudoulis, C., 2004, Improved $^{206}Pb/^{238}U$ microprobe geochronology by the monitoring of a trace-element-related matrix effect—SHRIMP, ID–TIMS, ELA–ICP–MS and oxygen isotope documentation for a series of zircon standards: Chemical Geology, v. 205, no. 1–2, p. 115–140. [Also available at https://doi.org/10.1016/j.chemgeo.2004.01.003.]

Bond, J.G., 1978, Geologic map of Idaho: Idaho Bureau of Mines and Geology, Geologic Map GM–1, scale 1:500,000.

Bookstrom, A.A., Johnson, B.R., Cookro, T.M., Lund, K., Watts, K.C., King, H.D., Kleinkopf, M.D., Pitkin, J.A., Sanchez, J.D., and Causey, J.D., 1998, Potential mineral resources, Payette Nation Forest, Idaho—Description and probabilistic estimation: U.S. Geological Survey Open-File Report 98–219–A, 254 p.

Brennan, D.T., Pearson, D.M., Link, P.K., and Chamberlain, K.R., 2020, Geologic map of the Bayhorse anticline, Custer County, Idaho: Idaho Geological Survey Technical Report 20–1, scale 1:24,000.

Capps, S.R., 1939, The Dixie placer district, Idaho—With notes on the lode mines, by Ralph J. Roberts: Idaho Bureau of Mines and Geology Pamphlet 48, 47 p.

Capps, S.R., 1940, Gold placers of the Secesh Basin, Idaho County, Idaho: Idaho Bureau of Mines and Geology Pamphlet 52, 59 p.

Capps, S.R., 1941, Faulting in western Idaho, and its relation to the high placer deposits: Idaho Bureau of Mines and Geology Pamphlet 56, 20 p.

Carr, J., and Link, P.K., 1999, Neoproterozoic conglomerate and breccia in the formation of Leaton Gulch, Grouse Peak, northern Lost River Range, Idaho—Relation to Beaverhead Impact Structure, *in* Hughes, S.S., and Thackray, G.D., eds., Guidebook to the Geology of Eastern Idaho: Pocatello, Idaho, Idaho Museum of Natural History, p. 21–29.

Cater, F.W., Pinckney, D.M., Hamilton, W.B., Parker, R.L., Weldin, R.D., Close, T.J., and Zilka, N.T., 1973, Mineral resources of the Idaho Primitive Area and vicinity, Idaho: U.S. Geological Survey Bulletin 1304, 431 p., 2 pls. in pocket. [Also available at https://pubs.er.usgs.gov/publication/b1304.]

Chang, Z., and Meinert, L.D., 2008, The Empire Cu-Zn mine, Idaho–Exploration implications of unusual skarn features related to high fluorine activity: Economic Geology, v. 103, no. 5, p. 909–938. [Also available at https://doi.org/10.2113/gsecongeo.103.5.909.]

Chauvot, I.P., 1986, Study of the gold deposits at the War Eagle mine, Idaho County, Idaho: Corvallis, Oreg., Oregon State University, M.S. thesis, 143 p.

Cook, E.F., 1956, Tungsten deposits of south-central Idaho: Idaho Bureau of Mines and Geology Pamphlet 108, 40 p.

Cookro, T.M., 1985, Depositional controls of breccia-fill and skarn tungsten deposits in the Challis quadrangle, chap. Q *of* McIntyre, D.H., ed., Symposium on the geology and mineral deposits of the Challis 1° × 2° quadrangle: U.S. Geological Survey Bulletin 1658–Q, p. 193-202. [Also available at https://doi.org/10.3133/b1658AS.]

Cookro, T.M., Silberman, M.L., and Berger, B.R., 1988, Gold-tungsten-bearing hydrothermal deposits in the Yellow Pine mining district, Idaho, *in* Schafer, R.W., Cooper, J.J., and Vikre, P.G., eds., Bulk mineable precious metal deposits of the western United States: Reno, Nev., Geological Society of Nevada, p. 577–624.

Cooper, J.R., 1951, Geology of the tungsten, antimony, and gold deposits near Stibnite, Idaho: U.S. Geological Survey Bulletin, v. 969–F, p. 151–197.

Currier, L. W., 1935, A preliminary report on the geology and ore deposits of the eastern part of the Yellow Pine district, Idaho: Idaho Bureau of Mines and Geology Pamphlet 43, 27 p.

Criss, R.E., Fleck, R.J., and Taylor, H.P., Jr., 1991, Tertiary meteoric hydrothermal systems and their relation to ore deposition, northwestern United States and southern British Columbia: Journal of Geophysical Research, v. 96, no. B8, p. 13335–13356. [Also available at https://doi.org/10.1029/91JB00640.]

Criss, R.E., and Taylor, H.P., 1983, An $^{18}O/^{16}O$ and D/H study of Tertiary hydrothermal systems in the southern half of the Idaho batholith: Geological Society of America Bulletin, v. 94, no. 5, p. 640–663. [Also available at https://doi.org/10.1130/0016-7606(1983)94<640:AOADSO>2.0.CO;2.]

Dail, C.M., and Zinsser, A., 2020, An update on the geology, geophysics, geochemistry and redevelopment of the world class Au-Sb-W Stibnite mining district, Idaho, *in* Koutz, F.R., and Pennell, W.M., eds., Vison for Discovery, Geological Society of Nevada 2020 Symposium Proceedings: Reno, Nevada, Geological Society of Nevada, p. 1–45.

du Bray, E.A., Holm-Denoma, C.S., Lund, K., and Premo, W.R., 2018, Review of the geochemistry and metallogeny of approximately 1.4 Ga granitoid intrusions of the conterminous United States: U.S. Geological Survey Scientific Investigations Report 2017–5111, 34 p., accessed March 23, 2021, at https://doi.org/10.3133/sir20175111.

Ekren, E.B., 1985, Eocene cauldron-related volcanic events in the Challis quadrangle, chap. C *of* McIntyre, D.H., ed., Symposium on the geology and mineral deposits of the Challis 1° × 2° quadrangle: U.S. Geological Survey Bulletin 1658–C, p. 43–58. [Also available at https://doi.org/10.3133/b1658AS.]

Erdman, J.A., Moye, F.J., Skipp, B., and Theobald, P.K., 1995, Geochemical evidence for epithermal metallization in Mississippian turbidites of the McGowan Creek Formation, Lava Creek Mining District, south-central Idaho, chap. O *of* Worl, R.G., Link, P.K., Winkler, G.R., and Johnson, K.M., eds., Geology and mineral resources of the Hailey 1° × 2° quadrangle and the western part of the Idaho Falls 1° × 2° quadrangle, Idaho: U.S. Geological Survey Bulletin 2064–O, 26 p. [Also available at https://doi.org/10.3133/b2064AR.]

Evans, B., Fredrich, J.T., and Wong, T.-F., 1990, The brittle-ductile transition in rocks—Recent experimental and theoretical progress, *in* Duba, A.G., Durham, W.B., Handin, J.W., Wang, H.F., eds., The brittle-ductile transition in rocks: Geophysical Monograph, v. 56, p. 1–20. [Also available at https://doi.org/10.1029/GM056p0001.]

Evans, K.V., and Zartman, R.E., 1990, U-Th-Pb and Rb-Sr geochronology of middle Proterozoic granite and augen gneiss, Salmon River Mountains, east-central Idaho: Geological Society of America Bulletin, v. 102, no. 1, p. 63–73. [Also available at https://doi.org/10.1130/0016-7606(1990)102<0063:UTPARS>2.3.CO;2.

Fayon, A.K., Tikoff, B., Kahn, M., and Gaschnig, R.M., 2017, Cooling and exhumation of the southern Idaho batholith: Lithosphere, v. 9, no. 2, p. 299–314, accessed March 23, 2021, at https://doi.org/10.1130/L565.1.

Fisher, F.S., 1985, Summary of the geology, mineral deposits, and resource potential for selected commodities in the Challis quadrangle, chap. A *of* McIntyre, D.H., ed., Symposium on the geology and mineral deposits of the Challis 1° × 2° quadrangle: U.S. Geological Survey Bulletin 1658–A, p. 3–28. [Also available at https://doi.org/10.3133/b1658AS.]

Fisher, F.S., McIntyre, D.H., and Johnson, K.M., 1992, Geologic map of the Challis 1° × 2° quadrangle, Idaho: U.S. Geological Survey Miscellaneous Investigations Series Map I–1819, 39 p., scale 1:250,000. [Also available at https://pubs.usgs.gov/imap/i-1819/.]

Gammons, C.H., 1988, Studies in hydrothermal phenomena—(2) a paragenesis and fluid inclusion study of polymetallic vein mineralization in the Big Creek mining district, Valley County, Idaho: University Park, Penn., Pennsylvania State University, Ph.D. thesis, p. 73–337.

Gammons, C.H., Rose, A.W., Snee, L.W., and Lund, K., 1985, Paragenesis, fluid inclusions, and Ar dating of the Big Creek mining district, Valley County, central Idaho [abs.]: Geological Society of America Abstracts with Programs, v. 17, p. 588.

Gaschnig, R.M., Vervoort, J.D., Lewis, R.S., and McClelland, W.C., 2010, Migrating magmatism in the northern US Cordillera—In situ U-Pb geochronology of the Idaho batholith: Contributions to Mineralogy and Petrology, v. 159, no. 6, p. 863–883. [Also available at https://doi.org/10.1007/s00410-009-0459-5.]

Gaschnig, R.M., Vervoort, J.D., Lewis, R.S., and Tikoff, B., 2013, Probing for Proterozoic and Archean crust in the northern U.S. Cordillera with inherited zircon from the Idaho batholith: Geological Society of America Bulletin, v. 125, no. 1–2, p. 73–88. [Also available at https://doi.org/10.1130/B30583.1.]

Gillerman, V.J.S., Schmitz, M.D., Benowitz, J.A., and Layer, P.W., 2019, Geology and temporal evolution of alteration and Au-Sb-W mineralization, Stibnite mining district, Idaho: Idaho Geological Survey Bulletin B–31, 149 p. [Also available at https://www.idahogeology.org/product/B-31.]

Grader, G.W., and Dehler, C.M., 1999, Devonian stratigraphy in east-central Idaho—New perspectives from the Lemhi Range and Bayhorse area, *in* Hughes, S.S., and Thackray, G.D., eds., Guidebook to the geology of eastern Idaho: Pocatello, Idaho, Idaho Museum of Natural History, p. 29–54.

Green, W.R., 1972, Delineation of mineral belts of northern and central Idaho: Idaho Bureau of Mines and Geology Information Circular, no. 22, 8 p.

Greenwood, W.R., and Morrison, D.A., 1973, Reconnaissance geology of the Selway-Bitterroot Wilderness Area: Idaho Bureau of Mines and Geology Pamphlet 154, 30 p.

Gustafson, J., 1987, Mining districts of the state of Idaho: Idaho Bureau of Mines and Geology Map 6, scale 1:1,000,000.

Hahn, G.A., and Hughes, G.J., 1984, Sedimentation, tectonism, and associated magmatism of the Yellowjacket Formation in the Idaho cobalt belt, Lemhi County, Idaho: Montana Bureau of Mines Special Publication 90, p. 65–67.

Hall, W.E., 1985, Stratigraphy of and mineral deposits in middle and upper Paleozoic rocks of the black-shale mineral belt, central Idaho, *in* McIntyre, D.H., ed., Symposium on the geology and mineral deposits of the Challis 1° × 2° quadrangle: U.S. Geological Survey Bulletin 1658–J, p. 118–131.

Hall, W.E., Rye, R.O., and Doe, B.R., 1978, Wood River mining district, Idaho Intrusion-related lead-silver deposits derived from country rock source: U.S. Geological Survey Journal of Research, v. 6, no. 5, p. 579–592. [Also available at https://pubs.er.usgs.gov/publication/70156358.]

Handy, M.R., Hirth, G., and Bürgmann, R., 2007, Continental fault structure and rheology from the frictional-to-viscous transition downward, chap. 6 *of* Handy, M.R., Hirth, G., and Hovius, N., eds., Tectonic faults—Agents of change on a dynamic Earth: Cambridge, Mass., The MIT Press, Dahlem Workshop Report 95, p. 139–181. [Also available at https://doi.org/10.7551/mitpress/6703.003.0008.]

Hardyman, R.F., 1985, The Twin Peaks Caldera and associated ore deposits, *in* McIntyre, D.H., ed., Symposium on the geology and mineral deposits of the Challis 1° × 2° quadrangle: U.S. Geological Survey Bulletin 1658–G, p. 97–106.

Hardyman, R.F., and Fisher, F.S., 1985, Rhyolite intrusions and associated mineral deposits in the Challis volcanic field, Challis quadrangle, *in* McIntyre, D.H., ed., Symposium on the geology and mineral deposits of the Challis 1° × 2° quadrangle: U.S. Geological Survey Bulletin 1658–N, p. 167–180.

Hobbs, W.S., 1985, Structural and stratigraphic controls of ore deposits in the Bayhorse area, Idaho, *in* McIntyre, D.H., ed., Symposium on the geology and mineral deposits of the Challis 1° × 2° quadrangle: U.S. Geological Survey Bulletin 1658–K, p. 133–140.

Hobbs, S.W., and Hays, W.H., 1990, Ordovician and older rocks of the Bayhorse area, Custer County, Idaho: U.S. Geological Survey Bulletin 1891, 40 p.

Hobbs, S.W., Hays, W.H., and McIntyre, D.H., 1991, Geologic map of the Bayhorse area, central Custer County, Idaho: U.S. Geological Survey Miscellaneous Geologic Investigations Map I–1882, scale 1:62,500.

Hughes, G.J., Jr., 1983, Basinal setting of the Idaho cobalt belt, Blackbird mining district, Lemhi County, Idaho, *in* Ranta, D.E., Kamilli, R.J., and Pansze, A.J., eds., The genesis of Rocky Mountain ore deposits—Changes with time and tectonics: Denver Region Exploration Geologists Society, 1983 Symposium Proceedings, p. 21–27.

Huss, C.E., Kirkham, G.D., Martin, C.J., Marek, J.M., Anderson, A.R., Kinder, R.C., and Kowalewski, P.E., 2019, Stibnite gold project—Prefeasibility study technical report: Midas Gold, M3 report, 650 p., accessed March 23, 2021, at https://perpetuaresources.com/wp-content/uploads/2019/10/midas-gold-stibnite-gold-project-2014-pfs.pdf.

Idaho State Historical Society, 1985, Mining in Idaho: Idaho State Historical Society Reference Series no. 9, 26 p.

Isaacson, P.E., Bachtel, S.L., and McFaddan, M.D., 1983, Stratigraphic correlation of the Paleozoic and Mesozoic rocks of Idaho: Idaho Bureau of Mines and Geology, Information Circular no. 37, 4 p.

Isakson, V.H., 2017, Geochronology of the tectonic, stratigraphic, and magmatic evolution of Neoproterozoic to early Paleozoic, North American Cordillera and Cryogenian glaciation: Boise, Idaho, Boise State University, Ph.D. thesis, 682 p.

Johnson, R., Close, T., and McHugh, E., 1998, Mineral resource appraisal of the Salmon National Forest, Idaho: U.S. Geological Survey Open-File Report 98–478, 277 p. [Also available at https://doi.org/10.3133/ofr98478.]

Kiilsgaard, T.H., and Bennett, E.H., 1985, Mineral deposits in the southern part of the Atlanta lobe of the Idaho batholith and their genetic relation to Tertiary intrusive rocks and to faults, *in* McIntyre, D.H., ed., Symposium on the geology and mineral deposits of the Challis 1° × 2° quadrangle: U.S. Geological Survey Bulletin 1658–M, p. 153–166.

Klein, T.L., and Sims, P.K., 2007, Control of epigenetic metal deposits by Paleoproterozoic basement architecture, *in* Lund, K., ed., Earth science studies in support of public policy development and land stewardship—Headwaters province, Idaho and Montana: U.S. Geological Survey Circular 1305, p. 17–26. [Also available at https://pubs.usgs.gov/circ/1305/.]

Knowles, C.R., and Bennett, E.H., 1978, Reconnaissance geology and geochemistry of the Gospel Peak-Buffalo Hump Wilderness Area, Idaho County, Idaho: Idaho Bureau of Mines and Geology Technical Report 78–5, 24 p. [Also available at https://www.idahogeology.org/product/T-78-5.]

Konyshev, S.A., and Muntean, J.L., 2016, Diversity of sedimentary-rock hosted gold deposits in the Stibnite mining district, Idaho [abs.]: Geological Society of America Abstracts with Programs, v. 48, no. 7. [Also available at https://doi.org/10.1130/abs/2016AM-281194.]

Krohe, N.J., Brennan, D.T., Link, P.K., Pearson, D.M., and Armstrong, L.T., 2020, Geologic map of the southern portion of the Clayton quadrangle, Custer County, Idaho: Idaho Geological Survey Technical Report 20–02, scale 1:24,000.

Larsen, E.S., and Livingston, D.C., 1921, Geology of the Yellow Pine cinnabar-mining district, Idaho: U.S. Geological Survey Bulletin, v. 715, p. 73–83.

Lasmanis, R., 1981, West End gold deposits, Yellow Pine mining district, Idaho—Preprint, *in* 87th Annual Northwest Mining Association Convention—Spokane, Washington, December 3–5, 1981 [proceedings]: Northwest Mining Association, 13 p.

Leonard, B.F., 1962, Old metavolcanic rocks of the Big Creek area, central Idaho, *in* Short papers in geology, hydrology, and topography; Articles 1–59: U.S. Geological Survey Professional Paper 450B, p. B11–B15. [Also available at https://doi.org/10.3133/pp450B.]

Leonard, B.F., 1985, Ore deposits related to the Thunder Mountain caldera complex, *in* McIntyre, D.H., ed., Symposium on the geology and mineral deposits of the Challis 1° × 2° quadrangle: U.S. Geological Survey Bulletin 1658–H, p. 107.

Leonard, B.F., and Christian, R.P., 1987, Residence of silver in mineral deposits of the Thunder Mountain caldera complex, central Idaho, U.S.A: Mineralogy and Petrology, v. 36, no. 3–4, p. 151–168. [Also available at https://doi.org/10.1007/BF01163257.]

Leonard, B.F., and Marvin, R., 1982, Temporal evolution of the Thunder Mountain caldera and related features, central Idaho, *in* Bonnichsen, B., and Breckenridge, R.M., eds., Cenozoic geology of Idaho: Idaho Bureau of Mines and Geology Bulletin 26, p. 23–41.

Lewis, R.D., 1984, Geochemical investigations of the Yellow Pine, Idaho and Republic, Washington mining districts: West Lafayette, Ind., Purdue University, Ph.D. thesis, 204 p.

Lewis, R.S., Burmester, R.F., and Bennett, E.H., 1998, Metasedimentary rocks between the Bitterroot and Atlanta lobes of the Idaho batholith and their relationship to the Belt Supergroup, *in* Berg, R.B., ed., Belt symposium III, Whitefish, Montana, August 14–21, 1993: Montana Bureau of Mines and Geology Special Publication 112, p. 130–144.

Lewis, R.S., Burmester, R.F., Bennett, E.H., and White, D.L., 1990, Preliminary geologic map of the Elk City region, Idaho County, Idaho: Idaho Geological Survey Technical Report 90–2, scale 1:100,000, 6 p.

Lewis, R.S., Link, P.K., and Long, S.P., 2012, Geologic map of Idaho: Idaho Geological Survey Map M–9, scale 1:750,000.

Lewis, R.S., Vervoort, J.D., Burmester, R.F., and Oswald, P.J., 2010, Detrital zircon analysis of Mesoproterozoic and Neoproterozoic metasedimentary rocks of north-central Idaho—Implications for development of the Belt-Purcell basin: Canadian Journal of Earth Sciences, v. 47, no. 11, p. 1383–1404. [Also available at https://doi.org/10.1139/E10-049.]

Lindgren, W., 1904, A geological reconnaissance across the Bitterroot Range and Clearwater Mountains in Montana and Idaho: U.S. Geological Survey Professional Paper 27, 123 p. [Also available at https://doi.org/10.3133/pp27.]

Link, P.K., Fanning, C.M., Lund, K., and Aleinikoff, J.N., 2007, Detrital-zircon populations and provenance of Mesoproterozoic strata of east-central Idaho, U.S.A.—Correlation with the Belt Supergroup of southwest Montana: Society for Sedimentary Geology Special Publication 86, p. 101–128.

Link, P.K., Mahon, R.C., Beranek, L.P., Campbell-Stone, E.A., and Lynds, R., 2014, Detrital zircon provenance of Pennsylvanian to Permian sandstones from the Wyoming craton and Wood River basin, Idaho, U.S.A: Rocky Mountain Geology, v. 49, no. 2, p. 115–136, accessed March 23, 2021, at https://doi.org/10.2113/gsrocky.49.2.115.

Link, P.K., Mahoney, J.B., Brimer, D.J., Batatian, L.D., Wilson, E., and Williams, F.J.C., 1995, Stratigraphic setting of sediment-hosted mineral deposits in the eastern part of the Hailey 1° × 2° quadrangle and part of the southern part of the Challis 1° × 2° quadrangle, south-central Idaho, chap. C *of* Worl, R.G., Link P.K., Winkler, G.R., and Johnson, K.M., eds., Geology and mineral resources of the Hailey 1° × 2° quadrangle and the western part of the Idaho Falls 1° × 2° quadrangle, Idaho: U.S. Geological Survey Bulletin 2064–C, 33 p., 1 pl., scale 1:100,000. [Also available at https://pubs.usgs.gov/bul/b2064-c/.]

Lithgow-Bertelloni, C., and Richards, M.A., 1998, The dynamics of Cenozoic and Mesozoic plate motions: Reviews of Geophysics, v. 36, no. 1, p. 27–78. [Also available at https://doi.org/10.1029/97RG02282.]

Liu, L., Spasojević, S., and Gurnis, M., 2008, Reconstructing Farallon plate subduction beneath North America back to the Late Cretaceous: Science, v. 322, no. 5903, p. 934–938. [Also available at https://doi.org/10.1126/science.1162921.]

Lorain, S.H., 1938, Gold mining and milling in Idaho County, Idaho: U.S. Bureau of Mines Information Circular 7039, 90 p.

Lorain, S.H., and Metzger, O.H., 1938, Reconnaissance of placer mining districts in Idaho County, Idaho: U.S. Bureau of Mines Information Circular 7023, 93 p.

Ludwig, K.R., 2003, Isoplot/Ex version 3.00, a geochronological toolkit for Microsoft Excel: Berkeley, Calif., Berkeley Geochronology Center Special Publication 4, 73 p.

Ludwig, K.R., 2009, SQUID 2—A user's manual, rev. 12 April, 2009: Berkeley Geochronology Center Special Publication 5, 110 p.

Lund, K., 1984, Tectonic history of a continent-island arc boundary—West-central Idaho: University Park, Penn., Pennsylvania State University, Ph.D. dissertation, 207 p.

Lund, K., 2004, Geology of the Payette National Forest and vicinity, Valley, Idaho, Washington, Adams, and Gem Counties, west-central Idaho: U.S. Geological Survey Professional Paper 1666, 89 p., 2 plates, scale 1:100,000, accessed September 30, 2022, at https://doi.org/10.3133/pp1666.

Lund, K., 2008, Geometry of the Neoproterozoic and Paleozoic rift margin of western Laurentia—Implications for mineral deposit settings: Geosphere, v. 4, no. 2, p. 429–444, accessed March 23, 2021, at https://doi.org/10.1130/GES00121.1.

Lund, K., Aleinikoff, J.N., Evans, K.V., duBray, E.A., Dewitt, E.H., and Unruh, D.M., 2010, SHRIMP U-Pb dating of recurrent Cryogenian and Late Cambrian-Early Ordovician alkalic magmatism in central Idaho—Implications for Rodinian rift tectonics: Geological Society of America Bulletin, v. 122, no. 3–4, p. 430–453, also available at https://doi.org/10.1130/B26565.1.

Lund, K., Aleinikoff, J.N., Evans, K.V., and Fanning, C.M., 2003, SHRIMP U-Pb geochronology of Neoproterozoic Windermere Supergroup, central Idaho—Implications for rifting of western Laurentia and synchroneity of Sturtian glacial deposits: Geological Society of America Bulletin, v. 115, no. 3, p. 349–372. [Also available at https://doi.org/10.1130/0016-7606(2003)115<0349:SUPGON>2.0.CO;2.]

Lund, K., Aleinkoff, J.N., Evans, K.V., and Kunk, M.J., 2004, Proterozoic basins and orogenic belts of central Idaho [abs.]: Geological Society of America Abstracts with Programs, v. 36, no. 5, p. 271.

Lund, K.I., Aleinikoff, J.N., Yacob, E.Y., Unruh, D.M., and Fanning, C.M., 2008, Coolwater culmination—Sensitive high-resolution ion microprobe (SHRIMP) U-Pb and isotopic evidence for continental delamination in the Syringa embayment, Salmon River suture, Idaho: Tectonics, v. 27, no. 2, article no. TC2009, 32 p. [Also available at https://doi.org/10.1029/2006TC002071.]

Lund, K., Box, S.E., Holm-Denoma, C.S., San Juan, C.A., Blakely, R.J., Saltus, R.W., Anderson, E.D., and DeWitt, E.H., 2015, Basement domain map of the conterminous United States and Alaska: U.S. Geological Survey Data Series 898, 41 p., accessed March 23, 2021, at https://doi.org/10.3133/ds898.

Lund, K., and Cheney, E.S., 2016, Unconformity-bounded sequences of the Neoproterozoic Windermere Supergroup in the Pacific Northwest, USA, *in* Cheney, E.S., Troost, K., and Sherrod, B., eds., The geology of Washington and beyond—From Laurentia to Cascadia: Seattle, Wash., University of Washington Press, p. 28–42.

Lund, K., and Esparza, L.E., 1990, Mineral resources of the Gospel-Hump Wilderness, Idaho County, Idaho: U.S. Geological Survey Bulletin 1812, 19 p.

Lund, K., and Snee, L.W., 1988, Metamorphic and structural development of the continent-island arc juncture in west-central Idaho, *in* Ernst, W.G., ed., Metamorphism and crustal evolution of the western conterminous United States: Rubey Colloquium no. 7, p. 296–331.

Lund, K., Snee, L.W., and Evans, K.V., 1986, Age and genesis of precious metals deposits, Buffalo Hump district, central Idaho—Implications for depth of emplacement of quartz veins: Economic Geology, v. 81, no. 4, p. 990–996. [Also available at https://doi.org/10.2113/gsecongeo.81.4.990.]

Lund, K., and Tysdal, R.G., 2007, Stratigraphic and structural setting of sediment-hosted Blackbird gold-cobalt-copper deposits, east-central Idaho, U.S.A., *in* Link, P.K., and Lewis, R.S., eds., Proterozoic geology of western North America and Siberia: Society for Sedimentary Geology Special Publication 86, p. 129–147. [Also available at https://doi.org/10.2110/pec.07.86.0129.]

Lund, K., Tysdal, R.G., Evans, K.V., Kunk, M.J., and Pillers, R.M., 2011, Structural controls and evolution of gold-, silver-, and REE-bearing copper-cobalt ore deposits, Blackbird district, east-central Idaho—Epigenetic origins: Economic Geology, v. 106, no. 4, p. 585–618. [Also available at https://doi.org/10.2113/econgeo.106.4.585.]

Lund, K., Zürcher, L., Hofstra, A.H., Van Gosen, B.S., Benson, M.E., Box, S.E., Anderson, E.D., Bleiwas, D.I., DeAngelo, J., Drake, R.M., II, Fernette, G.L., Giles, S.A., Glen, J.M.G., Haacke, J.E., Horton, J., John, D.M., Robinson, G.R., Jr., Rockwell, B.W., San Juan, C.A., Shaffer, B.N., Smith, S.M., and Williams, C.F., 2016, Geology and mineral resources of the North-Central Idaho Sagebrush Focal Area, chap. C *of* Mineral resources of the Sagebrush Focal Areas of Idaho, Montana, Nevada, Oregon, Utah, and Wyoming: U.S. Geological Survey Scientific Investigations Report 2016–5089–C, 147 p., accessed March 23, 2021, at https://doi.org/10.3133/sir20165089C.

Mahoney, J.B., Link, P.K., Burton, B.R., Geslin, J.K., and O'Brien, J.P., 1991, Pennsylvanian and Permian Sun Valley Group, Wood River Basin, south-central Idaho, *in* Cooper, J.D., and Stevens, C.H., eds., Paleozoic paleogeography of the Western United States-II—Pacific Section: Society of Economic Paleontologists and Mineralogists, Publication 67, v. 2, p. 551–580.

May, T.P., 1984, The geology of a portion of the Marshall Lake district, Idaho County, Idaho: Moscow, Idaho, University of Idaho, M.S. thesis, 101 p.

McCandless, D.O., 1982, A reevaluation of Cambrian through Middle Ordovician stratigraphy of the southern Lemhi Range: University Park, Pennsylvania, Pennsylvania State University, M.S. thesis, 157 p.

McFadden, M.D., Measures, E.A., and Isaacson, P.E., 1988, Early Paleozoic continental margin development, central Idaho, *in* Link, P.K., and Hackett, W.R., eds., Guidebook to the geology of central and southern Idaho: Idaho Geological Survey Bulletin 27, p. 129–152.

McIntyre, D.H., and Johnson, K.M., 1985, Epithermal gold-silver mineralization related to volcanic subsidence in the Custer graben, Custer County, Idaho, *in* McIntyre, D.H., ed., Symposium on the geology and mineral deposits of the Challis 1° × 2° quadrangle: U.S. Geological Survey Bulletin 1658–I, p. 110–115.

Mitchell, V.E., 2000, History of the Golden Anchor mine, Idaho County, Idaho: Idaho Geological Survey Staff Report 00-11, 28 p. [Also available at https://idahogeology.org/pub/Staff_Reports/2000/S-00-11.pdf.]

Montz, W.J., Kedenburg, M., Tikoff, B., Giorgis, S.D., Vervoort, J.D., Gaschnig, R.M., and Byerly, A., 2013, The Deadwood deformation zone, central Idaho—Constraints on timing and fabric development [abs.]: Geological Society of America Abstracts with Programs, v. 45, no. 7, p. 813.

Panneerselvam, K., Macfarlane, A.W., and Salters, V.J.M., 2012, Reconnaissance lead isotope characteristics of the Blackbird deposits—Implications for the age and origin of cobalt-copper mineralization in the Idaho cobalt belt, United States: Economic Geology, v. 107, no. 6, p. 1177–1188. [Also available at https://doi.org/10.2113/econgeo.107.6.1177.]

Parsley, P.G., 1997, Geology and ore mineralization of the Dewey deposit, Thunder Mountain mining district, Valley County, Idaho [abs], *in* Pacific Northwest Metals and Minerals Conference, Columbia Section, Spokane, Wash., April 23–25, 1997, Proceedings: Englewood, Colo., Society for Mining, Metallurgy, and Exploration, Inc., p. 13.

Pearson, D.M., and Link, P.K., 2021, Post-Belt Supergroup Mesoproterozoic to Cambrian rocks of the Leaton Gulch area, east of Challis, Idaho: Northwest Geology v. 50, p. 11-21. [Also available at https://www2.cose.isu.edu/~peardavi/_Pearson-Link_2021_NWGeo-article.pdf.]

Peterson, M.A., 1984, Geology and mineralization at the Quartz Creek tungsten mine, Yellow Pine, Idaho: Kent, Ohio, Kent State University, M.S. thesis, 80 p.

Reed, J.C., 1934, Gold-bearing gravel of the Nez Perce National Forest, Idaho County, Idaho: Idaho Bureau of Mines and Geology Pamphlet 40, 26 p.

Reed, J.C., 1937, Geology and ore deposits of the Warren mining district, Idaho County, Idaho: Idaho Bureau of Mines and Geology Pamphlet 45, 65 p.

Reed, J.C., 1939, Geology and ore deposits of the Florence district, Idaho County, Idaho: Idaho Bureau of Mines and Geology Pamphlet 46, 44 p.

Reid, R.R., 1959, Reconnaissance geology of the Elk City region, Idaho: Idaho Bureau of Mines and Geology Pamphlet 120, 100 p.

Reid, R.R., 1960, Placer deposits of the Elk City region: Idaho Bureau of Mines and Geology Pamphlet 121, 41 p.

Ross, C.P., 1931, A classification of the lode deposits of south-central Idaho: Economic Geology, v. 26, no. 2, p. 169–185. [Also available at https://doi.org/10.2113/gsecongeo.26.2.169.]

Ross, C.P., 1933, The Thunder Mountain mining district, Valley County, Idaho: Economic Geology, v. 28, no. 6, p. 587–600. [Also available at https://doi.org/10.2113/gsecongeo.28.6.587.]

Ross, C.P., 1934, Correlation and interpretation of Paleozoic stratigraphy in south-central Idaho: Geological Society of America Bulletin, v. 45, no. 5, p. 937–1000. [Also available at https://doi.org/10.1130/GSAB-45-937.]

Ross, C.P., 1936, Mining districts of the state of Idaho: Idaho Bureau of Mines and Geology in cooperation with the U.S. Geological Survey, scale 1:500,000.

Rostad, O.R., Armstrong, R.L., and Hollister, V.F., 1978, K-Ar dates for mineralization in the White Cloud-Cannivan porphyry molybdenum belt of Idaho and Montana—Discussion and reply: Economic Geology, v. 73, no. 7, p. 1366–1368. [Also available at https://doi.org/10.2113/gsecongeo.73.7.1366.]

Ross, C.P., and Forrester, J.D., 1947, Geologic map of the state of Idaho: U.S. Geological Survey and Idaho Bureau of Mines and Geology, scale 1:500,000.

Ruppel, E.T., and Lopez, D.A., 1988, Regional geology and mineral deposits in and near the central part of the Lemhi Range, Lemhi County, Idaho: U.S. Geological Survey Professional Paper 1480, 122 p. [Also available at https://doi.org/10.3133/pp1480.]

Sanford, R.F., and Wooden, J.L., 1995, Sources of lead in ore deposits of central Idaho, chap. N *of* Worl, R.G., Link, P.K., Winkler, G.R., and Johnson, K.M., eds., Geology and mineral resources of the Hailey 1° × 2° quadrangle and the western part of the Idaho Falls 1° × 2° quadrangle, Idaho: U.S. Geological Survey Bulletin 2064, p. N1–N24.

Savage, C.N., 1961, Economic geology of central Idaho black-sand placers: Idaho Bureau of Mines and Geology Bulletin 17, 160 p.

Savage, C.N., 1970, Evaluation of minerals and mineral potential of the Salmon River drainage basin in Idaho: Idaho Bureau of Mines and Geology Pamphlet 147, 64 p.

Schrader, F.C., and Ross, C.P., 1926, Antimony and quicksilver deposits in the Yellow Pine district: U.S. Geological Survey Bulletin, v. 780, p. 137–167.

Shannon, S.S., Jr., and Reynolds, S.J., 1975, A brief geological survey of the East Thunder Mountain mining district, Valley Co., Idaho: Idaho Bureau of Mines and Geology Information Circular 29, 13 p.

Shenon, P.J., and Reed, J.C., 1934, Geology and ore deposits of the Elk City, Orogrande, Buffalo Hump, and Tenmile districts, Idaho County, Idaho: U.S. Geological Survey Circular 9, 89 p. [Also available at https://doi.org/10.3133/cir9.]

Shenon, P.J., and Ross, C.P., 1936, Geology and ore deposits near Edwardsburg and Thunder Mountain, Idaho: Idaho Bureau of Mines and Geology Pamphlet 44, 45 p.

Skipp, B., and Kuntz, M.A., 2009, Geologic map of the Arco 30 × 60 minute quadrangle, south-central Idaho: Idaho Geological Survey Geologic Map 47, 32 p.

Skipp, B., Kuntz, M.A., and Morgan, L.A., 1989, Geologic map of Mackay 4 (Grouse) SE quadrangle, Butte County, Idaho: U.S. Geological Survey Open-File Report 89–431, scale 1:24,000. [Also available at https://doi.org/10.3133/ofr89431.]

Smitherman, J.R., 1988, Geologic map of the Stibnite roof pendant, Valley County, Idaho: Idaho Geological Survey, Technical Report T–88–2, scale 1:24,000.

Soulliere, S.J., Wilson, A.B., and Skipp, B.A., 1995, Jasperoid-associated precious-metal deposits in the northwestern part of the Idaho Falls 1° × 2° quadrangle, south-central Idaho, chap. J *of* Worl, R.G., Link, P.K., Winkler, G.R., and Johnson, K.M., eds., Geology and mineral resources of the Hailey 1° × 2° quadrangle and the western part of the Idaho Falls 1° × 2° quadrangle, Idaho: U.S. Geological Survey Bulletin 2064–J, p. J1–J15.

Stewart, D.E., Lewis, R.S., Stewart, E.D., and Link, P.K., 2013, Geologic map of the central and lower Big Creek drainage, central Idaho: Idaho Geological Survey Digital Web Map 161, scale 1:75,000, accessed March 23, 2021, at https://idahogeology.org/product/dwm-161.

Stewart, D.E., Stewart, E.D., and Lewis, R.S., 2017, Geologic map of the Burnt Log Creek area, Valley County, Idaho: Idaho Geological Survey, Digital Web Map 180, scale 1:36,000, accessed March 23, 2021, at https://idahogeology.org/product/dwm-180.

Stewart, D.E., Stewart, E.D., Lewis, R.S., Weppner, K.N., and Isakson, V.H., 2016, Geologic map of the Stibnite quadrangle, Valley County, Idaho: Idaho Geological Survey, Geologic Map GM-51, scale 1:24,000, accessed March 23, 2021, at https://idahogeology.org/product/gm-51.

Taylor, C.D., Winick, J.A., Unruh, D.M., and Kunk, M.J., 2007, Geochronology and geochemistry of the Idaho-Montana porphyry belt, *in* Lund, K., ed., Earth science studies in support of public policy development and land stewardship—Headwaters province, Idaho and Montana: U.S. Geological Survey Circular 1305, p. 26–39.

Thompson, F.A., and Ballard, S.M., 1924, Geology and gold resources of north-central Idaho: Idaho Bureau of Mines and Geology Bulletin 7, 127 p.

Tikoff, B., Kelso, P., Manduca, C., Markley, M.J., and Gillaspy, J., 2001, Lithospheric and crustal reactivation of an ancient plate boundary—The assembly and disassembly of the Salmon River suture zone, Idaho, USA: Geological Society, London, Special Publications 186, p. 213.

Turner, R.J.W., and Otto, B.R., 1995, Structural and stratigraphic setting of the Triumph stratiform zinc-lead-silver deposit, Devonian Milligen Formation, central Idaho, chap. E *of* Worl, R.G., Link, P.K., Winkler, G.R., and Johnson, K.M., eds., Geology and mineral resources of the Hailey 1° × 2° quadrangle and the western part of the Idaho Falls 1° × 2° quadrangle, Idaho: U.S. Geological Survey Bulletin 2064–E, 27 p. [Also available at https://doi.org/10.3133/b2064AR.]

Umpleby, J.B., and Livingston, D.C., 1920, A reconnaissance in south central Idaho embracing the Thunder Mountain, Big Creek, Stanley Basin, Sheep Mountain, and Seafoam districts: Idaho Bureau of Mines and Geology Bulletin 3, 232 p.

Unruh, D.M., Lund, K., Kuntz, M.A., and Snee, L.W., 2008, Uranium-lead zircon ages and Sr, Nd, and Pb isotope geochemistry of selected plutonic rocks from western Idaho: U.S. Geological Survey Open-File Report 2008–1142, 42 p., accessed March 23, 2021, at https://doi.org/10.3133/ofr20081142.

Watts, K.C., Jr., and King, H.D., 1999, Geochemistry of the Payette National Forest, Idaho: U.S. Geological Survey Open-File Report 98–219E, 44 p. [Also available at https://doi.org/10.3133/ofr98219E.]

Weis, P.L., Schmitt, L.J., Jr., and Tuchek, E.T., 1972, Mineral resources of the Salmon River Breaks Primitive Area, Idaho: U.S. Geological Survey Bulletin 1353-C, 91 p., scale 1:125,000. [Also available at https://doi.org/10.3133/b1353C.]

White, D.E., 1940, Antimony deposits of a part of the Yellow Pine district, Valley County, Idaho, a preliminary report: U.S. Geological Survey Bulletin 922–I, p. 247–279, 1 pl. in pocket. [Also available at https://doi.org/10.3133/b922I.]

White, D.E., 1945, Geologic map of the Yellow Pine district, Valley County, Idaho: U.S. Geological Survey Preliminary Strategic Map, Strategic Minerals Investigation, 6 p., scale 1:48,000.

Worl, R.G., and Johnson, K.M., 1995, Geology and mineral deposits of the Hailey 1° × 2° quadrangle and the western part of the Idaho Falls 1° × 2° quadrangle, south-central Idaho—An overview, chap. A *of* Worl, R.G., Link, P.K., Winkler, G.R., and Johnson, K.M., eds., Geology and mineral resources of the Hailey 1° × 2° quadrangle and the western part of the Idaho Falls 1° × 2° quadrangle, Idaho: U.S. Geological Survey Bulletin 2064–A, 22 p., 1 pl. in pocket. [Also available at https://pubs.er.usgs.gov/publication/b2064AR.]

Worthington, J.E., 2007, Porphyry and other molybdenum deposits of Idaho and Montana: Idaho Geological Survey Technical Report 2007–03, 25 p.

Publishing support provided by the Science Publishing Network, Denver Publishing Service Center

For more information concerning the research in this report, contact the

Center Director, USGS Geology, Geophysics, and Geochemistry Science Center

Box 25046, Mail Stop 973

Denver, CO 80225

(303) 236-1800

Or visit Geology, Geophysics, and Geochemistry Science Center website at

https://www.usgs.gov/centers/gggsc

ISSN 2330-7102 (online)
https://doi.org/10.3133/pp1884